Volume 26, Number 2, 2026 ISSN 1562-8353

NONLINEAR DYNAMICS AND SYSTEMS THEORY
An International Journal of Research and Surveys

Volume 26 Number 2 2026

CONTENTS

NONLINEAR DYNAMICS & SYSTEMS THEORY
Volume 26, No. 2, 2026

Nonlinear Dynamics and Systems Theory

An International Journal of Research and Surveys

 ISSN 1562-8353 Printed in Ukraine
To receive contents and abstracts by e-mail, visit our Website at: **http://www.e-ndst.kiev.ua**

InforMath Publishing Group
http://www.e-ndst.kiev.ua

Nonlinear Dynamics and Systems Theory

An International Journal of Research and Surveys

INSTRUCTIONS FOR CONTRIBUTORS

(1) General. Nonlinear Dynamics and Systems Theory (ND&ST) is an international journal devoted to publishing peer-refereed, high quality, original papers, brief notes and review articles focusing on nonlinear dynamics and systems theory and their practical applications in engineering, physical and life sciences. Submission of a manuscript is a representation that the submission has been approved by all of the authors and by the institution where the work was carried out. It also represents that the manuscript has not been previously published, has not been copyrighted, is not being submitted for publication elsewhere, and that the authors have agreed that the copyright in the article shall be assigned exclusively to InforMath Publishing Group by signing a transfer of copyright form. Before submission, the authors should visit the website:

http://www.e-ndst.kiev.ua

for information on the preparation of accepted manuscripts. Please download the archive Sample_NDST.zip containing example of article file (you can edit only the file Samplefilename.tex).

(2) Manuscript and Correspondence. Manuscripts should be in English and must meet common standards of usage and grammar. To submit a paper, send by e-mail a file in PDF format directly to

Professor A.A. Martynyuk, Institute of Mechanics,
Nesterov str.3, 03057, Kiev-57, Ukraine
e-mail: journalndst@gmail.com

or to one of the Regional Editors or to a member of the Editorial Board. Final version of the manuscript must typeset using LaTex program which is prepared in accordance with the style file of the Journal. Manuscript texts should contain the title of the article, name(s) of the author(s) and complete affiliations. Each article requires an abstract not exceeding 150 words. Formulas and citations should not be included in the abstract. AMS subject classifications and key words must be included in all accepted papers. Each article requires a running head (abbreviated form of the title) of no more than 30 characters. The sizes for regular papers, survey articles, brief notes, letters to editors and book reviews are: (i) 10-14 pages for regular papers, (ii) up to 24 pages for survey articles, and (iii) 2-3 pages for brief notes, letters to the editor and book reviews.

(3) Tables, Graphs and Illustrations. Each figure must be of a quality suitable for direct reproduction and must include a caption. Drawings should include all relevant details and should be drawn professionally in black ink on plain white drawing paper. In addition to a hard copy of the artwork, it is necessary to attach the electronic file of the artwork (preferably in PCX format).

(4) References. Each entry must be cited in the text by author(s) and number or by number alone. All references should be listed in their alphabetic order. Use please the following style:

Journal: [1] H. Poincare, Title of the article. *Title of the Journal* **volume** (issue) (year) pages. [Language]

Book: [2] A.M. Lyapunov, *Title of the Book.* Name of the Publishers, Town, year.

Proceeding: [3] R. Bellman, Title of the article. In: *Title of the Book.* (Eds.). Name of the Publishers, Town, year, pages. [Language]

(5) Proofs and Sample Copy. Proofs sent to authors should be returned to the Editorial Office with corrections within three days after receipt. The corresponding author will receive a sample copy of the issue of the Journal for which his/her paper is published.

(6) Editorial Policy. Every submission will undergo a stringent peer review process. An editor will be assigned to handle the review process of the paper. He/she will secure at least two reviewers' reports. The decision on acceptance, rejection or acceptance subject to revision will be made based on these reviewers' reports and the editor's own reading of the paper.

NONLINEAR DYNAMICS AND SYSTEMS THEORY
An International Journal of Research and Surveys
Published by InforMath Publishing Group since 2001

Volume 26 Number 2 2026

CONTENTS

Founded by A.A. Martynyuk in 2001.
Registered in Ukraine Number: KB No 5267 / 04.07.2001.

NONLINEAR DYNAMICS AND SYSTEMS THEORY

An International Journal of Research and Surveys

Impact Factor from SCOPUS for 2024: SJR – 0.262, SNIP – 1.098 and CiteScore – 1.5

Nonlinear Dynamics and Systems Theory (ISSN 1562–8353 (Print), ISSN 1813–7385 (Online)) is an international journal published under the auspices of the S.P. Timoshenko Institute of Mechanics of National Academy of Sciences of Ukraine and Curtin University of Technology (Perth, Australia). It aims to publish high quality original scientific papers and surveys in areas of nonlinear dynamics and systems theory and their real world applications.

AIMS AND SCOPE

Nonlinear Dynamics and Systems Theory is a multidisciplinary journal. It publishes papers focusing on proofs of important theorems as well as papers presenting new ideas and new theory, conjectures, numerical algorithms and physical experiments in areas related to nonlinear dynamics and systems theory. Papers that deal with theoretical aspects of nonlinear dynamics and/or systems theory should contain significant mathematical results with an indication of their possible applications. Papers that emphasize applications should contain new mathematical models of real world phenomena and/or description of engineering problems. They should include rigorous analysis of data used and results obtained. Papers that integrate and interrelate ideas and methods of nonlinear dynamics and systems theory will be particularly welcomed.

PUBLICATION AND SUBSCRIPTION INFORMATION

Nonlinear Dynamics and Systems Theory will have 6 issues in 2026, printed in hard copy (ISSN 1562–8353) and available online (ISSN 1813–7385), by InforMath Publishing Group, Nesterov str., 3, Institute of Mechanics, Kiev, MSP 680, Ukraine, 03057. Subscription prices are available upon request from the Publisher, EBSCO Information Services (`mailto:journals@ebsco.com`), or website of the Journal: `http://e-ndst.kiev.ua`. Subscriptions are accepted on a calendar year basis. Issues are sent by airmail to all countries of the world. Claims for missing issues should be made within six months of the date of dispatch.

ABSTRACTING AND INDEXING SERVICES

Papers published in this journal are indexed or abstracted in: Mathematical Reviews / MathSciNet, Zentralblatt MATH / Mathematics Abstracts, PASCAL database (INIST–CNRS) and SCOPUS.

Nonlinear Dynamics and Systems Theory, **26** (2) (2026) 115–124

On Chaotification and Stabilization of Zeraoulia-Sprott Map

Mamoune Aidel [1*] and Elhadj Zeraoulia [2]

[1] *University Larbi Ben M'hidi, Oum El Bouaghi, Algeria.*
[2] *University Larbi Tebassi, Tebessa, Algeria.*

Received: January 28, 2025; Revised: March 30, 2026

Abstract: This paper explores the stabilization of chaotic dynamics in the Zeraoulia-Sprott (Z-S) map using both feedback and non-feedback control strategies. By leveraging the stability theorem for discrete systems and the principle that lower energy correlates with greater stability, we systematically investigate the transition from chaos to periodic behavior. The study compares the effectiveness of feedback-based stabilization techniques with a minimum energy approach, analyzing their impact across different periodic orbits and dimensions. Numerical simulations validate the proposed methods, demonstrating their feasibility and efficiency in controlling chaos within the Z-S system. These findings contribute to a broader understanding of chaos suppression in discrete nonlinear systems and offer practical insights into their control applications.

Keywords: *discrete dynamical systems; Zeraoulia-Sprott map; chaos control; chaotification; stabilization; feedback control; minimum energy control.*

Mathematics Subject Classification (2020): 39A33, 39A05, 93-03, 39A70.

1 Introduction

Nonlinear dynamical systems are essential in many scientific and engineering fields, where discrete-time models can exhibit chaotic behavior, with applications in secure communication, cryptography, neural networks, and control theory. The Zeraoulia–Sprott (Z-S) map, a simple yet complex 2D rational mapping, shows diverse dynamics—periodic, quasi-periodic, and chaotic—making it a valuable model for studying stability and control [1].

* Corresponding author: mailto:smamoune.aidel@univ-khenchela.dz

Chaotic maps are key in nonlinear dynamics for understanding bifurcations, attractors, and stability in discrete systems. Recent studies on the Z-S map emphasize its high sensitivity to initial conditions and structural complexity [2], creating challenges for stability in practical uses. Control strategies, such as perturbation methods [3], stability criteria [4], and adaptive control [5,13,14,15,16], aim to regulate these behaviors, while chaotification has been explored for beneficial uses in coupled map lattices [6]. Despite applications like encryption [13], stabilizing chaotic maps, especially at p-periodic orbits, remain a crucial research focus [7].

The snap-back repeller theory is a common tool for analyzing discrete chaotic systems, offering criteria for chaos detection and control design [8–10]. Stabilization methods, both feedback and non-feedback, have proven effective for maps like the Hénon map [12]. This study applies these approaches to the chaotic Z-S map, targeting various periodic orbits. Using stability theorems and the principle linking lower energy states to greater stability, we evaluate and compare both methods through extensive numerical simulations, assessing their feasibility and potential applications.

The paper is organized as follows. After the Introduction, Section 2 examines the stability and instability regions of the system and studies how chaotification occurs within the stable region. Sections 3 and 4 focus on the unstable regions and develop a feedback control strategy to achieve stabilization. Section 5 presents numerical simulation for selected parameter values. Finally, Section 6 introduces a non-feedback (minimum energy) control approach for stabilization, supported by additional numerical results, followed by concluding remarks.

2 Problem and Formulation

The Z-S system is defined by the following recurrence:

$$\begin{cases} x_{k+1} = \dfrac{-ax_k}{1+y_k^2}, \\ y_{k+1} = x_k + by_k. \end{cases} \tag{1}$$

The system has several behaviors depending on the values of the parameters (a, b) according to G. Chen et al. [2].

Condition	$\lvert a\rvert$	$\lvert b\rvert$
1	< 1	< 1 : global asymptotic stability
2	< 1	> 1 : unbounded solutions
3	> 1	< 1 : nontrivial global attractor
4	> 1	> 1 : unbounded solutions

Table 1: Stability conditions based on parameters a and b.

In this paper, we will study the system behavior in the zone Ω defined by$\{(a,b)) \in \mathbb{R}^2 / \, |a| < 1, |b| < 1\}$ and $\{(a,b)) \in \mathbb{R}^2 / \, |a| > 1, |b| < 1\}$.

2.1 Chaotification of Z-S system

$$F\begin{pmatrix} x \\ y \end{pmatrix} = \begin{pmatrix} \dfrac{-ax}{1+y^2} \\ x + by \end{pmatrix}.$$

According to [2], the system is stable for $a \in]-1,1[$, $b \in]-1,1[$; we will chaotify it using the theorem from [10].

Theorem 2.1 *Consider the n-dimensional controlled system*

$$X_{k+1} = X_k + U_k \pmod 1, \tag{$*$}$$

where the controller is given by $U_k = cX_k - F(0)$.

If F is continuously differentiable and $\|F(X)\| < m$ for $\|X\| < 1$ and some positive constant m, then by choosing $|a| > 2m + \sqrt{n}$ such that all eigenvalues of $(DF(0) + cE)'(DF(0) + cE)$ exceed 1, and $|a|$ is suitably large, the controlled system $(*)$ will be chaotic in the sense of Li–Yorke.

If F is smooth and bounded, and a and c are chosen to satisfy certain eigenvalue and magnitude conditions, the controlled n-dimensional system becomes Li–Yorke chaotic.

2.1.1 Application

- F is C^1 with $DF(X) = \begin{pmatrix} \dfrac{-a}{1+y^2} & \dfrac{2axy}{1+y^2} \\ 1 & b \end{pmatrix}$, $\|F(X)\| \le \sqrt{5}$.
- Choosing $|c| = 6 > 2\sqrt{5} + \sqrt{2}$ gives $DF(0) + cE = \begin{pmatrix} -a+6 & 0 \\ 1 & b+6 \end{pmatrix}$ with the eigenvalues

$$\lambda_{1,2} = \frac{1}{2}\Big(d \pm \sqrt{f}\Big), \qquad \begin{aligned} d &= 12a - 12b + a^2 + b^2 + 73 \\ f &= (a^2 + 2ab + b^2 + 1)(a^2 - 2ab - 24a + b^2 + 24b + 145). \end{aligned}$$

- For $(a,b) \in (-1,1)^2$, $\lambda_1 > 1$ and $\lambda_2 > 1$, hence the system

$$\begin{cases} x(k+1) = \dfrac{-ax_k}{1+y_k^2} + 6x_k \,(\mathrm{mod}\, 1), \\ y(k+1) = x_k + by_k + 6y_k \,(\mathrm{mod}\, 1) \end{cases}$$

  is chaotic.

Numerical application. The system

$$\begin{cases} x_{k+1} = \dfrac{-0.5x_k}{1+y_k^2}, \\ y_{k+1} = x_k + 0.5y_k \end{cases} \tag{2}$$

is stable and admits the origin as a stable fixed point.

According to the theorem above, the system

$$\begin{cases} x_{k+1} = \dfrac{-0.5x_k}{1+y_k^2} + 6x_k \,(\mathrm{mod}\, 1), \\ y_{k+1} = x_k + 0.5y_k + 6y_k \,(\mathrm{mod}\, 1) \end{cases} \tag{3}$$

is chaotic.

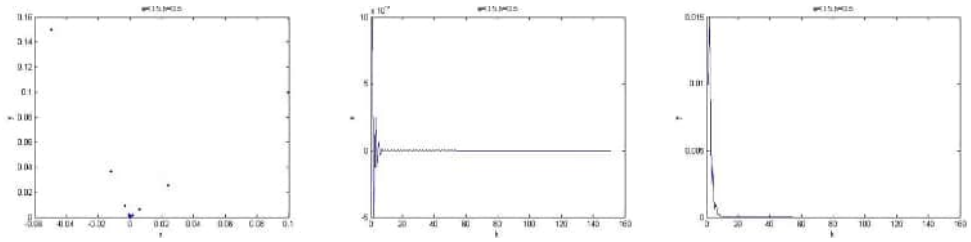

Figure 1: Phase spaces and evolution $(x,k),(y,k)$

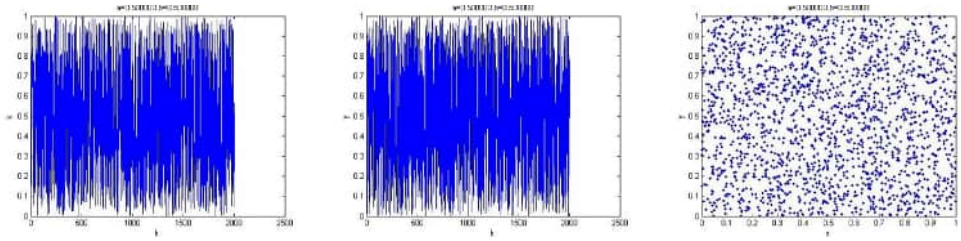

Figure 2: Chaotification.

3 Study of the Stability

Theorem 3.1 *If there exists at least one eigenvalue of the Jacobian matrix of the fixed point of one period greater than 1, the fixed point is unstable.*

The system has three fixed points:
$(0;0)$, $\left((1-b)\sqrt{-1-a};\sqrt{-1-a}\right)$, $\left((b-1)\sqrt{-1-a};-\sqrt{-1-a}\right)$.

3.1 Stability analysis

Fixed point $(0,0)$**:** For $a<-1$ and $-1<b<1$,

$$DF_{(0,0)}=\begin{pmatrix}-a & 0\\ 1 & b\end{pmatrix},\quad \lambda(DF)=(-a,\,b),\quad |-a|>1.$$

Hence $(0,0)$ is unstable in Ω.

Fixed point $\left((1-b)\sqrt{-1-a},\ \sqrt{-1-a}\right)$:

$$DF_{(x^*,y^*)}=\begin{pmatrix}1 & \frac{2(b-1)(a+1)}{a}\\ 1 & b\end{pmatrix},\quad \lambda_{1,2}=\frac{1+b\pm\sqrt{\frac{(b-1)(7a+ab+8)}{a}}}{2}.$$

- If $7a+ab+8>0$: $\lambda_1>1$ for $a>-1$, $\lambda_2>1$ has no solution in $a<-1$.
- If $7a+ab+8<0$: Eigenvalues are complex conjugates; $|\lambda_{1,2}|>1$ if $a<-2$.

4 Stabilizing Periodic Orbits of Z-S Map by Feedback Method

We consider the predictive control method with state feedback when the trajectory is near the fixed point. T. Ushio and S. Yamamoto [17] proposed, in this case, an alternative to the original method of Pyragas.

Supposing the system $X_{k+1} = f(X_k, U_k)$, Ushio and Yamamoto [17] propose a sequence in the form

$$U_k = K\left(f(X_k, o) - X^*\right) \diagup X^* = (x^*, y^*) \tag{4}$$

if it is desired that control be applied in an area such as

$$|X_k - X_{k-1}| < \varepsilon. \tag{5}$$

With ε being a positive enough number, the control will be determined as follows:

$$U_k = \begin{cases} K\left(f(X_k, o) - X^*\right) \text{if } |X_k - X_{k-1}| < \varepsilon, \\ o \quad \text{otherwise.} \end{cases} \tag{6}$$

4.1 Appliying the control law around fixed point $(0, 0)$

The control system is defined as follows: $f(X_k, 0) = f(X_k)$ with the vector

$$U_k = \begin{pmatrix} u_k^1 \\ u_k^2 \end{pmatrix} = \begin{pmatrix} K\left(\dfrac{-ax_k}{1+y_k^2} - 0\right) \\ 0\,(x_k + by_k - 0) \end{pmatrix}. \tag{7}$$

The system admits the origin as a fixed point, the gain K is chosen such that this fixed point becomes stable. We have

$$\begin{cases} x_{k+1} = \dfrac{-ax_k}{1+y_k^2} + u_k^1 \\ y_{k+1} = x_k + by_k + u_k^1 \end{cases} \Rightarrow \begin{cases} x_{k+1} = \dfrac{-ax_k}{1+y_k^2} + K\left(\dfrac{-ax_k}{1+y_k^2}\right) \\ y_{k+1} = x_k + by_k. \end{cases} \tag{8}$$

We linearize the system around the origin $Df\,(0,0)) = \begin{pmatrix} (1+K)\,(-a) & 0 \\ 1 & b \end{pmatrix}$ with the eigenvalues $-a - Ka, b$, $|b| \prec 1, |(1+K)\,(-a)| < 1$. The system is stable if $-1 < a(1+K) < 1$.

5 Numerical Simulation

Case $a = -7,\ b = -0.1$**.** All three fixed points are unstable; the bifurcation diagram and a positive Lyapunov exponent indicate chaos. Choose a scalar gain K so that $-1 < 7 + 7K < 1$ gives

$$K \in \left(-\tfrac{8}{7}, -\tfrac{6}{7}\right) \approx (-1.14, -0.85),$$

which places both closed-loop eigenvalues inside the unit disk, ensuring local stabilization of the targeted fixed point. For example, with $K = -1.1$ and control

$$U_k = \begin{pmatrix} -1.1\,\dfrac{-10\,x_k}{1+y_k^2} \\ 0 \end{pmatrix},$$

the uncontrolled system

$$\begin{cases} x_{k+1} = \dfrac{7x_k}{1+y_k^2}, \\ y_{k+1} = x_k - 0.1\, y_k \end{cases}$$

is stabilized under the chosen feedback.

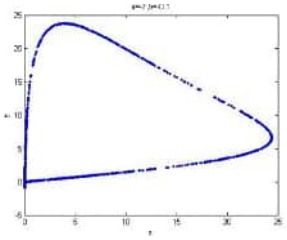

Figure 3: Zerraoulia-Sprotts attractor for $a = -7, b = -0.1$.

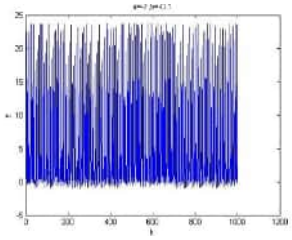

Figure 4: Synchronization (k, y).

The system under control is

$$\begin{cases} x_{k+1} = \dfrac{7x_k}{1+y_k^2} - 1.1\left(\dfrac{7x_k}{1+y_k^2}\right), \\ y_{k+1} = x_k - 0.1y_k. \end{cases} \tag{9}$$

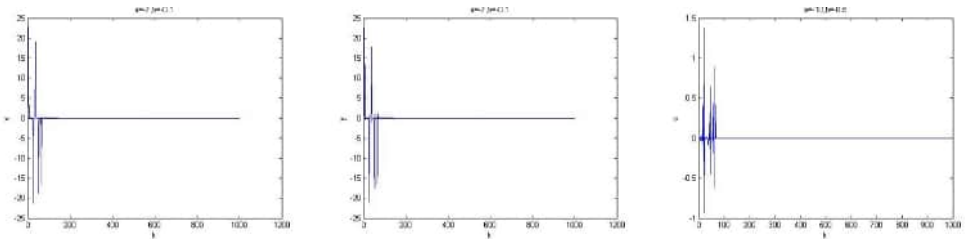

Figure 5: Stabilization (k,x), (k,y) and the control.

Around the fixed point $\left((1-b)\sqrt{-1-a}; \sqrt{-1-a}\right) = (x^*; y^*)$,

$$\begin{cases} x_{k+1} = \dfrac{-ax_k}{1+y_k^2} + k\left(\dfrac{-ax_k}{1+y_k^2} - x^*\right), \\ y_{k+1} = x_k + by_k + 0(x_k + by_k - y^*), \end{cases}$$

$$Df\,(x^*; y^*) = \begin{pmatrix} 1+k & \dfrac{2(1+k)(b-1)(1+a)}{a} \\ 1 & b \end{pmatrix}.$$

For $a = -7$, $b = -0.1$, the three fixed points are unstable. From the bifurcation diagram and the fact that one of Lyapunov's exponents is positive, the system is chaotic. We now calculate the gain K:

$$-1 < 7 + 7K < 1 \quad \Longrightarrow \quad -1.14 < K < -0.85.$$

When K belongs to this interval, the control system admits two eigenvalues less than 1, so the fixed point is surely stable. We take $K = -1.1$. The control is

$$U_k = \begin{pmatrix} u_1(k) \\ u_2(k) \end{pmatrix} = \begin{pmatrix} -1.1 \left(\dfrac{-10x_k}{1+y_k^2} \right) \\ 0 \end{pmatrix}.$$

The uncontrolled system is

$$\begin{cases} x_{k+1} = \dfrac{7x_k}{1+y_k^2}, \\ y_{k+1} = x_k - 0.1y_k. \end{cases}$$

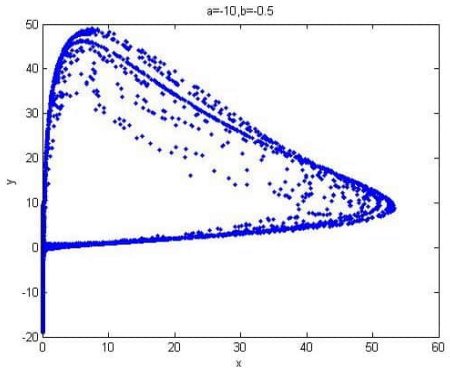

Figure 6: Zeraoulia–Sprott attractor.

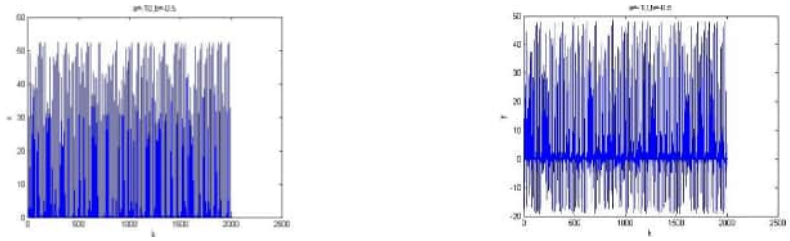

Figure 7: Zeraoulia-Sprott attractor for a=-10,b=-0.5 and the evolution (k,x) (k,y).

We take $K = -0.9$. The system under control becomes

$$\begin{cases} x_{k+1} = \dfrac{10x_k}{1+y_k^2} - 0.9 \left(\dfrac{10x_k}{1+y_k^2} - 4.5 \right), \\ y_{k+1} = x_k - 0.5y_k + 0(x_k - 0.5y_k - 3). \end{cases} \tag{10}$$

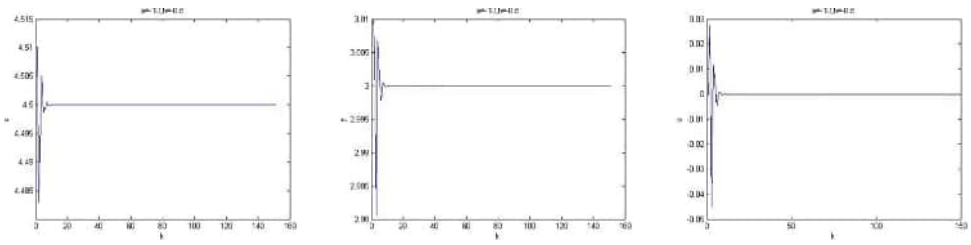

Figure 8: Stabilization (k,x), (k,y) and control.

6 Stabilizing Periodic Orbits of Z-S Map by Minimum Energy Method

For discrete chaotic systems, stabilizing high-periodic orbits with feedback is difficult due to the large gains required. Instead, we propose a non-feedback method for the Zeraoulia–Sprott map: by reducing the generalized energy (Lyapunov function) below a chosen threshold $E_m < E_{\text{av}}$, the system can be driven to periodic orbits.

6.1 Application of the method around unstable fixed point $(\mathbf{0}, \mathbf{0})$

The system is defined by the recurrence

$$\begin{cases} x_{k+1} = \dfrac{-ax}{1+y_k^2} \\ y_{k+1} = x_k + by_k \end{cases} \quad \diagup (a,b) \in (\Omega)\,. \tag{11}$$

From the diagram below, we can notice the areas that can be chaotic.

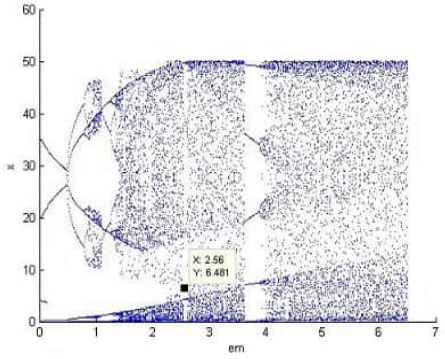

Figure 9: Bifurcation diagram (em, x).

We take as an example $a = -10, b = -0.1, x_0 = 0.1,\ y_0 = 0.1$. The chaotic behavior was confirmed by Lyapunov's exponent.

The Control.

We chose as a function of Lyapunov $E(x,y) = \dfrac{1}{a^2}\left(x^2+y^2\right)$. The average value of E

for 100000 iterations is equal to 6.4485, now we will apply the control

$$\begin{cases} E_k = 0.01\left(x_k^2 + y_k^2\right), \\ x_{k+1} = \dfrac{10x_k}{1+y_k^2}, \\ y_{k+1} = \widetilde{y_k} \end{cases} \tag{12}$$

as

$$\widetilde{y_k} = \begin{cases} x_k - 0.1y_k\ , & E_k < E_m, \\ -\sqrt{E_m - x_k^2}, & E_k \geq E_m \ \ et\ \widetilde{y_k} < 0, \\ \sqrt{E_m - x_k^2}, & E_k \geq E_m \ \ et \widetilde{y_k} \geq 0. \end{cases}$$

According to the diagram, we distinguish the zone where the system has periodic unstable orbits, we will apply the method to make these orbits stable. We chose some samples: em=0.1 (7 periods), em=0.67 (14 periods), em=1.18 (14periodes), em=2.56 (22 periods), em=3.8 (15 periods).

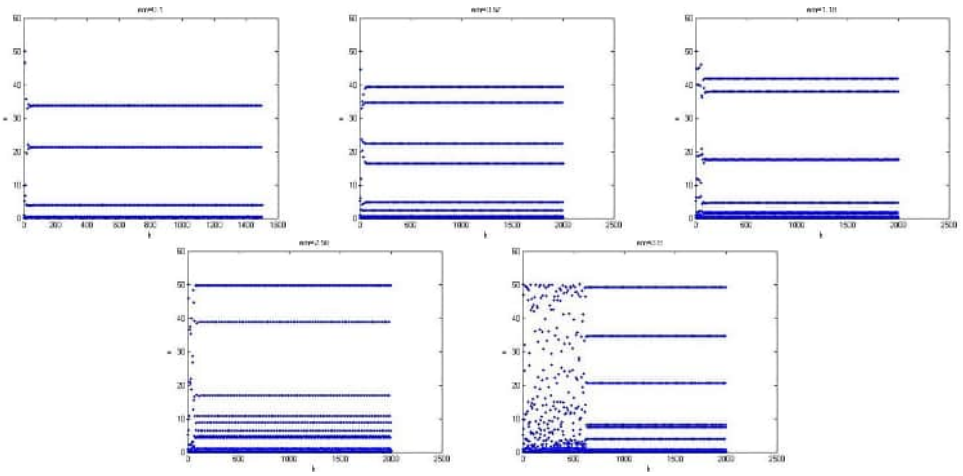

Figure 10: Different types of stabilisation.

Although $E \leq E_m$ is not always maintained, simulations show that the proposed method can stabilize the Z-S map at various p-periodic orbits by adjusting $E_m \in [0, 6.4485]$. Control starts at $n = 60$ and works for both low- and high-periodic orbits, with iteration costs ranging from ≈ 10 (1-periodic) to ≈ 30 (7-periodic).

7 Conclusion

This study examined the stabilization of the chaotic Zeraoulia-Sprott (Z-S) map using feedback and non-feedback control methods. By applying the stability theorem for discrete systems, we demonstrated the effectiveness of both approaches in directing the system toward periodic orbits. Numerical simulations confirmed the feasibility of these techniques, highlighting their potential for controlling chaos in nonlinear discrete systems. Future research may explore extensions to higher-dimensional maps and adaptive control strategies.

References

[1] Z. Elhadj and J. C. Sprott. On the dynamics of a new simple 2-d rational discrete mapping. *International Journal of Bifurcation and Chaos* **21** (1) (2011) 155–160.

[2] G. Chen, E. V. Kudryashova, N. V. Kuznetsov and G. A. Leonov. Dynamics of the zeraoulia–sprott map revisited. *International Journal of Bifurcation and Chaos* **26** (7) (2016) 1650126.

[3] L. Zhang and Y.Shi. Time-varying perturbations of chaotic discrete systems. *International Journal of Bifurcation and Chaos* **22** (3) (2012) 1250066.

[4] A. Iggidr and M. Bensoubaya. *Stability of Discrete-time Systems: New Criteria and Applications to Control Problems*. RR–3003, INRIA, 1996.

[5] E. G. da Silva. *Introduction to Dynamic Systems and Chaos*. 2004.

[6] R. Senkerik, Z. Oplatkova and I. Zelinka. Investigation on evolutionary chaos controller synthesis for hénon map stabilization. In: *AIP Conference Proceedings*, vol. 1389, 1027–1030. American Institute of Physics, September, 2011.

[7] P. Li, Z. Li, W. A. Halang and G. Chen. Chaotification of a spatiotemporal coupled map lattice. In: *Proceedings of the 3rd International Conference Physics and Control (PhysCon)*, 2007.

[8] M. Wang. Chaotic control of lü system via three methods. *International Journal of Modern Nonlinear Theory and Application* **3** (2) (2014).

[9] Y. Shi and P. Yu. Chaos induced by regular snap-back repellers. *Journal of Mathematical Analysis and Applications*, **337**(2) (2008) 1480–1494.

[10] C. Li and G. Chen. An improved version of the marotto theorem. *Chaos, Solitons & Fractals* **18** (1) (2003) 69–77.

[11] K. L. Liao and C. W. Shih. Snapback repellers and homoclinic orbits for multi-dimensional maps. *Journal of Mathematical Analysis and Applications* **386** (1) (2012) 387–400.

[12] T. Wang, X. Wang, and M. Wang. Chaotic control of hénon map with feedback and nonfeedback methods. *Communications in Nonlinear Science and Numerical Simulation*, 16(8):3367–3374, 2011.

[13] S. Adoui and B. Benzeghli. Using a 2-d discrete chaotic map to create safe data in symmetric systems. *Nonlinear Dynamics and Systems Theory*, 24(6), 2024.

[14] K. Daas and N. Hamri. Inducing chaos through timescales in a three-species food chain model. *Nonlinear Dynamics and Systems Theory*, 24(6), 2024.

[15] R. Ramar, V. Sandhiya, N. Santhiya, R. Vinothini, and S. Vinothini. Complex dynamics of novel chaotic system with no equilibrium point: Amplitude control and offset boosting control, its adaptive synchronization. *Nonlinear Dynamics and Systems Theory* **24** (5) (2024) 505–516.

[16] F. Hannachi and R. Amira. On the dynamics and fshp synchronization of a new chaotic 3-d system with three nonlinearities. *Nonlinear Dynamics and Systems Theory* **23** (3) (2023) 283–294.

[17] T. Ushio and S. Yamamoto. Prediction-based control of chaos. *Physics Letters A* **264** (1999) 30–35.

Nonlinear Dynamics and Systems Theory, **26** (2) (2026) 125–137

Some New 4D Fractional-Order Hyperchaotic Rabinovich Systems: Dynamical Analysis and Control

S. Beghou, S. Rouar * and O. Zehrour

Dynamical Systems and Control Laboratory, University of Oum El Bouaghi, Algeria.

Received: March 21, 2025; Revised: March 23, 2026

Abstract: This paper proposes some new 4D fractional-order hyperchaotic Rabinovich systems with Caputo derivatives. Using an exhaustive computer search, 20 simple hyperchaotic systems are found according to system parameters, initial conditions, and fractional-order derivatives of the 4D fractional-order Rabinovich system. These 20 systems are listed in this paper, and based on the Lyapunov exponents, the basic dynamical behaviors of these 20 systems have been investigated. By designing linear and nonlinear feedback controllers, the problems of local and global asymptotic stabilization are investigated for the first system of the proposed hyperchaotic systems. Furthermore, the numerical simulations show the feasibility and the effectiveness of the results.

Keywords: *fractional-order derivative; hyperchaotic Rabinovich system; Lyapunov exponents; feedback controller.*

Mathematics Subject Classification (2020): 34C28, 37D45, 37M22, 70K20, 93-04.

1 Introduction

Hyperchaos, characterized as a chaotic system with at least two positive Lyapunov exponents, has attracted many researchers due to its potential applications in science and engineering, such as neural networks, generation, control, synchronization, secure communications, lasers, image encryption [15], and so on. The hyperchaotic system is a higher dimensional chaotic system; its dynamics are richer and more extended in the phase plane, it has more complex behavior and abundant dynamics than chaotic systems.

* Corresponding author: mailto:salim.rouar@univ-oeb.dz

Historically, hyperchaos was first described by Rössler in 1979 as a model of a particular chemical reaction. After that, many hyperchaotic systems have been studied, including the Lorenz system, Rabinovich system, and Chua system [3, 4], among others.

Nonlinear dynamical systems exhibit unpredictable characteristics due to the disproportionate interactions that exist among their variables (inputs and outputs). The exploration of nonlinear dynamics contributes significantly to a more profound understanding, modeling, prediction, and control of the behaviors exhibited by complex systems that manifest in both natural and engineered systems. Nonlinear dynamics with their interdisciplinary applications can be found in almost every area of scientific research, such as physics, economics, and biology [8]. Chaos, as a dynamical behavior, is one of the most extensively studied topics in nonlinear dynamics in recent years. Comprehending chaos and nonlinear dynamics not only improves knowledge but also provides tools to find creative solutions to real-world phenomena.

Fractional-order calculus is a branch of applied mathematics that deals with differentiation and integration under an arbitrary order of these operations. In recent decades, fractional calculus has been a fruitful field of research, and it has been applied to almost every field of mathematics, science, engineering, and technology. During the last few years, fractional calculus and its applications have been undergoing rapid development, with more and more convincing applications in the real world. In fact, many applications of fractional calculus can be found in physics, signal processing, science and engineering, and many other domains (see e.g. [9] as well as the references therein). Fractional-order systems are closer to real-world phenomena due to their efficacy in modeling the memory and heredity properties of some phenomena [1].

A variety of fractional-order chaotic systems have been extensively investigated in the literature, for example, the fractional-order Lorenz, Chua, Chen, and Rabinovich systems, as well as systems exhibiting hidden dynamics, hyperchaotic behavior, and multi-scroll attractors [4, 14].

Many scientists and engineers have discovered the valuable applications of fractional-order chaos in many fields of science such as engineering, physics, mathematical biology, and psychology [12].

The Rabinovich differential system was first introduced as an important physical system in [10]. It is a nonlinear dynamical system recognized for displaying complex behaviors, including chaos and hyperchaos. Fractional-order chaotic Rabinovich systems have demonstrated significant potential across various advanced technological domains, including secure communication and cryptography, signal processing, artificial intelligence and machine learning, as well as the modeling of complex systems exhibiting memory-dependent dynamics [2]. Liu et al. [7] proposed a new 4D hyperchaotic system, which is generated via adding a controller to the 3D Rabinovich system, and studied its fundamental dynamics.

He and Chen in [4] proposed a 4D fractional-order hyperchaotic system and investigated its stability, hyperchaos, control of chaos, and synchronization for fixed system parameters ($a = 4,\ b = 1,\ h = 6.75,\ d = 1,\ k = 2$) and fixed initial conditions $(5.5, -1.25, 8.4, 2.75)$.

This paper proposes new 4D fractional-order hyperchaotic Rabinovich systems according to varied system parameters, initial conditions, and fractional-order derivatives. We also develop linear and nonlinear feedback controllers to address the problems of local and global asymptotic stability for the first system of these proposed systems.

The rest of this paper is organized as follows. Section 2 presents some preliminaries

such as Caputo's fractional-order derivative and the theory of fractional-order nonlinear dynamical systems. Section 3 describes the proposed fractional-order hyperchaotic Rabinovich systems. Section 4 analyzes the stability and hyperchaos of these proposed systems. Section 5 investigates the local and global asymptotic stabilization problems for the first system of the proposed hyperchaotic systems by designing linear and nonlinear feedback controllers, respectively. In the end, the conclusions are drawn in Section 6.

2 Preliminaries

2.1 Caputo fractional derivative

Among several fractional-order derivative approaches considered in the literature, Caputo's approach has the feature that the initial conditions for fractional differential equations take on the same form as for integer-order differential equations. Due to this feature, the Caputo fractional derivative is perfect for use in real applications. The reader can refer to [11] for more details.

Definition 2.1 The α-th order Caputo fractional derivative of function $f(t)$ with respect to t and the terminal 0 is given by

$$ {}_0D_t^{\alpha} f = \frac{d^{\alpha} f(t)}{dt^{\alpha}} = \frac{1}{\Gamma(m-\alpha)} \int_0^t \frac{f^{(m)}(\tau)}{(t-\tau)^{\alpha+1-m}} d\tau, $$

where m is an integer such that $m-1 \leq \alpha < m$, and Γ is a well-known Gamma function.

2.2 Stability of the fractional-order nonlinear dynamical system

We define the Caputo fractional-order nonlinear dynamical system as follows:

$$ {}^{C}D^{\alpha} x_i = f_i(x_1, x_2, ..., x_n), \left(i = \overline{1,n}, 0 < \alpha < 1\right). \tag{1} $$

We obtain the equilibrium points of the system (1) via solving the system $f_i(x_1, x_2, ..., x_n) = 0, \left(i = \overline{1,n}, 0 < \alpha < 1\right)$.

To study the stability of the system (1), the following theorem is crucial.

Theorem 2.1 *[5] System* (1) *is asymptotically stable if all the eigenvalues* $\lambda_i, i = \overline{1,n}$, *of the Jacobian matrix* J *calculated at the equilibrium point of the system* (1) *satisfy the condition*

$$ |\arg(\lambda_i)| > \alpha.\frac{\pi}{2}, \left(i = \overline{1,n}, 0 < \alpha < 1\right), $$

where the Jacobian matrix is defined as

$$ J = \frac{\partial f}{\partial x}, \ f = (f_1, f_2, ..., f_n)^T, \ x = (x_1, x_2, ..., x_n)^T. $$

Theorem 2.2 *[5] Let* $x(t) \in R^n$ *be a vector of continuous and differentiable function, then the inequality*

$\frac{1}{2}{}_a^{C}D_t^{q} x^T(t) x(t) \leq x^T(t) D_t^{q} x(t)$ *holds.*

Theorem 2.3 *[5] The equilibrium point of system* (1) *is stable if for each* x, $x(t)^T f(x(t)) \leq 0$, *and it is asymptotically stable if* $\forall x \neq 0$, $x(t)^T f(x(t)) < 0$.

3 New Fractional-Order Hyperchaotic Rabinovich Systems

He and Chen [4] proposed a 4D fractional-order hyperchaotic Rabinovich system as follows:

$$\begin{cases} D^{\alpha_1}x = hy - ax + yz, \\ D^{\alpha_2}y = hx - by - xz + w, \\ D^{\alpha_3}z = -dz + xy, \\ D^{\alpha_4}w = -ky, \end{cases} \tag{2}$$

where D^{α_i} denotes the derivatives of order α_i, $(0 < \alpha_i < 1, i = \overline{1,n})$ in the sense of Caputo, with fixed system parameter $(a, b, d, h, k) = (4, 1, 1, 6.75, 2)$.

The stability and hyperchaos of the system (2) with the fixed system parameter were analyzed by He and Chen in [4]. They showed that the origin is the only equilibrium point and it is unstable. Also, they demonstrated that there is a hyperchaotic behavior for the system (2) with varying fractional order α.

The authors propose new 4D fractional-order hyperchaotic Rabinovich systems according to different system parameters and different initial conditions.

Twenty 4D fractional-order hyperchaotic Rabinovich systems are introduced and listed in Table 1 as $FE_1 - FE_{20}$.

4 Stability and Hyperchaotic Behaviors of Proposed Systems

This section studies the dynamical behaviors of the new hyperchaotic proposed systems $FE_1 - FE_{20}$, including equilibria, stability, and hyperchaos.

4.1 Equlibria

In order to obtain the equlibrium points of systems $FE_1 - FE_{20}$, we must have

$$\begin{cases} hy - ax + yz = 0, \\ hx - by - xz + w = 0, \\ -dz + xy = 0, \\ -ky = 0. \end{cases}$$

By calculation, we get that $\left(\overset{*}{x}, \overset{*}{y}, \overset{*}{z}, \overset{*}{w}\right) = (0, 0, 0, 0)$ is the only equilibrium point for all systems $FE_1 - FE_{20}$.

4.2 Stability

The Jacobian matrix of the system (2) is given by

$$J = \begin{bmatrix} -a & h+z & y & 0 \\ h-z & -b & -x & 1 \\ y & x & -d & 0 \\ 0 & -k & 0 & 0 \end{bmatrix}.$$

The characteristic equation $|J - \lambda I| = 0$ at the equilibrium point $(0, 0, 0, 0)$ is

$$(\lambda + d)\left[\lambda^3 + (a+b)\lambda^2 + \left(ab + k - h^2\right)\lambda + ak\right] = 0.$$

For all systems $FE_1 - FE_{20}$ (see Table 1), we have

$$\min_{1\leq i\leq 4} |\arg(\lambda_i)| = |\arg(\lambda_1)| = |\arg(\lambda_2)| = 0 < \alpha.\frac{\pi}{2} \qquad (0 < \alpha < 1).$$

According to Theorem 2.1, the equilibrium points $(0, 0, 0, 0)$ are unstable for all systems $FE_1 - FE_{20}$.

4.3 Hyperchaos of the new proposed systems

We have used an exhaustive computer search by Matlab tools, considering combinations of the system parameters, fractional orders, and initial conditions to find the cases in which the Rabinovich system (2) shows hyperchaotic dynamics. Twenty simple examples $FE_1 - FE_{20}$ are found in this way.

All the cases have the origin as the only equilibrium point. For each case that is found, there are two positive Lyapunov exponents (≥ 0.001), which implies that this cases are hyperchaotic systems.

The Kaplan-Yorke dimension [6] is an estimate of the fractal dimension based on the spectrum of Lyapunov exponents of a chaotic system. Arrange the Lyapunov exponents in order from largest to smallest $LE_1 \geq LE_2 \geq ... \geq LE_n$, let j be the largest index for which $\sum_{i=1}^{j} LE_i \geq 0$ and $\sum_{i=1}^{j+1} LE_i < 0$, then the Kaplan-Yorke (Lyapunov) dimension is defined as

$$D_{KY} = j + \frac{1}{|LE_{j+1}|}\sum_{i=1}^{j} LE_i.$$

The Lyapunov spectra (which are calculated by Wolf's method [13]) and Kaplan-York dimensions are listed in Table 1 along with system parameters, fractional orders, and initial conditions.

The attractor dimensions of all cases $FE_1 - FE_{20}$ are just over 3.0, and the largest of them is FE_{16} with $D_{KY} = 3.0847$. In addition, Lyapunov exponents according to the time of some proposed systems are shown in Fig.1.

The projections of the strange attractors in the $xyz-$space for the cases $FE_1 - FE_{20}$ are shown in Fig.2.

Case	Paremeters	Eigenvalues	(x_0, y_0, z_0, w_0)	Fractional order	LEs	D_{KY}
FE_1	$a = 4, b = 1, d = 1,$ $h = 6.75, k = 2$	$\lambda_1 = 4.1236$ $\lambda_2 = 0.2079$ $\lambda_3 = -9.3315$ $\lambda_4 = -1$	$(0.1, 0, 1, 0.1)$	0.9	0.4843 0.01015 -0.000 -9.7903	3.0505
FE_2				0.85	0.5784 0.1133 0.0009 -12.0538	3.0574
FE_3				0.7	0.7732 0.0849 -0.0019 -21.8128	3.0392
FE_4	$a = 4, b = 1, d = 1,$ $h = 6, k = 3$	$\lambda_1 = 3.1019$ $\lambda_2 = 0.4522$ $\lambda_3 = -8.5541$ $\lambda_4 = -1$	$(1, 0, 1, 1)$	0.99	0.2352 0.0237 -0.0014 -6.5205	3.0395
FE_5				0.95	0.3149 0.0125 0.000 -7.7631	3.0422
FE_6				0.9	0.3566 0.0033 -0.0061 -9.5511	3.0370
FE_7	$a = 2, b = 1, d = 1,$ $h = 5, k = 2$	$\lambda_1 = 3.2577$ $\lambda_2 = 0.0966$ $\lambda_3 = -6.3543$ $\lambda_4 = -1$	$(-0.5, 0.5, 1, 0)$	0.97	0.2331 0.0025 -0.0588 -4.7335	3.0373

Table1. New 4D fractional−order hyperchaotic Rabinovich systems.

Case	Paremeters	Eigenvalues	(x_0, y_0, z_0, w_0)	Fractional order	LEs	D_{KY}
FE_8	$a = 4, b = 1, d = 1,$ $h = 5, k = 1$	$\lambda_1 = 2.4624$ $\lambda_2 = 0.2117$ $\lambda_3 = -7.6741$ $\lambda_4 = -1$	$(0.1, 0, 0.1, 1)$	0.99	0.1511 0.0594 0.0021 −6.4748	3.0328
FE_9				0.95	0.1827 0.0524 0.0025 −7.6661	3.0310
FE_{10}				0.9	0.2173 0.0683 0.0014 −9.4593	3.0303
FE_{11}				0.75	0.3198 0.0546 0.0006 −17.2426	3.0217
FE_{12}	$a = 4, b = 1, d = 2,$ $h = 7, k = 2$	$\lambda_1 = 4.3867$ $\lambda_2 = 0.1904$ $\lambda_3 = -9.5771$ $\lambda_4 = -2$	$(0.1, 0.1, 1, 0.1)$	0.99	0.3367 0.0269 −0.0006 −7.6700	3.0473
FE_{13}				0.97	0.3784 0.0285 −0.0000 −8.3725	3.0486
FE_{14}				0.95	0.4129 0.0285 −0.000 −9.1221	3.0484
FE_{15}				0.85	0.6263 0.0054 −0.0003 −13.8996	3.0454

Table 1. (**Continued**.)

Case	Paremeters	Eigenvalues	(x_0, y_0, z_0, w_0)	Fractional order	LEs	D_{KY}
FE_{16}	$a = 4, b = 1, d = 1,$ $h = 8, k = 1$	$\lambda_1 = 5.5329$ $\lambda_2 = 0.0682$ $\lambda_3 = -10.6011$ $\lambda_4 = -1$	$(0.1, 0, 1, 0.5)$	0.99	0.5358 0.0423 0.0013 −6.8434	3.0847
FE_{17}				0.95	0.6251 0.0530 −0.0016 −8.1228	3.0833
FE_{18}				9	0.7695 0.0639 −0.0012 −10.0625	3.0827
FE_{19}				0.8	1.1437 0.0692 −0.0001 15.3143	3.0792
FE_{20}				0.7	0.6733 0.0109 −0.0490 −22.38	3.0284

Table 1. (**Continued**.)

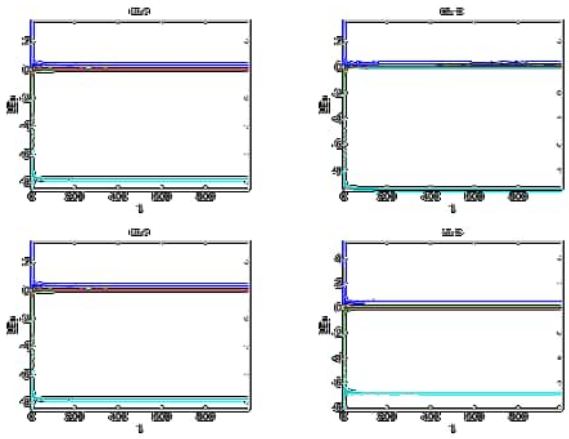

Figure 1: Lyapunov exponents with respect to time for some proposed 4D fractional-order hyperchaotic systems.

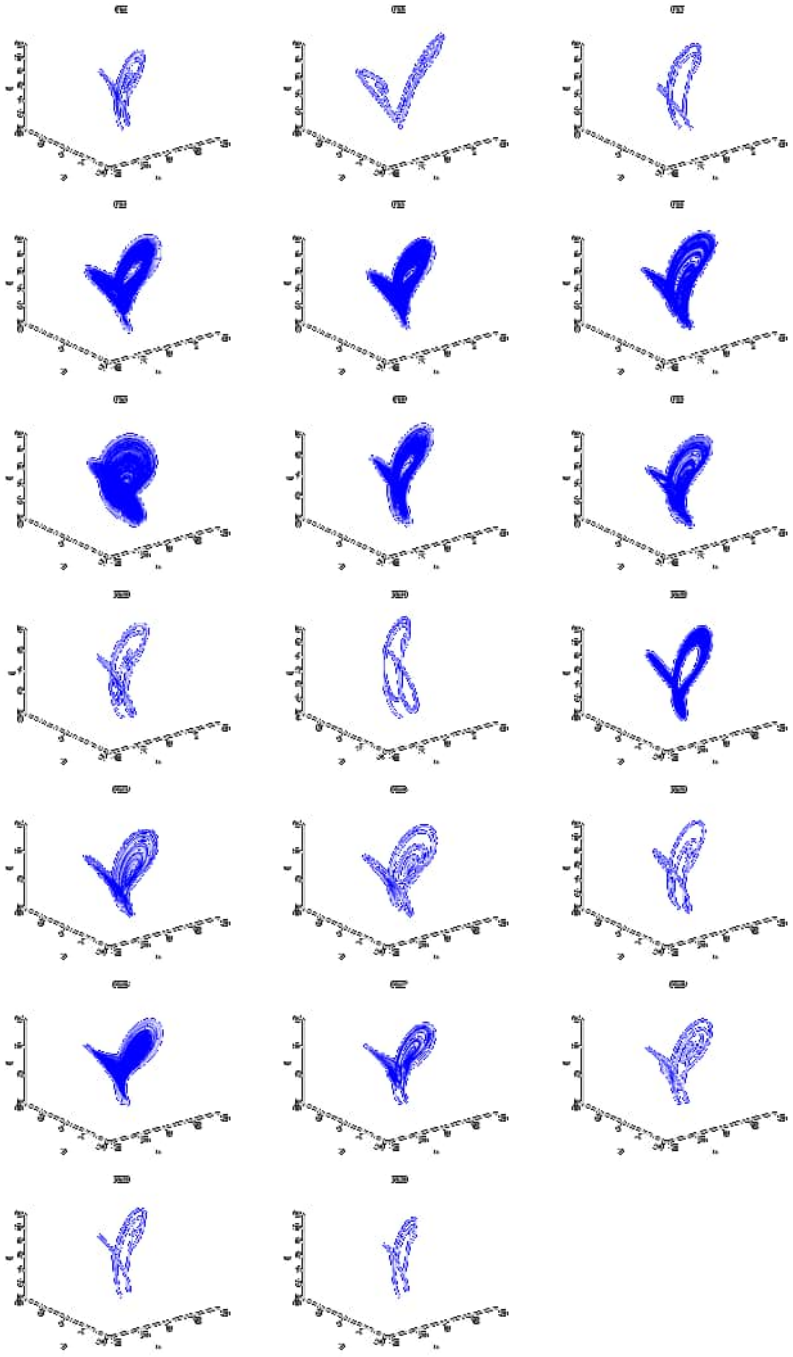

Figure 2: Attractors for the proposed 4D fractional order Rabinovich systems in the xyz-plane with initial conditions given in Table 1.

5 Chaotic Control of the Fractional-Order Rabinovich System FE_1

5.1 Linear feedback control

In this section, we study the chaotic control of system FE_1 by using the linear feedback control.

The linear controlled fractional-order Rabinovich system is as follows:

$$\begin{aligned} {}_a^c D_t^\beta x &= hy - ax + yz - k_1(x - x^*), \\ {}_a^c D_t^\beta y &= hx - by - xz + w - k_2(y - y^*), \\ {}_a^c D_t^\beta z &= -dz + xy - k_3(z - z^*), \\ {}_a^c D_t^\beta w &= -ky - k_4(w - w^*), \end{aligned} \tag{3}$$

with the fractional order $\beta = 0.9$, and the parameters $a = 4$, $b = 1$, $h = 6.75$, $d = 1$, $k = 2$. $(x^*, y^*, z^*, w^*) = (0; 0; 0; 0)$ is the equilibrium point of system FE_1 and k_1, k_2, k_3, k_4 are four linear control parameters.

The Jacobian matrix J of system (3) at the equilibrium point (x^*, y^*, z^*, w^*) is

$$J(x^*, y^*, z^*, w^*) = \begin{bmatrix} -a - k_1 & h + z^* & y^* & 0 \\ h - z^* & -b - k_2 & -x^* & 1 \\ y^* & x^* & -d - k_3 & 0 \\ 0 & -k & 0 & -k_4 \end{bmatrix}$$

and the corresponding characteristic equation for the parameters $a = 4$, $b = 1$, $h = 6.75$, $d = 1$, $k = 2$ is

$$f(\lambda) = \begin{vmatrix} \lambda + 4 + k_1 & -6.75 & 0 & 0 \\ -6.75 & \lambda + 1 + k_2 & 0 & -1 \\ 0 & 0 & \lambda + d + k_3 & 0 \\ 0 & 2 & 0 & \lambda + k_4 \end{vmatrix} = 0. \tag{4}$$

We selected the control parameters k_1, k_2, k_3 and k_4 in such a way that all eigenvalus λ of equation (4) should satisfy the condition $|\arg(\lambda_i)| > \pi > \beta.\pi/2$ to stabilize system (2).

5.1.1 Stabilization of the equilibrium point E

Lemma 5.1 *System* (3) *is locally asymptotically stable at the equilibrium point* $(0; 0; 0; 0)$ *with the control parameters* $k_1 = 2$; $k_2 = 10$; $k_3 = 1$; $k_4 = 10$.

Proof. Substitute the value of k_1; k_2; k_3 and k_4 into the characteristic equation (5), we can get

$$\begin{aligned} f(t) &= \begin{vmatrix} \lambda + 6 & -6.75 & 0 & 0 \\ -6.75 & \lambda + 11 & 0 & -1 \\ 0 & 0 & \lambda + 2 & 0 \\ 0 & 2 & 0 & \lambda + 10 \end{vmatrix} \\ &= \lambda^4 + 29\lambda^3 + 246.4375\lambda^2 + 601.25\lambda + 432.75 = 0, \end{aligned} \tag{5}$$

and the characteristic roots of equation (5) are $\lambda_1 \simeq -15.4531$, $\lambda_2 \simeq -10.1701$, $\lambda_3 \simeq -2$, $\lambda_4 \simeq -1.3767$.

By Theorem 2.1, $|\arg(\lambda_i)| = \pi > (0.9).\pi/2$, $i = 1, 2, 3, 4$, so the controlled fractional-order Rabinovich system (3) is locally asymptotically stable at $(0; 0; 0; 0)$.

As depicted in Fig.3(a), the controllers are activated at $t = 20s$. The fractional order Rabinovich system FE_1 is hyperchaotic when $t < 20s$, and after activating the controllers ($t \geq 20$), the state $x(t)$, $y(t)$, $z(t)$, and $w(t)$ approaches the equilibium point gradually; when $t = 25$, the system is controled entirely to the equilibrium point $(x^*, y^*, z^*, w^*) = (0; 0; 0; 0)$.

If the controllers are activated at $t = 30$, Fig.3(b) shows that the fractional-order Rabinovich system FE_1 is hyperchaotic when $t < 30s$, and it is controlled entirely to the equilibrium point when $t = 35$.

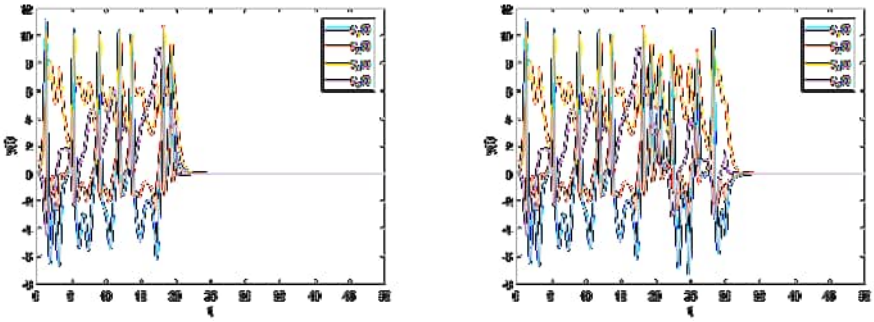

Figure 3: Stabilization of the fractional-order hyperchaotic Rabinovich system FE_1 for $k_1 = 2$, $k_2 = 10$, $k_3 = 1$ and $k_4 = 10$.

5.2 Nonlinear feedback control

By using the nonlinear feedback control method, we will enable the system (2) to achieve the global asymptotical stability.

The nonlinear controlled fractional-order Rabinovich system is

$$\begin{aligned} {}_a^c D_t^\alpha x &= hy - ax + yz - U_1, \\ {}_a^c D_t^\alpha y &= hx - by - xz + w + U_2, \\ {}_a^c D_t^\alpha z &= -dz + xy + U_3, \\ {}_a^c D_t^\alpha w &= -ky + U_4, \end{aligned} \tag{6}$$

where $U_1;\ U_2;\ U_3;\ U_4$ are the nonlinear controllers to be designed later.

Lemma 5.2 *System* (2) *can achieve the global asymptotical stability under the controllers*

$$U_1 = -k_1 x;\ U_2 = -k_2 y;\ U_3 = -k_3 - z - xy;\ U_4 = -k_4 w - y \tag{7}$$

if and only if the conditions $k_1 > h^2 - a;\ k_2 > \frac{3}{2} - b;\ k_3 > -d;\ k_4 > \frac{k^2}{2}$ *hold, where* $k_1;\ k_2;\ k_3;\ k_4$ *are control parameters.*

Proof. Choosing a positive definite Lyapunov function

$$V = \frac{1}{2}\left(x^2 + y^2 + z^2 + w^2\right) \tag{8}$$

and applying Theorem 2.2 and the controllers (7), the fractional derivative of the Lyapunov function (8) of the nonlinear controlled system (6) is obtained as

$$\begin{aligned}
{}_a^c D_t^q V \leq & {}_a^c D_t^{\alpha 1} x + {}_a^c D_t^{\alpha 2} y + {}_a^c D_t^{\alpha 3} z + {}_a^c D_t^{\alpha 4} w \\
& = x\left(hy - ax + yz - U_1\right) + y\left(hx - by - xz + w + U_2\right) \\
& + z\left(-dz + xy + U_3\right) + w\left(-ky + U_4\right) \\
& = x\left(hy - ax + yz - k_1 x_1\right) + y\left(hx - by - xz + w - k_2 y\right) \\
& + z\left(-dz + xy - k_3 z - xy\right) + w\left(-ky - k_4 w - y\right) \\
& = -\left(hx - y\right)^2 - \left(a - h^2 + k_1\right) x^2 - \left(b - \frac{3}{2} + k_2\right) y^2 \\
& - \left(d + k_3\right) z^2 - \frac{1}{2}\left(y + kw\right)^2 - \frac{1}{2}\left(-k^2 + 2k_4\right) w^2,
\end{aligned}$$

where $k_1 > h^2 - a$; $k_2 > \frac{3}{2} - b$; $k_3 > -d$; $k_4 > \frac{k^2}{2}$ hold, the fractional derivative of the Lyapunov function is negative definite (${}_a^c D_t^q V < 0$), according to Theorem 2.3, so the controlled system (6) is globaly asymptotically stable.

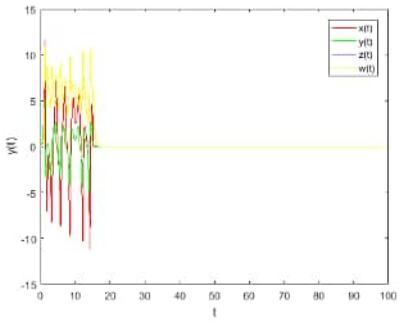

Figure 4: Stabilization of the fractional-order hyperchaotic Rabinovich system FE_1 for $k_1 = 45$, $k_2 = 1$, $k_3 = 0$ and $k_4 = 10$.

Fig.4 shows that with the parameters $a = 4$, $b = 1$, $h = 6.75$, $d = 1$, $k = 2$, $q = 0.9$ and the control parameters $k_1 = 45$, $k_2 = 1$, $k_3 = 0$, $k_4 = 10$, the Rabinovich system FE_1 is hyperchaotic if $t < 20$. After activating the controlers at $t = 20$, the system achieve global stability gradually.

6 Conclusion

The paper proposed 20 new four-dimensional fractional-order hyperchaotic Rabinovich systems with Caputo derivatives. Each system possessed a single equilibrium point located at the origin, and the stability at this point was analyzed. Based on the computation of Lyapunov exponents, it was demonstrated that the proposed systems exhibited hyperchaotic behavior under certain combinations of system parameters, initial conditions, and fractional-order derivatives. The attractors, their dimensions, and the Lyapunov exponents of selected systems were presented. Furthermore, the local and global asymptotic stabilization problems for the first of the proposed hyperchaotic systems were addressed through the design of linear and nonlinear feedback controllers, respectively.

This study contributes to the development of theoretical research in chaos and control theory by introducing novel fractional-order hyperchaotic Rabinovich systems and proposing an effective control strategy for system stabilization. Additionally, the results suggest potential practical applications in areas such as secure communication systems, modeling of memory-dependent materials (e.g., viscoelastic materials), and improved modeling of anomalous diffusion processes in plasma dynamics. Future research may further explore the dynamical properties and behaviors of these newly proposed hyperchaotic systems

References

[1] D. Baleanu, S. S. Sajjadi, J. H. Asad, A. Jajarmi and E. Estiri. Hyperchaotic behaviours, optimal control, and synchronization of a nonautonomous cardiac conduction system. *Advances in Difference Equation* **2021** (1) (2021) 1–24.

[2] C. T. Deressa. On the chaotic nature of the Rabinovich system through Caputo and Atangana–Baleanu–Caputo fractional derivatives. *Advances in Continuous and Discrete Models* **2022** (1) (2022), article number 66.

[3] Y. Ghettout, L. Meddour, T. Hamaizia, and R. Ouahabi. Dynamic Analysis of a New Hyperchaotic System with Infinite Equilibria and Its Synchronization. *Nonlinear Dynamics and Systems Theory* **24**(2) (2024) 147–158.

[4] J. He and F. Chen. A new fractional order hyperchaotic Rabinovich system and its dynamical behaviors. International Journal of Non-Linear Mechanics **95** (2017) 73-81.

[5] J. He and F. Chen. Dynamical analysis of a new fractional-order Rabinovich system and its fractional matrix projective synchronization. *Chinese Journal of Physics* **56** (5) (2018) 2627–2637.

[6] J. Kaplan and J. York. Functional differential equations and approximations of fixed points. Lecture Notes in Mathematics **730** (1979) 204–227.

[7] Y. J. Liu, Q. G. Yang and G. P. Pang. A hyperchaotic system from the Rabinovich system. Journal of Computational and Applied Mathematics **234** (1) (2010) 101–113.

[8] E. Mosekilde. Topics in Nonlinear Dynamics: Applications to Physics, Biology and Economic Systems. World Scientific, Singapore, (1996).

[9] S. Patnaik, J. P. Hollkamp and F. Semperlotti. Applications of variable-order fractional operators: a review. *Proceedings of the Royal Society A* **476** (2234) (2020) 20190498.

[10] A. S. Pikovski, M. I. Rabinovich, and V. Y. Trakhtengerts. On set of stochasticity in decay confinement of parametric instability. *Soviet Journal of Experimental and Theoretical Physics* **47** (4) (1978) 715–719.

[11] I. Podlubny. *Fractional Differential Equations*. Academic Press, San Diego, 1999.

[12] M. S. Tavazoei. Fractional order chaotic systems: history, achievements, applications, and future challenges. *The European Physical Journal Special Topics* **229** (2020) 887–904.

[13] A. Wolf, J. B. Swift, H. L. Swinney, and J. A. Vastano. Determining Lyapunov exponents from a time series. *Physica* **16** (3) (1985) 285–317.

[14] F. Yu, S. Xu, Y. Lin, T. He, C. Wu and H. Lin. Design and analysis of a novel fractional-order system with hidden dynamics, hyperchaotic behavior and multi-scroll attractors. *Mathematics* **12** (14) (2024) 1–22.

[15] G. Zhao, H. Zhao, Y. Zhang and X. An. A new memristive system with extreme multistability and hidden chaotic attractors and with application to image encryption. *International Journal of Bifurcation and Chaos* **34** (01) (2024) 2450010.

Nonlinear Dynamics and Systems Theory, **26** (2) (2026) 138–147

Numerical Resolution of Transport-Diffusion Systems via Taylor Collocation Method

A. Chettouh [1,2] and H. Laib [2,3*]

[1] *Laboratory of Applied Mathematics and Didactics, Higher Normal School El Katiba Assia Djebar, Constantine, Algeria.*
[2] *University of Abdelhafid Boussouf, Mila, Algeria.*
[3] *Higher Normal School Echeikh Mohamed Elbachir Elibrahimi, Algiers, Algeria.*

Received: February 3, 2025; Revised: April 9, 2026

Abstract: The primary objective of this paper is to develop a numerical approach for solving a system of transport-diffusion equations. The proposed method is based on Taylor polynomials, which are employed within a collocation method in the space $S_{p-1}^{(-1)}(\Pi_{N,M})$ to approximate the solution of the corresponding Volterra integro-differential equation. The convergence of the method is established, and numerical experiments are conducted to demonstrate its accuracy. This work contributes to the field of system dynamics by introducing a new computational approach to understanding and predicting the behavior of transport-diffusion systems. The Taylor collocation method enables precise numerical approximations of these equations, which is fundamental in modeling dynamic processes such as pollutant dispersion in a moving fluid and thermal diffusion in engineered systems.

Keywords: *system of transport-diffusion equations; Volterra integro-differential equation; collocation method; Taylor polynomials; error analysis.*

Mathematics Subject Classification (2020): 35K15, 35R09, 65M70, 93A99.

* Corresponding author: mailto:hafida.laib@gmail.com

1 Introduction

The transport-diffusion system is given by

$$\partial_t u(t,x) + v(t) \cdot \nabla u(t,x) - \kappa \Delta u(t,x) = g(t,x,u(t,x)) \tag{1}$$

for all $(t,x,u) \in \mathbb{R}^+ \times \mathbb{R}^n \times \mathbb{R}^d$. This system is classified as a parabolic partial differential equation (for a mathematical analysis, see [8], which provided essential theoretical foundations for the existence and uniqueness of the solution to this system). It is used to model the process of transport and diffusion of a substance contained in a fluid, or a property within a moving fluid.

Here, u represents the amount of the substance or the intensity of the property being transported and diffused, v is the velocity vector of transport, κ is the diffusion coefficient (a positive constant), and g is the source or reaction term. This equation has applications in various fields, including the analysis of dynamical systems and atmospheric problems such as air pollution. It can also model water pollution problems in seas and other aquatic systems.

In the study of this equation, two main cases arise depending on the value of g. The first case is when $g = 0$. Many researchers have studied this case numerically in the domain $0 < x < L$ under initial and boundary conditions, using different numerical methods such as the compact finite differences method of sixth order [7] and B-spline exponential collocation method [10]. The second case is when $g \neq 0$. Many researchers have investigated this scenario. In [1], Alhumaizi analyzed a convection-diffusion system with reaction using various standard reduction techniques. In [9], Liu presented a numerical analysis of a diffusion-migration (transport) model with a reaction describing the interaction between prey and predator in one-dimensional space under periodic boundary conditions.

The main goal of this paper is to resolve the system of transport-diffusion equations in a one-dimensional domain under initial conditions using an algorithm based on the Taylor collocation method. This method is known for its powerful performance in solving differential, integral, and integro-differential equations numerically (see, for example, [2,3,5]). Recently, a Taylor-based numerical framework was proposed for delay Volterra integral equations with mixed kernels and spatial variables, demonstrating high accuracy and reliable convergence properties [11]. Motivated by these results, the present work extends the Taylor collocation strategy to the case of proportional-delay Volterra equations.

The paper is organized as follows. In Section 2, we will pose the problem and convert it to a Volterra integro-differential equation of the second kind. In Section 3, we will approximate the solution of the Volterra integro-differential equation. We will also explore the convergence analysis and its order for the Volterra integro-differential equation. Section 4 will present a numerical example to illustrate the theoretical results. Finally, we will conclude with a summary of our research and prospects for further study.

2 Statement of the Problem

Consider the following system of transport-diffusion equations:

$$\frac{\partial u(t,x)}{\partial t} + v(t)\frac{\partial u(t,x)}{\partial x} - \kappa \frac{\partial^2 u(t,x)}{\partial x^2} = g(t,x,u(t,x)), \quad (t,x) \in D,$$

where $D = [0,T] \times [0,X] \subset \mathbb{R}^+ \times \mathbb{R}$ and $u = (u_1, u_2, \ldots, u_d)^T \in \mathbb{R}^d$ (here, κ is a strictly positive constant), subject to the initial conditions

$$u(0,x) = u_0(x),\ u(t,0) = h(t),\ u_0(0) = h(0),\ \frac{\partial u(t,0)}{\partial x} = l(t).$$

Here, $h, l, g \in \mathbb{R}^d$ and $v = \mathrm{diag}(v_1, v_2, \ldots, v_d)$ is a diagonal matrix.

We assume that $g(t,x,u(t,x))$ is affine in the third variable, i.e.,

$$g(t,x,u(t,x)) = a(t,x) \cdot u(t,x) + b(t,x),$$

such that a (reaction term) is a $d \times d$ matrix and $b = (b_1, b_2, \ldots, b_d)^T$ represents the vector source term.

Integrating twice both sides of (1) from 0 to x with respect to the second variable yields a system of two-dimensional Volterra integro-differential equation of the form

$$\begin{aligned} u(t,x) = &\int_0^x \left[\frac{s-x}{\kappa}(a(t,s)\cdot u(t,s) + b(t,s))\right] ds + \left(I_d - \frac{x}{\kappa}v(t)\right) h(t) + xl(t) \\ &+ \frac{1}{\kappa}\int_0^x \left[(x-s)\frac{\partial u(t,s)}{\partial t} + v(t)u(t,s)\right] ds, \end{aligned}$$

then

$$u(t,x) = f(t,x) + \frac{1}{\kappa}\int_0^x \left[(x-s)\left(\frac{\partial u(t,s)}{\partial t} - a(t,s)\cdot u(t,s)\right) + v(t)u(t,s)\right] ds, \qquad (2)$$

where

$$f(t,x) = \int_0^x \frac{s-x}{\kappa} b(t,s)\, ds + \left(I_d - \frac{x}{\kappa}v(t)\right) h(t) + xl(t).$$

The functions f, a, and v are smooth, with f and a defined on $D = [0,T]\times[0,X] \subset \mathbb{R}^2$, and v defined on $[0,T] \subset \mathbb{R}$.

3 Description of the Method

Let $\Pi_N = \{t_i \mid t_i = ih,\ i = 0,1,\ldots,N\}$ and $\Pi_M = \{x_j \mid x_j = jk,\ j = 0,1,\ldots,M\}$ denote the uniform partitions of the intervals $[0,T]$ and $[0,X]$, respectively, with step sizes given by $h = \frac{T}{N}$ and $k = \frac{X}{M}$. These partitions define a grid for D:

$$\Pi_{N,M} = \Pi_N \times \Pi_M = \{(t_n, x_m),\ 0 \le n \le N,\ 0 \le m \le M\}.$$

We define the subintervals as follows:

$$\sigma_n = [t_n, t_{n+1}), \quad n = 0,1,\ldots,N-2; \quad \sigma_{N-1} = [t_{N-1}, t_N],$$

$$\delta_m = [x_m, x_{m+1}), \quad m = 0,1,\ldots,M-2; \quad \delta_{M-1} = [x_{M-1}, x_M],$$

and we define $D_{n,m} := \sigma_n \times \delta_m$ for all $n = 0,1,\ldots,N-1$; $m = 0,1,\ldots,M-1$. Moreover, let π_{p-1} represent the set of all real polynomials in $\mathbb{R}$ of degree not exceeding $p-1$ in t and x. We define the real polynomial spline space of degree $p-1$ as follows:

$$S_{p-1}^{(-1)}(\Pi_{N,M}) = \{\bar{u} : \bar{u}_{n,m} = \bar{u}|_{D_{n,m}} \in \pi_{p-1}^d,\ n = 0,\ldots,N-1;\ m = 0,\ldots,M-1\}.$$

Its dimension is $dNMp^2$, which corresponds to the total number of coefficients of the polynomials $\bar{u}_{n,m}$ for $n = 0, \ldots, N-1$; $m = 0, \ldots, M-1$. To determine these coefficients, we apply the Taylor polynomial on each rectangle.

First, we approximate u in the rectangles $D_{0,0}$ by the polynomials

$$\bar{u}_{0,0}(t,x) = \sum_{i+j=0}^{p-1} \frac{1}{i!j!} \frac{\partial^{i+j} u(0,0)}{\partial t^i \partial x^j} t^i x^j \ ; \quad (t,x) \in D_{0,0}, \tag{3}$$

where $\dfrac{\partial^{i+j} u(0,0)}{\partial t^i \partial x^j}$ is the exact value of $\dfrac{\partial^{i+j} u}{\partial t^i \partial x^j}$ at the point $(0,0)$.
To obtain $\dfrac{\partial^{i+j} u}{\partial t^i \partial x^j}$, we differentiate equation (2) j times with respect to x and i times with respect to t, considering three distinct cases.

- If $j = 0$, then we have

$$\begin{aligned} \frac{\partial^i u(t,x)}{\partial t^i} &= \frac{\partial^i f(t,x)}{\partial t^i} + \frac{1}{\kappa} \int_0^x \frac{\partial^i (v(t) \cdot u(t,s))}{\partial t^i} ds \\ &\quad + \frac{1}{\kappa} \int_0^x (x-s) \left(\frac{\partial^{i+1} u(t,s)}{\partial t^{i+1}} - \frac{\partial^i (a(t,s) \cdot u(t,s))}{\partial t^i} \right) ds. \end{aligned}$$

- If $j = 1$, then we obtain

$$\begin{aligned} \frac{\partial^{i+1} u(t,x)}{\partial t^i \partial x} &= \frac{\partial^{i+1} f(t,x)}{\partial t^i \partial x} + \frac{1}{\kappa} \frac{\partial^i (v(t) u(t,x))}{\partial t^i} \\ &\quad + \frac{1}{\kappa} \int_0^x \left[\frac{\partial^{i+1} u(t,s)}{\partial t^{i+1}} - \frac{\partial^i (a(t,s) \cdot u(t,s))}{\partial t^i} \right] ds. \end{aligned}$$

- If $j \geq 2$, then we find

$$\begin{aligned} \frac{\partial^{i+j} u(t,x)}{\partial t^i \partial x^j} &= \frac{\partial^{i+j} f(t,x)}{\partial t^i \partial x^j} + \frac{1}{\kappa} \frac{\partial^i \left(v(t) \frac{\partial^{j-1} u(t,x)}{\partial x^{j-1}} \right)}{\partial t^i} \\ &\quad + \frac{1}{\kappa} \frac{\partial^{i+j-1} u(t,x)}{\partial t^{i+1} \partial x^{j-2}} - \frac{1}{\kappa} \frac{\partial^{i+j-2} (a(t,x) \cdot u(t,x))}{\partial t^i \partial x^{j-2}}. \end{aligned}$$

Second, we approximate u in the rectangles $D_{n,m}, n = 0, ..., N-1, \ m = 0, ..., M-1$ and $(n,m) \neq (0,0)$, by the polynomials

$$\bar{u}_{n,m}(t,x) = \sum_{i+j=0}^{p-1} \frac{1}{i!j!} \frac{\partial^{i+j} \hat{u}_{n,m}(t_n, x_m)}{\partial t^i \partial x^j} (t-t_n)^i (x-x_m)^j \ ; \quad (t,x) \in D_{n,m}, \tag{4}$$

where $\hat{u}_{n,m}$ is the exact solution of the integral equation

$$\begin{aligned} \hat{u}_{n,m}(t,x) = f(t,x) &+ \frac{1}{\kappa} \sum_{\rho=0}^{m-1} \int_{x_\rho}^{x_{\rho+1}} (x-s) \left(\frac{\partial \bar{u}_{n,\rho}(t,s)}{\partial t} - a(t,s) \cdot \bar{u}_{n,\rho}(t,s) \right) ds \\ &+ \frac{1}{\kappa} \left(\sum_{\rho=0}^{m-1} \int_{x_\rho}^{x_{\rho+1}} v(t) \bar{u}_{n,\rho}(t,s) ds + \int_{x_m}^{x} v(t) \hat{u}_{n,m}(t,s) ds \right) \\ &+ \frac{1}{\kappa} \int_{x_m}^{x} (x-s) \left(\frac{\partial \hat{u}_{n,m}(t,s)}{\partial t} - a(t,s) \cdot \hat{u}_{n,m}(t,s) \right) ds. \end{aligned} \tag{5}$$

To find $\frac{\partial^{i+j}u}{\partial t^i \partial x^j}$, we differentiate equation (5) j times with respect to x and i times with respect to t, considering three different cases.

- If $j = 0$, then we get

$$\begin{aligned}\frac{\partial^i \hat{u}_{n,m}(t,x)}{\partial t^i} &= \frac{\partial^i f(t,x)}{\partial t^i} + \int_{x_m}^{x} \frac{x-s}{\kappa}\left(\frac{\partial^{i+1}\hat{u}_{n,m}(t,s)}{\partial t^{i+1}} - \frac{\partial^i(a(t,s)\cdot \hat{u}_{n,m}(t,s))}{\partial t^i}\right) ds \\ &+ \frac{1}{\kappa}\sum_{\rho=0}^{m-1}\int_{x_\rho}^{x_{\rho+1}} (x-s)\left(\frac{\partial^{i+1}\bar{u}_{n,\rho}(t,s)}{\partial t^{i+1}} - \frac{\partial^i(a(t,s)\cdot \bar{u}_{n,\rho}(t,s))}{\partial t^i}\right) ds \\ &+ \frac{1}{\kappa}\left(\sum_{\rho=0}^{m-1}\int_{x_\rho}^{x_{\rho+1}} \frac{\partial^i\left(v(t)\bar{u}_{n,\rho}(t,s)\right)}{\partial t^i} ds + \int_{x_m}^{x} \frac{\partial^i\left(v(t)\hat{u}_{n,m}(t,s)\right)}{\partial t^i} ds\right).\end{aligned}$$

- If $j = 1$, then we get

$$\begin{aligned}\frac{\partial^{i+1}\hat{u}_{n,m}(t,x)}{\partial t^i \partial x} &= \frac{\partial^{i+1} f(t,x)}{\partial t^i \partial x} + \frac{1}{\kappa}\frac{\partial^i\left(v(t)\hat{u}_{n,m}(t,x)\right)}{\partial t^i} \\ &+ \frac{1}{\kappa}\sum_{\rho=0}^{m-1}\int_{x_\rho}^{x_{\rho+1}}\left(\frac{\partial^{i+1}\bar{u}_{n,\rho}(t,s)}{\partial t^{i+1}} - \frac{\partial^i(a(t,s)\cdot \bar{u}_{n,\rho}(t,s))}{\partial t^i}\right) ds \\ &+ \frac{1}{\kappa}\int_{x_m}^{x}\left(\frac{\partial^{i+1}\hat{u}_{n,m}(t,s)}{\partial t^{i+1}} - \frac{\partial^i(a(t,s)\cdot \hat{u}_{n,m}(t,s))}{\partial t^i}\right) ds.\end{aligned}$$

- If $j \geq 2$, then we get

$$\begin{aligned}\frac{\partial^{i+j}\hat{u}_{n,m}(t,x)}{\partial t^i \partial x^j} &= \frac{\partial^{i+j} f(t,x)}{\partial t^i \partial x^j} + \frac{1}{\kappa}\frac{\partial^i\left(v(t)\frac{\partial^{j-1}\hat{u}_{n,m}(t,x)}{\partial x^{j-1}}\right)}{\partial t^i} \\ &+ \frac{1}{\kappa}\frac{\partial^{i+j-1}\hat{u}_{n,m}(t,x)}{\partial t^{i+1}\partial x^{j-2}} - \frac{1}{\kappa}\frac{\partial^{i+j-2}(a(t,x)\cdot \hat{u}_{n,m}(t,x))}{\partial t^i \partial x^{j-2}}.\end{aligned}$$

4 Study of the Convergence and the Error of the Numerical Method

This section will focus on studying the convergence of the method above and evaluating its error. The following lemmas will be important in this analysis.

Lemma 4.1 (*Taylor's theorem for functions of two independent variables*) *Let f be p times continuously differentiable on $D = [0,a]\times[0,b]$ and let $(x_0,y_0)\in D$. Then for all $(x,y)\in D$, we have*

$$\begin{aligned}f(x,y) &= \sum_{i+j=0}^{p-1}\frac{1}{i!j!}\frac{\partial^{i+j}f(x_0,y_0)}{\partial x^i \partial y^j}(x-x_0)^i(y-y_0)^j \\ &+ \sum_{i+j=p}\frac{1}{i!j!}\frac{\partial^{i+j}f(x_1,y_1)}{\partial x^i \partial y^j}(x-x_0)^i(y-y_0)^j,\end{aligned}$$

where

$$\begin{cases} x_1 = \theta x + (1-\theta)x_0 \in [0,a], \\ y_1 = \theta y + (1-\theta)y_0 \in [0,b], \end{cases} \qquad \theta \in (0,1).$$

Lemma 4.2 (*Discrete Gronwall-type inequality [6]*) *Let* $\{k_j\}_{j=0}^{n}$ *be a given non-negative sequence and the sequence* $\{\varepsilon_n\}$ *satisfy* $\varepsilon_0 \leq p_0$ *and*

$$\varepsilon_n \leq p_0 + \sum_{i=0}^{n-1} k_i \varepsilon_i, \quad n \geq 1,$$

with $p_0 \geq 0$. *Then* ε_n *can be bounded by* $\varepsilon_n \leq p_0 \exp\left(\sum_{j=0}^{n-1} k_j\right), \quad n \geq 1.$

Lemma 4.3 *Let* f *and* v *be* p*-times continuously differentiable on their respective domains. Then, under the assumptions*

$$k < \min\left\{\frac{\kappa}{A}, \frac{-V + \sqrt{V^2 + 2\kappa(1+A)}}{2(1+A)}\right\},$$

where $V = \max\left\{\binom{i}{r}\left\|\frac{\partial^{i-r} v}{\partial t^{i-r}}\right\|, \quad i = 0, ..., p, \quad r = 0, ..., i\right\}$, $A = \max\left\{\binom{i}{r}\left\|\frac{\partial^{i-r} a}{\partial t^{i-r}}\right\|, \quad i = 0, ..., p, \quad r = 0, ..., i\right\}$, *there exists a positive number* $C(p)$ *such that for all* $n = 0, \ldots, N-1$, $m = 0, \ldots, M-1$ *and* $i + j = 0, 1, ..., p$, *we have*

$$\left\|\frac{\partial^{i+j} \hat{u}_{n,m}}{\partial t^i \partial x^j}\right\|_{L^\infty(D_{n,m})} \leq C(p),$$

where $\hat{u}_{0,0}(t,x) = u(t,x)$ *for* $(t,x) \in D_{0,0}$.

Proof. The proof follows from a more straightforward generalization of the techniques applied in Lemma 5 of [4]. □

The following theorem will give the convergence of the presented method.

Theorem 4.1 *Let* $f, a,$ *and* v *be* p *times continuously differentiable on their respective domains. Assume that* $\bar{u} \in S_{p-1}^{(-1)}(\Pi_{N,M})$ *in equations (3) and (4) defines a unique approximate solution. Then the error function* $e = u - \bar{u}$ *satisfies the condition*

$$\|e\|_{L^\infty(D)} \leq C(h+k)^{p-1},$$

C *is a finite constant independent of* h *and* k.

Proof. Define the error $e(t,x)$ on $D_{n,m}$ by $e_{n,m}(t,x) = u(t,x) - \bar{u}_{n,m}(t,x)$ for all $n \in \{0, \ldots, N-1\}$ and $m \in \{0, \ldots, M-1\}$.
Claim 1. There exists a constant β_1 independent of h and k such that $\|e_{0,0}\|_{L^\infty(D_{0,0})} \leq \beta_1(h+k)^p$.

Let $(t,x) \in D_{0,0}$, by using Lemma 4.1, we obtain from (3) that

$$|e_{0,0}(t,x)| \leq \sum_{i+j=p} \frac{1}{i!j!}\left\|\frac{\partial^{i+j} u}{\partial t^i \partial x^j}\right\| h^i k^j.$$

Hence, by Lemma 4.3, we have

$$|e_{0,0}(t,x)| \leq \underbrace{\frac{C(p)}{p!}}_{\beta_1}(h+k)^p.$$

Claim 2. There exists a constant β_2 independent of h and k such that $\|e_{n,m}\|_{L^\infty(D_{n,m})} \leq \beta_2(h+k)^{p-1}$ for all $n = 0, \ldots, N-1$ and $m = 1, \ldots, M-1$.

Let $(t,x) \in D_{n,m}$, we have from (5) that

$$|u(t,x) - \hat{u}_{n,m}(t,x)| \leq c_1 k \sum_{\rho=0}^{m-1} (\|\partial_t e_{n,\rho}\| + \|e_{n,\rho}\|) + c_2 \int_{x_m}^{x} \|\partial_t u(t,s) - \partial_t \hat{u}_{n,m}(t,s)\| ds + c_2 \int_{x_m}^{x} \|u(t,s) - \hat{u}_{n,m}(t,s)\| ds, \tag{6}$$

where c_1 and c_2 are positive numbers.

On the other hand, by differentiating (5) with respect to t, we have, for $x \neq x_m$,

$$\begin{aligned}\int_{x_m}^{x} (x-s)(\partial_t u(t,s) - \partial_t \hat{u}_{n,m}(t,s)) ds &= \kappa(u(t,x) - \hat{u}_{n,m}(t,x)) \\ &+ \int_{x_m}^{x} ((x-s)a(t,s) - v(t))(u(t,s) - \hat{u}_{n,m}(t,s)) ds \\ &- \sum_{\rho=0}^{m-1} \int_{x_\rho}^{x_{\rho+1}} (x-s)(\partial_t u(t,s) - \partial_t \bar{u}_{n,\rho}(t,s)) + v(t)(u(t,s) - \bar{u}_{n,\rho}(t,s)) ds.\end{aligned}$$

Hence

$$c_3 \|\partial_t u - \partial_t \hat{u}_{n,m}\| \leq \kappa \|u - \hat{u}_{n,m}\| + k c_4 \|u - \hat{u}_{n,m}\| + k c_5 \sum_{\rho=0}^{m-1} (\|\partial_t e_{n,\rho}\| + \|e_{n,\rho}\|),$$

then

$$\|\partial_t u - \partial_t \hat{u}_{n,m}\| \leq \frac{\kappa + k c_4}{c_3} \|u - \hat{u}_{n,m}\| + \frac{k c_5}{c_3} \sum_{\rho=0}^{m-1} (\|\partial_t e_{n,\rho}\| + \|e_{n,\rho}\|). \tag{7}$$

If $x = x_m$: by differentiating (5) with respect to t, we obtain

$$\|\partial_t u - \partial_t \hat{u}_{n,m}\| \leq \frac{k c_6}{\kappa} \sum_{\rho=0}^{m-1} (\|\partial_t e_{n,\rho}\| + \|e_{n,\rho}\|), \tag{8}$$

using (7) and (8), we get

$$\|\partial_t u - \partial_t \hat{u}_{n,m}\| \leq \Big(\frac{\kappa + k c_4}{c_3}\Big) \|u - \hat{u}_{n,m}\| + k c_7 \sum_{\rho=0}^{m-1} (\|\partial_t e_{n,\rho}\| + \|e_{n,\rho}\|), \tag{9}$$

where c_3, c_4, c_5 and c_6 are positive numbers and $c_7 = k(\frac{c_5}{c_3} + \frac{c_6}{\kappa})$.

Then, from (6) and (9), we have

$$\begin{aligned}\|u - \hat{u}_{n,m}\| + \|\partial_t u - \partial_t \hat{u}_{n,m}\| &\leq k(c_1 + c_7) \sum_{\rho=0}^{m-1} (\|\partial_t e_{n,\rho}\| + \|e_{n,\rho}\|) \\ &+ c_2 X \|\partial_t u - \partial_t \hat{u}_{n,m}\| + \Big(c_2 X + \frac{1}{c_3} + \frac{X c_4}{\kappa c_3}\Big) \|u - \hat{u}_{n,m}\|,\end{aligned}$$

denote by $c_8 = \max\{c_2X, c_2X + \frac{1}{c_3} + \frac{Xc_4}{\kappa c_3}\}$, then

$$\|u - \hat{u}_{n,m}\| + \|\partial_t u - \partial_t \hat{u}_{n,m}\| \leq k(c_1 + c_7) \sum_{\rho=0}^{m-1} (\|\partial_t e_{n,\rho}\| + \|e_{n,\rho}\|) + c_8(\|u - \hat{u}_{n,m}\| + \|\partial_t u - \partial_t \hat{u}_{n,m}\|).$$

Hence

$$\|u - \hat{u}_{n,m}\| + \|\partial_t u - \partial_t \hat{u}_{n,m}\| \leq \underbrace{\frac{c_1 + c_7}{1 - c_8}}_{c_9} k \sum_{\rho=0}^{m-1} (\|\partial_t e_{n,\rho}\| + \|e_{n,\rho}\|),$$

and by Lemma 4.3, we deduce that

$$\begin{aligned}\|\partial_t e_{n,m}\| + \|e_{n,m}\| &\leq \|\partial_t u - \partial_t \hat{u}_{n,m}\| + \|\partial_t \hat{u}_{n,m} - \partial_t \bar{u}\| + \|u - \hat{u}_{n,m}\| + \|\hat{u}_{n,m} - \bar{u}\| \\ &\leq c_9 k \sum_{\rho=0}^{m-1} (\|\partial_t e_{n,\rho}\| + \|e_{n,\rho}\|) + \frac{C(p)}{(p-1)!} \left(\frac{T+X}{p} + 1\right) (h+k)^{p-1}.\end{aligned}$$

Using Lemma 4.2, we obtain

$$\|\partial_t e_{n,m}\| + \|e_{n,m}\| \leq \underbrace{\frac{C(p)}{(p-1)!} \left(\frac{T+X}{p} + 1\right) \exp(c_9 X)}_{\beta_2} (h+k)^{p-1}.$$

This implies that for all $n = 0, ..., N-1$ and $m = 0, ..., M-1$,

$$\|e_{n,m}\| \leq \beta (h+k)^{p-1},$$

where $\beta = \max\{\beta_1, \beta_2\}$.

Thus, the proof of Theorem 4.1 is completed. □

5 Numerical Example

In this section, we will examine the practical application of the method discussed in detail in the previous sections to solve a transport-diffusion system. The calculations were performed using Maple 17 running under Windows 7 on a computer equipped with an Intel Core i7-2630QM CPU @2.00 GHz and 8,00 Go of RAM.

Example 5.1 Consider the linear two-dimensional Volterra integro-differential system of two equations

$$\begin{cases} u_1(t,x) &= f_1(t,x) + \frac{1}{3}\int_0^x (x-s)\left(\dfrac{\partial u_1(t,s)}{\partial t} + 3t^2 s u_1(t,s) - \ln(2) t^2 u_2(t,s)\right) + \\ &\quad + e^{-t^2} u_1(t,s) ds \\ u_2(t,x) &= f_2(t,x) + \frac{1}{3}\int_0^x (x-s)\left(\dfrac{\partial u_2(t,s)}{\partial t} - t^3 e^{-t} u_1(t,s) - (t+s) u_2(t,s)\right) + \\ &\quad + t^3 u_2(t,s) ds \end{cases}$$

for $t, x \in [0,1]$, where $f_1(t,x)$ and $f_2(t,x)$ are chosen so that the exact solution is $(u_1(t,x), u_2(t,x)) = (t^4 \sin(-x^2), -t^3 \cos(x))$. We can easily show that this system of equations is equivalent to the following transport-diffusion system:

$$\begin{cases} \frac{\partial u_1(t,x)}{\partial t} + e^{-t^2} \frac{\partial u_1(t,x)}{\partial x} - 3\frac{\partial^2 u_1(t,x)}{\partial x^2} & = -3t^2 x u_1(t,x) + \ln(2) t^2 u_2(t,x) - 3\frac{\partial^2 f_1(t,x)}{\partial x^2} \\ \frac{\partial u_2(t,x)}{\partial t} + t^3 \frac{\partial u_2(t,x)}{\partial x} - 3\frac{\partial^2 u_2(t,x)}{\partial x^2} & = t^3 e^{-t} u_1(t,x) + (t+x) u_2(t,x) - 3\frac{\partial^2 f_2(t,x)}{\partial x^2} \end{cases}$$

with the initial conditions $u_1(0,x) = u_1(t,0) = \frac{\partial u_1(t,0)}{\partial x} = 0$, $u_2(0,x) = \frac{\partial u_2(t,0)}{\partial x} = 0$, and $u_2(t,0) = -t^3$. The numerical results for $p = 3$ and $(N, M) = (5,5), (10,10)$ of the Taylor collocation method are shown in Table 1.

	$N = M = 5$		$N = M = 10$	
(t,x)	$e1$	$e2$	$e1$	$e2$
$(0,0)$	0	0	0	0
$(0.1,0.1)$	$9.99e-07$	$9.95e-04$	$1.13e-08$	$3.67e-08$
$(0.2,0.2)$	$1.48e-06$	$1.96e-06$	$5.84e-07$	$7.80e-07$
$(0.3,0.3)$	$2.39e-04$	$5.54e-04$	$5.30e-06$	$3.70e-06$
$(0.4,0.4)$	$7.98e-05$	$3.15e-05$	$2.53e-05$	$9.52e-06$
$(0.5,0.5)$	$1.64e-03$	$4.22e-04$	$8.48e-05$	$1.39e-05$
$(0.6,0.6)$	$7.31e-04$	$3.09e-05$	$2.26e-04$	$7.26e-06$
$(0.7,0.7)$	$4.90e-03$	$6.83e-04$	$5.08e-04$	$1.45e-04$
$(0.8,0.8)$	$3.29e-03$	$1.23e-03$	$9.87e-04$	$6.94e-04$
$(0.9,0.9)$	$8.14e-03$	$4.99e-03$	$1.66e-03$	$2.49e-03$
CPU time/sec	20.43 s		654.18s	

Table 1: Comparison of the absolute errors in Example 5.1.

6 Conclusion

This work presents a method for solving the transport-diffusion equation using the Taylor collocation method. This approach effectively approximates solutions to Volterra integro-differential equations, and a thorough analysis of the proposed method's convergence properties has been conducted.

The numerical experiments demonstrate the efficacy of the Taylor collocation method in solving the transport-diffusion system, even in the presence of reaction terms. These results confirm the method's utility in this context and highlight its potential for applications in other fields involving the spread of pollutants in a moving fluid or thermal diffusion in engineered systems in modeling dynamic processes, transport, and diffusion processes, such as environmental and atmospheric modeling.

Future research will aim to extend this approach to more complex systems and higher-dimensional domains. Additionally, the effect of various boundary conditions on the convergence and accuracy of the numerical solutions will be investigated.

Acknowledgment

Authors are grateful to the anonymous referees and editor for their constructive comments. Additionally, heartfelt appreciation is extended to Professor Azzeddine Bellour

for their guidance and suggestions throughout this work.

References

[1] K. Alhumaizi, R. Henda and M. Soliman. Numerical analysis of a reaction-diffusion-convection system. *Computers & Chemical Engineering* **27** (4) (2003) 579–594.

[2] A.Bellour and M. Bousselsal. A Taylor collocation method for solving delay integral equations. *Numerical Algorithms* **65** (4) (2014) 843–857.

[3] A. Bellour and M. Bousselsal. Numerical solution of delay integro-differential equations by using Taylor collocation method. *Mathematical Methods in the Applied Sciences* **37** (10) (2014) 1491–1506.

[4] F. Birem, A. Boulmerka, H. Laib and C. Hennous. Goursat problem in hyperbolic partial differential equations with variable coefficients solved by Taylor collocation method. *Iranian Journal of Numerical Analysis and Optimization* **14** (2) (2024) 613–637.

[5] H. Bouzeraieb, H. Laib and A. Boulmerka. Numerical solution of neutral double delay Volterra integral equations using Taylor collocation method. *Nonlinear Dynamics and Systems Theory* **23** (3) (2024) 236–245.

[6] H. Brunner. *Collocation Methods for Volterra Integral and Related Functional Differential Equations*. Cambridge University Press, Cambridge, 2004.

[7] G. Gurarslan, H. Karahan, D. Alkaya, M. Sari and M. Yasar. Numerical solution of advection-diffusion equation using a sixth-order compact finite difference method. *Mathematical Problems in Engineering* **2013** (2013) Article ID 672936.

[8] O. A. Ladyzhenskaia, V. A. Solonnikov and N. N. Ural'tseva. *Linear and Quasi-Linear Equations of Parabolic Type*. American Mathematical Society, Providence, 1968.

[9] P. P. Liu. An analysis of a predator-prey model with both diffusion and migration. *Mathematical and Computer Modelling Journal* **51** (9–10) (2010) 1064–1070.

[10] R. Mohammadi. Exponential B-spline solution of convection-diffusion equations. *Applied Mathematics* **4** (6) (2013) 933–944.

[11] S. Saidane and H. Laib. A Numerical Approach for Solving Delay Volterra Integral Equations with a Spatial Variable and Mixed Kernels. *Nonlinear Dynamics and Systems Theory* **25** (6) (2025) 669–678.

Nonlinear Dynamics and Systems Theory, **26** (2) (2026) 148–161

Study of a Delay Viscoelastic Problem Involving a Generalized Fractional Proportional Derivative

N. Chihi [1], A. Chidouh [2*] and D. Boucenna[1]

[1] *Laboratory of Physical Chemistry and Biology of Materials, Higher Normal School of Technological Education (ENSET), Skikda 21000, Algeria.*
[2] *Laboratory of Computer Science and Applied Mathematics, Chadli Bendjedid University, El Tarf, Algeria.*

Received: February 5, 2025; Revised: March 29, 2026

Abstract: In this paper, we study a nonlinear fractional viscoelastic problem with multiple delays. We consider the fractional model of Voigt in terms of generalized fractional proportional derivative. Using the Banach contraction principle, we prove the existence and uniqueness of the solution under some assumptions, then we confirm the dependence of the latter upon the initial data. The Hyers-Ulam-Rassias stability is established and the results are illustrated by a numerical example.

Keywords: *fractional calculus; Ulam stability; Banach contraction; fractional proportional derivative; rheological models.*

Mathematics Subject Classification (2020): 74D10; 34A12; 26A33; 47H10.

Introduction

In recent years, fractional calculus has proven to be a powerful and versatile tool for modeling many physical and mechanical phenomena, despite the existence of many definitions and formulas for fractional derivatives, see [1–5]. The fractional derivative is an integral operator that has a memory term in the kernel, which is its advantage in modeling rheological phenomena. It can accurately describe the behavior of viscoelastic materials and well define the stress-strain relationships.

When we apply stress to an elastic material, the stress causes deformation, and the material will instantly return to its initial shape when this stress is removed. We say that the elastic deformation here is instantaneous and recoverable and the work is stored in the form of elastic energy.

* Corresponding author: mailto:chidouh-amar@univ-eltarf.dz

Hooke's law describes the behavior of a purely elastic ideal solid as follows:

$$\sigma = E\gamma, \tag{1}$$

where σ is the stress applied, γ is the strain and E is the elastic modulus.

By definition, the viscosity is the measure of fluid's resistance to flow. It also reflects the rate of dissipation of the material's strain energy in the flow. Once there is a dissipation of energy and the stress stops, the deformation becomes permanent and that behavior can be expressed by the following equation:

$$\sigma = \mu \frac{d\gamma}{dt}, \tag{2}$$

where the stress is proportional to the strain velocity and μ is the coefficient of viscosity.

Elastic materials that have the ability to dissipate mechanical energy due to viscous effects are called viscoelastic materials. There are many models that can describe viscoelastic phenomena, for example the Maxwell and Kelvin-Voigt models or combinations of them. The Kelvin-Voigt model is a purely viscous damper and a purely elastic spring connected in parallel, modelled by the following constitutive equation:

$$\mu \frac{d\gamma}{dt} + E\gamma = \sigma. \tag{3}$$

The above equation was studied by A. Chidouh et al. in [6]. They considered the generalized nonlinear equation (3) involving fractional derivative, where the existence results are established by means of the Guo-Krassnosl'ski theorem. In fact, there are many works and papers that focused on studying rheological models that make use of the fractional derivative due to the important role of the latter in studying viscoelastic phenomena. F. Mainardi and G. Spada in [7] have provided a general survey of the fractional viscoelastic models. Their analysis covered the creep, relaxation and viscosity properties of basic fractional models. The papers dealing with rheological models have usually relied on classical fractional derivatives such as the Rieman-Lioville, Caputo and Caputo-Fabrizio ones, see [1–3, 7, 8] and the references therein.

Recently, many definitions of the fractional derivative have appeared, similar to those of the conformable fractional derivative, and many have succeeded in generalizing the fractional derivative in a way that preserves its properties, see [9, 10] and the references therein. In 2017, F. Jarad et al. [11] generalized the fractional proportional integral and derivative, both containing the exponential function in their kernels. Those fractional operators are well-behaved and have several advantages over the classical derivatives, such as being an accurate generalization of the existing fractional derivatives and integrals of Caputo and Riemann-Liouville.

We point out that in rheological models, delay terms appear naturally in certain equations because the response of a viscoelastic material is not instantaneous, and here we consider materials that are not at rest for t belonging to $[-r, 0]$. We also refer to [12], one of the works that inspired us to study fractional differential equations involving delays, where the authors established the existence and stability of solutions for the following nonlinear fractional problem:

$$\begin{cases} D_{0+}^{\alpha} x(t) = \sum\limits_{j=1}^{n} a_j(t) f(t, x(t), x(t-\tau_j)); \quad t \in (0,T], 0 < \alpha < 1, \\ I_{0+}^{1-\alpha} x(t)\big|_{t=0^+} = 0; \quad x(t) = \phi(t), t < 0 \text{ and } \lim\limits_{t\to 0} \phi(t) = 0. \end{cases}$$

Motivated by the above papers and also dealing with the nonlinear Kelvin-Voigt model containing the new generalized proportional Caputo derivative defined in [11], we consider the following problem:

$$ {}^{PC}D_{0^+}^{\alpha,\rho}\gamma(t) + \omega\gamma(t) = \sum_{j=1}^{n} a_j(t)\sigma_j(\gamma(t-\tau_j)),\ (t>0, \omega>0), \tag{4} $$

and

$$ \gamma(t) = \varsigma(t),\ t \in [-r, 0], \tag{5} $$

where ${}^{PC}D_{0^+}^{\alpha,\rho}$ denotes the generalized proportional Caputo derivative of order $0 < \alpha < 1$ and $0 < \rho \leq 1$, taking into account that $0 < r = \max_{j=1,\ldots,n}\{\tau_j\} \leq T$ and $\gamma(0) = \varsigma(0) = 0$.

The content of this paper is arranged as follows. In the first section, we will give some basic definitions and some lemmas that will serve as an analysis tool in the rest of this paper. In Section 2, we rely mainly on two results of [11, Theorem 3.8 and Theorem 5.3] and transform our fractional problem into an equivalent integral equation in a very particular Banach space so that it allows us, under some assumptions, to study the existence and uniqueness of the solution to the above equations. The dependence of the solution on the initial data will also be discussed. In Section 3, we will use the approach of Ulam-Hyers-Rassias to study the stability. Finally, our results will be illustrated by a numerical example.

1 Method and Preliminaries

Here, we employ an effective method based on fixed-point theorems, along with some functional analysis tools. The selection of appropriate functional spaces and sets is crucial to facilitating the task. To achieve this, we first define a Banach space and a suitable subset of it, which forms the basis of this method. Then, we transform our fractional problem into an equivalent integral equation. Finally, from this derived equation, we construct a continuous operator from a compact subset to itself, and via the fixed-point theorems, prove the existence and uniqueness of the solution. All of this will be accomplished with the aid of some functional analysis tools, requiring the following concepts and definitions. We will begin with an important definition of a new fractional derivative which is called the generalized proportional fractional derivative, see [11].

Definition 1.1 For $\rho \in [0,1]$, let the functions $k_0, k_1 : [0,1] \times [0,T] \to [0,\infty)$ be continuous such that for all $t \in [0,T]$, we have

$\lim_{\rho\to 0^+} k_1(\rho,t) = 1$, $\lim_{\rho\to 1^-} k_1(\rho,t) = 0$, and $k_1(\rho,t) \neq 0, \rho \in [0,1)$,

$\lim_{\rho\to 0^+} k_0(\rho,t) = 0$, $\lim_{\rho\to 1^-} k_1(\rho,t) = 1$, and $k_1(\rho,t) \neq 0, \rho \in [0,1)$.

Then the adjusted conformable derivative operator of order ρ is defined by

$$ D^{\rho}u(t) = k_1(\rho,t)u(t) + k_0(\rho,t)u'(t). \tag{6} $$

The derivative mentioned in (6) is called a proportional derivative.

Here, consider $k_1(\rho,t) = 1-\rho$ and $k_0(\rho,t) = \rho$. The equality (6) takes the form

$$ D^{\rho}u(t) = (1-\rho)u(t) + \rho u'(t), \tag{7} $$

which will be the focus of our study regarding the proportional derivative in the rest of this paper. For more details, see [1, 8] and the references therein.

Definition 1.2 Let $\rho \in (0,1]$ and $\alpha > 0$. The generalized proportional fractional integral of the function u is defined by

$$(I_{0^+}^{\alpha,\rho}u)(t) = \frac{1}{\rho^\alpha \Gamma(\alpha)} \int_0^t \exp\left(\frac{\rho-1}{\rho}(t-s)\right)(t-s)^{\alpha-1}u(s)ds,\ t \in [0,T]. \tag{8}$$

Definition 1.3 Let $\rho, \alpha \in (0,1]$. The generalized proprotional Caputo derivative of the function u is defined by

$$({}^{PC}D_{0^+}^{\alpha,\rho})u(t) = \frac{1}{\rho^{1-\alpha}\Gamma(1-\alpha)} \int_0^t \exp\left(\frac{\rho-1}{\rho}(t-s)\right)(t-s)^{-\alpha}(D^\rho u)(s)ds,\ t \in [0,T].$$

Note that, if $\rho = 1$, we get

$$({}^{PC}D^{\alpha,1}u)(t) = ({}^{C}D^{\alpha}u)(t),$$

where ${}^{C}D^{\alpha}$ denotes the Caputo derivative of order α, which means that the latter is a particular case of the generalized proportional Caputo derivative.

Now, let us give important lemmas which play a key role in this work.

Lemma 1.1 *[11] If $\rho \in (0,1], \beta > 0$ and $\alpha \in (0,1]$. Then, for u being a real continuous function on $[0,T]$, we have the following statements:*

1.
$$I^{\alpha,\rho}(I_{0^+}^{\beta,\rho}u)(t) = I^{\beta,\rho}(I_{0^+}^{\alpha,\rho}u)(t) = (I_{0^+}^{\alpha+\beta,\rho}u)(t); \tag{9}$$

2.
$$I_{0^+}^{\alpha,\rho}\ \left({}^{PC}D_{0^+}^{\alpha,\rho}u\right)(t) = u(t) - u(0)\exp\left(\frac{\rho-1}{\rho}t\right). \tag{10}$$

Lemma 1.2 *[13] Let $0 < \alpha < 1$ and $\beta \geq \alpha$, then we have*

$$E_{\alpha,\beta}(-z) \leq \frac{1}{\Gamma(\beta)}; t > 0, \tag{11}$$

where $E_{\alpha,\beta}(z)$ is the Mittag-Leffler function defined as follows:

$$E_{\alpha,\beta}(z) = \sum_{n=0}^{\infty} \frac{z^n}{\Gamma(\alpha n + \beta)}; (z, \alpha, \beta \in C; \mathrm{Re}\,\alpha > 0). \tag{12}$$

2 Existence Results

First of all, we consider the constitutive equation as a linear generalized proportional fractional problem involving the Voigt model

$$({}^{PC}D_{0^+}^{\alpha,\rho}\gamma)(t) + \omega\gamma(t) = \sigma(t), \gamma(0) = 0; (t > 0, \omega > 0). \tag{13}$$

Mechanical phenomena are usually described by differential equations, while we can also describe the phenomena by integral equations which are very suitable for theoretical

work such as studying the stability of solutions or other tasks, where it is sufficient for these integral equations to be equivalent to the differential ones.

Now, we transform our equations (13) into an equivalent integral equation, where we work on highlighting the space to which the solution belongs, so that we ensure the equivalence between our two equations, which is what was not addressed in [11] as the author used the Laplace transform.

Theorem 2.1 *Let $0 < \alpha < 1, \omega > 0$ and $\sigma \in C([0;T],\mathbb{R})$. Then the initial value problem (13) is equivalent to the following integral equation:*

$$\gamma(t) = \frac{1}{\rho^{\alpha}} \int_0^t \exp\left(\frac{\rho-1}{\rho}(t-s)\right)(t-s)^{\alpha-1} E_{\alpha,\alpha}\left(-\omega\left(\frac{t-s}{\rho}\right)^{\alpha}\right)\sigma(s)ds \tag{14}$$

in the Banach space of continuous functions.

Proof. Apply the generalized proportional fractional integral to equations (13). Then, using the first statement (9) of Lemma (1.1), we get

$$\begin{aligned}\gamma(t) &= (I_{0^+}^{\alpha,\rho}\sigma)(t) - \omega(I_{0^+}^{\alpha,\rho}\gamma)(t) + \gamma(0)\exp\left(\frac{\rho-1}{\rho}t\right)\\ &= \frac{1}{\rho^{\alpha}\Gamma(\alpha)}\int_0^t \exp\left(\frac{\rho-1}{\rho}(t-s)\right)(t-s)^{\alpha-1}\sigma(s)ds\\ &- \frac{\omega}{\rho^{\alpha}\Gamma(\alpha)}\int_0^t \exp\left(\frac{\rho-1}{\rho}(t-s)\right)(t-s)^{\alpha-1}\gamma(s)ds.\end{aligned}$$

We will use the successive approximations method to derive the solution, taking into account

$$\gamma_0(t) = (I_{0^+}^{\alpha,\rho}\sigma)(t) = \frac{1}{\rho^{\alpha}\Gamma(\alpha)}\int_0^t \exp\left(\frac{\rho-1}{\rho}(t-s)\right)(t-s)^{\alpha-1}\sigma(s)ds \tag{15}$$

and

$$\gamma_m(t) = \gamma_0(t) - \omega(I_{0^+}^{\alpha,\rho}\gamma_{m-1})(t). \tag{16}$$

By (10), the second statement of Lemma 1.1, we get

$$\begin{aligned}\gamma_1(t) &= \gamma_0(t) - \omega(I_{0^+}^{\alpha,\rho}\gamma_0)(t)\\ &= (I_{0^+}^{\alpha,\rho}\sigma)(t) - \omega(I_{0^+}^{2\alpha,\rho}\sigma)(t)\end{aligned}$$

and

$$\begin{aligned}\gamma_2(t) &= \gamma_0(t) - \omega(I_{0^+}^{\alpha,\rho}\gamma_1)(t)\\ &= (I_{0^+}^{\alpha,\rho}\sigma)(t) - \omega(I_{0^+}^{2\alpha,\rho}\sigma)(t) + \omega^2(I_{0^+}^{3\alpha,\rho}\sigma)(t).\end{aligned}$$

Continuing this process, we obtain

$$\gamma_m(t) = \frac{1}{\rho^{\alpha}}\int_0^t \exp\left(\frac{\rho-1}{\rho}(t-s)\right)(t-s)^{\alpha-1}\sum_{k=0}^{m}\frac{(t-s)^{k\alpha}}{\rho^{k\alpha}\Gamma(k\alpha+\alpha)}(-\omega)^k\sigma(s)ds.$$

Taking the limit as $m \to \infty$, denote $\lim_{m\to\infty} \gamma_m(t) = \gamma(t), t \in [0,T]$ (γ is the unique solution which belongs to the Banach space of real continous functions) and consider (12), we obtain

$$\gamma(t) = \frac{1}{\rho^\alpha} \int_0^t \exp\left(\frac{\rho-1}{\rho}(t-s)\right)(t-s)^{\alpha-1} E_{\alpha,\alpha}\left(-\omega\left(\frac{t-s}{\rho}\right)^\alpha\right)\sigma(s)ds. \tag{17}$$

The proof is complete.

Now, we turn our attention to the nonlinear problem (13), where

$$\sigma(t) = \sum_{j=1}^{n} a_j(t)\sigma_j(\gamma(t-\tau_j))$$

and

$$\gamma(t) = \varsigma(t),\ t \in [-r, 0],$$

taking into account that $0 < r = \max_{j=1,\dots,n}\{\tau_j\} \le T$ and $\gamma(0) = \varsigma(0) = 0$.

Let us introduce the following hypotheses.

(C1) $a_j : [0,T] \to \mathbb{R}$ are continuous functions with $A_j = \sup_{t\in[0,T]} |a_j(t)|$.

(C2) $\sigma_j : C[-v,T] \to C[-v,T]$ are Lipschitz functions, i.e., there exists $B_j > 0$ such that

$$\|\sigma_j(\gamma_1) - \sigma_j(\gamma_2)\|_{C[-v,T]} \le B_j \|\gamma_1 - \gamma_2\|_{C[-v,T]}; \gamma_1, \gamma_2 \in C[-v,T]. \tag{18}$$

We suppose that $\Sigma = \sum_{j=1}^{n} A_j B_j$ and $\sigma_j(0) \neq 0$.

Theorem 2.2 *Assume that (C1) and (C2) are satisfied. If*

$$\frac{T^\alpha \Sigma}{\rho^\alpha \Gamma(\alpha+1)} \le 1, \tag{19}$$

then problem (4) and (5) has a unique solution $\gamma \in (C[-r,T],\mathbb{R})$.

Proof. Let us define the following space:

$$X = \left\{\gamma \in (C[-v,T],\mathbb{R}) : \gamma\big|_{[-r,0]} = \varsigma\right\},$$

which is a Banach space endowed with the sup-norm

$$\|\gamma\|_X = \sup_{t\in[-r,T]} |\gamma(t)|.$$

We consider the operator $P : X \to X$ defined by

$$(P\gamma)(t) = \begin{cases} \varsigma(t) & \text{for } t \in [-r,0], \\ \frac{1}{\rho^\alpha}\int_0^t \exp\left(\frac{\rho-1}{\rho}(t-s)\right)(t-s)^{\alpha-1} E_{\alpha,\alpha}\left(-\omega\left(\frac{t-s}{\rho}\right)^\alpha\right) \\ \quad \times \sum_{j=1}^{n} a_j(s)\sigma_j(\gamma(s-\tau_j))ds & \text{for } t \in [0,T]. \end{cases}$$

From Theorem 2.1, finding a solution of (4) and (5) in $(C[-r,T],\mathbb{R})$ is equivalent to finding a fixed point of the operator P.

For any $\gamma_1,\gamma_2 \in (C[-v,T],\mathbb{R})$ and each $t\in[-r,T]$, we have

$$|(P\gamma_1)(t)-(P\gamma_2)(t)| \leq \frac{1}{\rho^\alpha}\int_0^t \exp\left(\frac{\rho-1}{\rho}(t-s)\right)(t-s)^{\alpha-1}E_{\alpha,\alpha}\left(-\omega\left(\frac{t-s}{\rho}\right)^\alpha\right) \times\left(\sum_{j=1}^n |a_j(s)|\,B_j\,|\gamma_1(s-\tau_j)-\gamma_2(s-\tau_j)|\right)ds.$$

Putting $z=(s-\tau_j)$, we get

$$\begin{aligned}|(P\gamma_1)(t)-(P\gamma_2)(t)| &\leq \sum_{j=1}^n \frac{1}{\rho^\alpha}\int_{-\tau_j}^0 \exp\left(\frac{\rho-1}{\rho}(t-z-\tau_j)\right)(t-z-\tau_j)^{\alpha-1}\\ &\quad\times E_{\alpha,\alpha}\left(-\omega\left(\frac{t-z-\tau_j}{\rho}\right)^\alpha\right)|a_j(s)|\,B_j\,|\gamma_1(z)-\gamma_2(z)|\,dz\\ &\quad+\sum_{j=1}^n \frac{1}{\rho^\alpha}\int_0^{t-\tau_j} \exp\left(\frac{\rho-1}{\rho}(t-z-\tau_j)\right)(t-z-\tau_j)^{\alpha-1}\\ &\quad\times E_{\alpha,\alpha}\left(-\omega\left(\frac{t-z-\tau_j}{\rho}\right)^\alpha\right)|a_j(s)|\,B_j\,|\gamma_1(z)-\gamma_2(z)|\,dz.\end{aligned}$$

We have $\gamma_1(t)=\gamma_2(t)=\varsigma(t)$ for $t\in[-r,0]$. Taking into account

$$\exp\left(\frac{\rho-1}{\rho}(t-z-\tau_j)\right)\leq 1,\ \text{for } \rho\in(0,1], \tag{20}$$

and (11), we get

$$|(P\gamma_1)(t)-(P\gamma_2)(t)| \leq \frac{1}{\rho^\alpha\Gamma(\alpha)}\sum_{j=1}^n\int_0^{t-\tau_j}(t-z-\tau_j)^{\alpha-1}\,|a_j(s)|\,B_j\,|\gamma_1(z)-\gamma_2(z)|\,dz.$$

Therefore,

$$\|(P\gamma_1)(t)-(P\gamma_2)(t)\|_X \leq \left(\frac{T^\alpha\Sigma}{\rho^\alpha\Gamma(\alpha+1)}\right)\|\gamma_1-\gamma_2\|_X.$$

In view of (19) and Banach's fixed point, we deduce that P is a contraction. Hence, the problem (4)-(5) has a unique solution on $(C[-r,T],\mathbb{R})$. This completes the proof.

Corollary 2.1 *Under the conditions (18), the unique solution of (4) and (5) depends continuously on function $\varsigma(t)$.*

Proof. Let γ_1 and γ_2 be solutions of problem (4)-(5), corresponding to the functions ς_1 and ς_2, respectively. Then we have

$$|\gamma_1(t)-\gamma_2(t)| = \left|\frac{1}{\rho^\alpha}\int_0^t \exp\left(\frac{\rho-1}{\rho}(t-s)\right)(t-s)^{\alpha-1}E_{\alpha,\alpha}\left(-\omega\left(\frac{t-s}{\rho}\right)^\alpha\right)\right.$$

$$\times\sum_{j=1}^{n}a_j(s)\left|\sigma_j(\gamma_1(s-\tau_j))-\sigma_j(\gamma_2(s-\tau_j))\right|\Bigg|.$$

Putting $z=(s-\tau_j)$ and taking into account (20) and (11), we get

$$\begin{aligned}
|\gamma_1(t)-\gamma_2(t)| &\leq \frac{\Sigma}{\rho^{\alpha}\Gamma(\alpha)}\int_{-\tau_j}^{t-\tau_j}(t-z-\tau_j)^{\alpha-1}\left|\gamma_1(z)-\gamma_2(z)\right|dz\\
&\leq \frac{\Sigma}{\rho^{\alpha}\Gamma(\alpha)}\int_{-\tau_j}^{0}(t-z-\tau_j)^{\alpha-1}\left|\gamma_1(z)-\gamma_2(z)\right|dz\\
&+\frac{\Sigma}{\rho^{\alpha}\Gamma(\alpha)}\int_{0}^{t-\tau_j}(t-z-\tau_j)^{\alpha-1}\left|\gamma_1(z)-\gamma_2(z)\right|dz\\
&\leq \frac{\Sigma}{\rho^{\alpha}\Gamma(\alpha)}\sup_{z\in[-v,0]}|\gamma_1(z)-\gamma_2(z)|\int_{-\tau_j}^{0}(t-z-\tau_j)^{\alpha-1}dz\\
&+\frac{\Sigma}{\rho^{\alpha}\Gamma(\alpha)}\sup_{z\in[0,T]}|\gamma_1(z)-\gamma_2(z)|\int_{0}^{t-\tau_j}(t-z-\tau_j)^{\alpha-1}dz\\
&\leq \frac{(t^{\alpha}-(t-\tau_j)^{\alpha})\,\Sigma}{\rho^{\alpha}\Gamma(\alpha+1)}\left\|\varsigma_1-\varsigma_2\right\|_{C[-v,0]}\\
&+\frac{(t-\tau_j)^{\alpha}\Sigma}{\rho^{\alpha}\Gamma(\alpha+1)}\left\|\gamma_1-\gamma_2\right\|_{C[0,T]}.
\end{aligned}$$

Consequently, we have

$$\left\|\gamma_1-\gamma_2\right\|_{C[0,T]}\leq\frac{T^{\alpha}\Sigma}{\rho^{\alpha}\Gamma(\alpha+1)}\left\|\gamma_1-\gamma_2\right\|_{C[0,T]}+\frac{T^{\alpha}\Sigma}{\rho^{\alpha}\Gamma(\alpha+1)}\left\|\varsigma_1-\varsigma_2\right\|_{C[-r,0]}.$$

Then, in view of (9), we get

$$\left\|\gamma_1-\gamma_2\right\|_{C[0,T]}\leq\frac{T^{\alpha}\Sigma}{\rho^{\alpha}\Gamma(\alpha+1)-T^{\alpha}\Sigma}\left\|\varsigma_1-\varsigma_2\right\|_{C[-r,0]}.$$

This implies the dependence of $\gamma(t)$ on the initial data $\varsigma(t)$ and completes the proof.

3 Stability Results

Definition 3.1 The problem (4)-(5) has the Ulam-Hyers stability if for each $\varepsilon>0$ and each $y\in C([-v,T],\mathbb{R})$, there exists a solution of the following problem:

$$\begin{cases}\left|({}^{PC}D_{0^+}^{\alpha,\rho}y)(t)+\omega y(t)-\sum_{j=1}^{n}a_j(t)\sigma_j((t-\tau_j))\right|\leq\varepsilon, t\in[0,T],\\ y(t)=\varsigma(t), t\in[-r,0],\ \varsigma(0)=0.\end{cases}\tag{21}$$

There exist a solution $\gamma\in C([-v,T],\mathbb{R})$ of (4)-(5) and a real number $k>0$ such that

$$|y(t)-\gamma(t)|\leq k\varepsilon.$$

Remark 3.1 A function $y \in C([-v,T],\mathbb{R})$ is a solution of the problem (21) if and only if there exists a function $h \in C([0,T],\mathbb{R})$ such that for every $t \in [0,T]$, we have $|h(t)| \leq \varepsilon$ and

$$\begin{cases} ({}^{PC}D_{0^+}^{\alpha,\rho}y)(t) + \omega y(t) = \sum_{j=1}^{n} a_j(t)\sigma_j(y(t-\tau_j)) + h(t), t \in [0,T], \\ y(t) = \varsigma(t), t \in [-r,0],\ \varsigma(0) = 0. \end{cases} \tag{22}$$

Lemma 3.1 *If $y \in C([-v,T],\mathbb{R})$ is a solution of the problem (21), then for $t \in [0,T]$, y satisfies the relation*

$$\begin{aligned} &\left| y(t) - \frac{1}{\rho^\alpha}\int_0^t \exp\left(\frac{\rho-1}{\rho}(t-s)\right)(t-s)^{\alpha-1}E_{\alpha,\alpha}\left(-\omega\left(\frac{t-s}{\rho}\right)^\alpha\right)\right. \\ &\left.\times\sum_{j=1}^{n} a_j(t)\sigma_j(y(s-\tau_j))ds\right| \\ &\leq \frac{T^\alpha}{\rho^\alpha\Gamma(\alpha+1)}\varepsilon. \end{aligned} \tag{23}$$

Proof. For $y(t) = \varsigma(t),\ t \in [-r,0]$, the solution of (22) satisfies

$$\begin{aligned} y(t) = &\frac{1}{\rho^\alpha}\int_0^t \exp\left(\frac{\rho-1}{\rho}(t-s)\right)(t-s)^{\alpha-1}E_{\alpha,\alpha}\left(-\omega\left(\frac{t-s}{\rho}\right)^\alpha\right) \\ &\times\left(\sum_{j=1}^{n} a_j(t)\sigma_j(y(s-\tau_j)) + h(t)\right)ds. \end{aligned}$$

On the other hand,

$$\begin{aligned} &\left| y(t) - \frac{1}{\rho^\alpha}\int_0^t \exp\left(\frac{\rho-1}{\rho}(t-s)\right)(t-s)^{\alpha-1}E_{\alpha,\alpha}\left(-\omega\left(\frac{t-s}{\rho}\right)^\alpha\right)\right. \\ &\left.\times\sum_{j=1}^{n} a_j(t)\sigma_j(y(s-\tau_j))ds\right| \\ &\leq \left|\frac{1}{\rho^\alpha}\int_0^t \exp\left(\frac{\rho-1}{\rho}(t-s)\right)(t-s)^{\alpha-1}E_{\alpha,\alpha}\left(-\omega\left(\frac{t-s}{\rho}\right)^\alpha\right)h(t)ds\right| \\ &\leq \frac{1}{\rho^\alpha}\int_0^t \exp\left(\frac{\rho-1}{\rho}(t-s)\right)(t-s)^{\alpha-1}E_{\alpha,\alpha}\left(-\omega\left(\frac{t-s}{\rho}\right)^\alpha\right)|h(t)|\,ds \\ &\leq \left(\frac{T^\alpha}{\rho^\alpha\Gamma(\alpha+1)}\right)\varepsilon. \end{aligned}$$

The proof is complete.

Theorem 3.1 *If the problem (4)-(5) has a unique solution, then it is Ulam-Hyers stable.*

Proof. From Theorem 2.1, the problem (4)-(5) has a unique solution γ in $C([-v,T],\mathbb{R})$. Let y be a solution of (21), then we obtain, for each $t \in [-r,T]$,

$$|y(t) - \gamma(t)| = \left| y(t) - \frac{1}{\rho^\alpha}\int_0^t \exp\left(\frac{\rho-1}{\rho}(t-s)\right)(t-s)^{\alpha-1}E_{\alpha,\alpha}\left(-\omega\left(\frac{t-s}{\rho}\right)^\alpha\right)\right.$$

$$
\begin{aligned}
&\times\sum_{j=1}^{n}a_j(s)\sigma_j(\gamma(s-\tau_j))ds\Bigg| \\
&\leq \left|y(t)-\frac{1}{\rho^{\alpha}}\int_0^t \exp\left(\frac{\rho-1}{\rho}(t-s)\right)(t-s)^{\alpha-1}E_{\alpha,\alpha}\left(-\omega\left(\frac{t-s}{\rho}\right)^{\alpha}\right)\right. \\
&\times\sum_{j=1}^{n}a_j(s)\sigma_j(y(s-\tau_j))ds\Bigg| \\
&+\frac{1}{\rho^{\alpha}}\int_0^t \exp\left(\frac{\rho-1}{\rho}(t-s)\right)(t-s)^{\alpha-1}E_{\alpha,\alpha}\left(-\omega\left(\frac{t-s}{\rho}\right)^{\alpha}\right) \\
&\times\sum_{j=1}^{n}|a_j(s)|\,|\sigma_j(y(s-\tau_j))-\sigma_j(\gamma(s-\tau_j))|\,ds.
\end{aligned}
$$

By Lemma 3.1, we get

$$
|y(t)-\gamma(t)| \leq \frac{T^{\alpha}}{\rho^{\alpha}\Gamma(\alpha+1)}\varepsilon+\frac{\sum_{j=1}^{n}A_jB_j}{\rho^{\alpha}\Gamma(\alpha)}\int_{-\tau_j}^{t-\tau_j}(t-z-\tau_j)^{\alpha-1}\,|y(z)-\gamma(z)|\,dz
$$

As $y(z)=x(z)=\varsigma(z)$ for $z\in[-\tau_j,0]$, we get

$$
\begin{aligned}
|y(t)-x(t)| &\leq \frac{T^{\alpha}}{\rho^{\alpha}\Gamma(\alpha+1)}\varepsilon+\frac{\Sigma}{\rho^{\alpha}\Gamma(\alpha)}\int_{0}^{t-\tau_j}(t-z-\tau_j)^{\alpha-1}\,|y(z)-\gamma(z)|\,dz \\
&\leq \frac{T^{\alpha}}{\rho^{\alpha}\Gamma(\alpha+1)}\varepsilon+\frac{T^{\alpha}\Sigma}{\rho^{\alpha}\Gamma(\alpha+1)}\left\|y-\gamma\right\|_{C[0,T]}.
\end{aligned}
$$

Hence,

$$
\left\|y-\gamma\right\|_{C[0,T]} \leq \frac{T^{\alpha}}{\rho^{\alpha}\Gamma(\alpha+1)-T^{\alpha}\Sigma}\varepsilon
$$

and (4)-(5) is Ulam-Hyers stable with the constant $k=\frac{T^{\alpha}}{\rho^{\alpha}\Gamma(\alpha+1)-T^{\alpha}\Sigma}$.

Let us now give a generalized results on stability that is known as the Ulam-Hyers-Rassias stability.

Definition 3.2 The equation (4)-(5) has the Ulam-Hyers-Rassias stability with respect to $\phi(t)$ if there exists a real number $C>0$ such that for each $\varepsilon>0$ and for each $y\in C([-v,T],\mathbb{R})$, there is a solution of the following problem:

$$
\begin{cases}
\left|({}^{PC}D_{0^+}^{\alpha,\rho}y)(t)+\omega y(t)-\sum_{j=1}^{n}a_j(t)\sigma_j(y(t-\tau_j))\right| \leq \varepsilon\phi(t), t\in[0,T], \\
y(t)=\varsigma(t), t\in[-r,0],\ \varsigma(0)=0.
\end{cases} \tag{24}
$$

There exists a solution $\gamma\in C([-v,T],\mathbb{R})$ of (4)-(5) such that

$$
|y(t)-\gamma(t)| \leq C\phi(t)\,\varepsilon.
$$

Before we give the following lemma, we assume that for a continous function $\phi(t)$, there is a positive constant θ such that

$$\int_0^t (t-s)^{\alpha-1}\phi(s)ds \leq \theta\phi(t).$$

Lemma 3.2 *If $y \in C([-v,T],\mathbb{R})$ is a solution of the problem (24), then for $t \in [0,T]$, y satisfies the relation*

$$\begin{aligned}&\left|y(t) - \frac{1}{\rho^\alpha}\int_0^t \exp\left(\frac{\rho-1}{\rho}(t-s)\right)(t-s)^{\alpha-1}E_{\alpha,\alpha}\left(-\omega\left(\frac{t-s}{\rho}\right)^\alpha\right)\right.\\ &\left.\times\sum_{j=1}^n a_j(t)\sigma_j(y(s-\tau_j))ds\right|\\ &\leq \frac{\theta\varepsilon}{\rho^\alpha\Gamma(\alpha)}\phi(t). \end{aligned} \tag{25}$$

Proof. For $y(t) = \varsigma(t),\ t \in [-r,0]$, the solution of (24) satisfies

$$\begin{aligned}y(t) = &\frac{1}{\rho^\alpha}\int_0^t \exp\left(\frac{\rho-1}{\rho}(t-s)\right)(t-s)^{\alpha-1}E_{\alpha,\alpha}\left(-\omega\left(\frac{t-s}{\rho}\right)^\alpha\right)\\ &\times\left(\sum_{j=1}^n a_j(t)\sigma_j(y(s-\tau_j)) + h(t)\right)ds,\end{aligned}$$

where $|h(t)| \leq \varepsilon\phi(t)$. Then

$$\begin{aligned}&\left|y(t) - \frac{1}{\rho^\alpha}\int_0^t \exp\left(\frac{\rho-1}{\rho}(t-s)\right)(t-s)^{\alpha-1}E_{\alpha,\alpha}\left(-\omega\left(\frac{t-s}{\rho}\right)^\alpha\right)\right.\\ &\left.\times\sum_{j=1}^n a_j(t)\sigma_j(y(s-\tau_j))ds\right|\\ &\leq \frac{1}{\rho^\alpha}\int_0^t \exp\left(\frac{\rho-1}{\rho}(t-s)\right)(t-s)^{\alpha-1}E_{\alpha,\alpha}\left(-\omega\left(\frac{t-s}{\rho}\right)^\alpha\right)|h(t)|\,ds\\ &\leq \frac{\varepsilon}{\rho^\alpha}\int_0^t \exp\left(\frac{\rho-1}{\rho}(t-s)\right)(t-s)^{\alpha-1}E_{\alpha,\alpha}\left(-\omega\left(\frac{t-s}{\rho}\right)^\alpha\right)\phi(s)ds\\ &\leq \frac{\varepsilon\theta}{\rho^\alpha\Gamma(\alpha)}\phi(s).\end{aligned}$$

The proof is complete.

Theorem 3.2 *If problem (4)-(5) has a unique solution, then it is Ulam-Hyers-Rassias stable.*

Proof. From Theorem 2.1, the problem (4)-(5) has a unique solution γ in $C([-v,T],\mathbb{R})$. Let y be a solution of (24), then we obtain, for each $t \in [-v,T]$, that

$$|y(t)-\gamma(t)| = \left|y(t) - \frac{1}{\rho^\alpha}\int_0^t \exp\left(\frac{\rho-1}{\rho}(t-s)\right)(t-s)^{\alpha-1}E_{\alpha,\alpha}\left(-\omega\left(\frac{t-s}{\rho}\right)^\alpha\right)\right.$$

$$
\begin{aligned}
&\times\sum_{j=1}^{n}a_j(s)\sigma_j(\gamma(s-\tau_j))ds\Bigg| \\
&\leq \left|y(t)-\frac{1}{\rho^{\alpha}}\int_0^t \exp\left(\frac{\rho-1}{\rho}(t-s)\right)(t-s)^{\alpha-1}E_{\alpha,\alpha}\left(-\omega\left(\frac{t-s}{\rho}\right)^{\alpha}\right)\right. \\
&\times\sum_{j=1}^{n}a_j(s)\sigma_j(y(s-\tau_j))ds\Bigg| \\
&+\frac{1}{\rho^{\alpha}}\int_0^t \exp\left(\frac{\rho-1}{\rho}(t-s)\right)(t-s)^{\alpha-1}E_{\alpha,\alpha}\left(-\omega\left(\frac{t-s}{\rho}\right)^{\alpha}\right) \\
&\times\sum_{j=1}^{n}|a_j(s)|\,|\sigma_j(y(s-\tau_j))-\sigma_j(\gamma(s-\tau_j))|\,ds.
\end{aligned}
$$

By Lemma 3.2, we get

$$
|y(t)-\gamma(t)| \leq \frac{\theta\varepsilon}{\rho^{\alpha}\Gamma(\alpha)}\phi(t)+\frac{\sum_{j=1}^{n}B_jl_j}{\rho^{\alpha}\Gamma(\alpha)}\int_{-\tau_j}^{t-\tau_j}(t-z-\tau_j)^{\alpha-1}\,|y(z)-\gamma(z)|\,dz.
$$

As $y(z)=\gamma(z)=\varsigma(z)$ for $z\in[-\tau_j,0]$, we get

$$
\begin{aligned}
|y(t)-\gamma(t)| &\leq \frac{\theta\varepsilon}{\rho^{\alpha}\Gamma(\alpha)}\phi(t)+\frac{\sum_{j=1}^{n}A_jB_j}{\rho^{\alpha}\Gamma(\alpha)}\int_{0}^{t-\tau_j}(t-z-\tau_j)^{\alpha-1}\,|y(z)-\gamma(z)|\,dz \\
&\leq \frac{\theta\varepsilon}{\rho^{\alpha}\Gamma(\alpha)}\phi(t)+\frac{T^{\alpha}\Sigma}{\rho^{\alpha}\Gamma(\alpha+1)}\,\|y-\gamma\|_{C[0,T]}\,.
\end{aligned}
$$

Hence,

$$
\|y-\gamma\|_{C[0,T]} \leq \frac{\alpha\theta}{\rho^{\alpha}\Gamma(\alpha+1)-T^{\alpha}\Sigma}\varepsilon\phi(t),
$$

and (4)-(5) is Ulam-Hyers-Rassias stabe with respect to $\phi\,(t)$, where

$$
C=\frac{\alpha\theta}{\rho^{\alpha}\Gamma(\alpha+1)-T^{\alpha}\Sigma}.
$$

Example

Consider the following delay fractional problem:

$$
\begin{cases}
{}^{PC}D_{0^+}^{\frac{1}{2},\frac{1}{2}}\gamma(t)+\pi\gamma(t)=\sum_{j=1}^{2}\frac{1}{7j}\cos(jt)\sin(j\gamma(t-j)+1),\ t\in[0,\pi], \\
\gamma(t)=t,\ t\in[-2,0],
\end{cases}
\tag{26}
$$

where ${}^{PC}D_{0^+}^{\frac{1}{2},\frac{1}{2}}$ denotes the generalized proportional Caputo derivative of order $\alpha=\frac{1}{2}$ and $\rho=\frac{1}{2}$.

Here, $\sigma_j(x) = \frac{\sin(jx+1)}{7j}$, $j = \overline{1,2}$. Take into account that in this example, we have two stress functions $\sigma_1(x) = \frac{1}{7}\sin(x+1)$ and $\sigma_2(x) = \frac{1}{14}\sin(2x+1)$ which are Lipschitz functions such that $\sigma_j(0) \neq 0$ and the Lipschitz constant $B_j = \frac{1}{7}$ for $j = \overline{1,2}$.

On the other hand, $a_j(t) = \cos(jt)$ such that $\max_{0\leq t\leq\pi} |a_j(t)| = \max_{0\leq t\leq\pi} |\cos(jt)| = 1$ for $j = \overline{1,2}$.

Then we obtain that $\Sigma = \sum_{j=1}^{2} A_j B_j = \frac{2}{7}$. So, the assumptions (C1) and (C2) of Theorem 2.2 are fulfilled as well as condition (19):

$$\frac{T^\alpha \Sigma}{\rho^\alpha \Gamma(\alpha+1)} = \frac{8}{7\sqrt{2\pi}} = 0.46 < 1.$$

Therefore, from Theorem 2.2, we conclude that our problem (26) has a unique solution in $C([-2,\pi],\mathbb{R})$, which makes it Ulam-Hyers stable as follows from the above analysis.

4 Discussion

In this work, we studied a fractional differential equation involving a generalized fractional proportional derivative. Our equation is a generalization of the classical viscoelastic Kelvin-Voigt model with the addition of a delay term. Using a fractional-order derivative in the model gives us a more accurate representation of memory than integer order, while the delay term reflects the viscoelastic behavior observed in certain mechanical systems. The existence and uniqueness of the solutions were established using the fixed point technique. This technique is very effective when appropriate assumptions are made regarding the nonlinear terms and delay functions, thus ensuring the validity of the proposed fractional delayed model. So, our technique is not only a tool for solving many types of equations, but it is also a powerful means that facilitates the study of stability in a way that has never been done before. The stability of the solutions was analyzed according to the Ulam concept. These stability properties confirm that approximate solutions remain close to precise solutions, highlighting the reliability of the proposed model. The results obtained appear to be very strong and generalize many previous findings. These results were further confirmed by a numerical example that explains the method used in detail.

Acknowledgment

The authors would like to express sincere gratitude to the editors and the anonymous reviewers for their valuable comments and constructive suggestions.

References

[1] K. D. Papoulia, V. P. Panoskaltsis, N. V. Kurup and Igor Korovajchuk. Rheological representation of fractional order viscoelastic material models. *Rheologica Acta.* **49** (2010) 381–400.

[2] M. Fukunaga and S. Nobuyuki. Fractional derivative constitutive models for finite deformation of viscoelastic materials. *Journal of Computational and Nonlinear Dynamics* **10** (6) (2015) 061002.

[3] J. Hristov. Response functions in linear viscoelastic constitutive equations and related fractional operators. *Mathematical Modelling of Natural Phenomena* **14** (3) (2019) 305.

[4] N. Allouch, S. Hamani and J. Henderson. Boundary value problem for fractional q-difference equations. *Nonlinear Dynamics and Systems Theory* **24** (2) (2024) 111–122.

[5] A. Khalouta. Conformable Fractional Khalouta Transform and Its Applications to Fractional Differential Equations. *Nonlinear Dynamics and Systems Theory* **24** (5) (2024) 495–504.

[6] A. Chidouh, A. Guezane-Lakoud, R. Bebbouchi, A. Bouaricha and D. F. Torres. Linear and nonlinear fractional Voigt models. *Theory and Applications of Non-integer Order Systems, 8th Conference on Non-integer Order Calculus and Its Applications*, Zakopane, Poland. Springer International Publishing (2017) 157–167.

[7] F. Mainardi and S. Giorgio. Creep, relaxation and viscosity properties for basic fractional models in rheology. *The European Physical Journal Special Topics* **193** (1) (2011) 133–160.

[8] A. Chidouh, R. Atmania and D. F. Torres. Study of a fractional creep problem with multiple delays in terms of Boltzmann's superposition principle. *Fractal and Fractional* **6** (8) (2022) 434.

[9] R. Khalil, M. Al Horani, A. Yousef and M. Sababheh. A new definition of fractional derivative. *J. Comput. Appl. Math.* **264** (2014) 65–70.

[10] T. Abdeljawad. On conformable fractional calculus. *J. Comput. Appl. Math.* **279** (2015) 57–66.

[11] F. Jarad, T. Abdeljawad and J. Alzabut. Generalized fractional derivatives generated by a class of local proportional derivatives. *The European Physical Journal Special Topics* **226** (2017) 3457–3471.

[12] Z. H. Gao, L. Yang and Z. G. Luo. Stability of the solutions for nonlinear fractional differential equations with delays and integral boundary conditions. *Adv. Difference Equ.* **2013** (43) (2013) 8 pp.

[13] W. R. Schneider. Completely monotone generalized Mittag-Leffler functions. *Expositiones Mathematicae* **14** (1996) 3–16.

Nonlinear Dynamics and Systems Theory, **26** (2) (2026) 162–172

A Scaled Nonlinear Conjugate Gradient Method for Unrestricted Optimizations

Isam H. Halil [1] and Marwan S. Jameel [2*]

[1] *Department of Mathematics, College of Science, University of Kerkuk, Kerkuk, Iraq.*
[2] *Department of Climate Change, University of Mosul, Mosul, Iraq.*

Received: November 8, 2025; Revised: March 12, 2026

Abstract: The conjugate gradient (CG) methods are a family of iterative algorithms used to repeatedly (or iteratively) solve nonlinear systems and control theory problems that can be formulated as unconstrained optimisation. The conjugate gradient method is used for some algorithms; a subclass of it is the hybrid conjugate gradient method. This paper provides new spectral and hybrid conjugate gradient methods. The innovative spectral conjugate gradient technique demonstrates global convergence features, supported by many presumptions and a rigorous Wolfe line search. Moreover, the hybrid conjugate gradient technique fulfils the requirements for achieving global convergence when employing accurate line searches. Additionally, we demonstrate that the approaches provided in this study meet the necessary conditions for descent. The suggested solutions exhibit a high level of competitiveness and efficiency, as evidenced by the numerical results obtained from several test problems.

Keywords: *conjugate gradient approach; spectral conjugate gradient; global convergence analysis; Wolfe line condition.*

Mathematics Subject Classification (2020): 90-XX, 93-XX, 90C06, 70Kxx.

1 Introduction

In numerous nonlinear dynamic systems, the objective is to determine the best state or combination of parameters that leads to the desired behavior. Optimizing parameters in control systems is frequently required to ensure stability and prevent oscillations. Gradient methods can also be applied to address nonlinear systems that arise from electronic and electrical circuits. Hence, the difficulty arising from the concerns mentioned above

* Corresponding author: mailto:marwan.jameel@uomosul.edu.iq

can be framed as an optimization problem, and an attempt can be made to resolve it using iterative techniques such as the way suggested in this paper, see [1, 2].

Consider the following problem with unconstrained optimization:

$$minf(x),\ x \in R^n. \tag{1}$$

Let $f : \mathbb{R}^{\kappa} \to \mathbb{R}$, if we think intuitively in terms of the graph of f, then we have a gradient map $(\nabla f)(x)$ mapping smoothly on the set R. In mathematics, we have 3 types of solutions exact, approximate and numeric methods. Numerical methods to solve Eq. (1) are a lot of them. Newton technique, conjugate gradient (CG), steepest descent(SD), and quasi-Newton(QN) methods belong to these types two. This means that for huge problems where the conjugate gradient method is not only extremely simple but also takes much less memory. Conjugate gradient method is quite efficient. Conjugate gradient methods enabled the numerical type classification. The bracketing method begins with an initial guess x^0 and then provides new guesses which converge to a solution of Eq. (1) by repetitively enhancing the bound via an iteration x^n. From here we are going to compute our target function f(x) for the first object and then calculate it for the other iterations x^1, x^2, x^3, x^4 and so on. Typically, in a non-linear conjugate gradient procedure, it is an iterative approach to solve for the optimal solution.

$$x_{k+1} = x_k + \alpha_k p_k, \tag{2}$$

The step-length α_k is usually determined by means of one of the line searches. A Wolfe, Goldstein or Armijo criterion provides a proper step of $x^(k)$ so as to calculate some decrease in the function value without taking small steps. The first two terms guarantee that the attention flows in the direction p^k is given by

$$p_{k+1} = \begin{cases} -g_{k+1} & if \quad k{=}0, \\ \\ -g_{k+1}+\beta_k p_k & if \quad k{>}0. \end{cases} \tag{3}$$

Within the framework of a three-term conjugate gradient approach (TTCG), as elucidated by N. Andrei [2], it is possible to choose from various generic formats

$$p_{k+1} = \begin{cases} -g_{k+1} & if \quad k{=}0, \\ \\ -g_{k+1}-\alpha s_k - b y_k & if \quad k{>}0. \end{cases} \tag{4}$$

A search direction is determined by adding the values of g_{k+1}, s_k, y_k, when α_k and b_k implemented the mathematical formula associated with the terms $||g_k||^2, ||g_{k+1}||^2, ||y_k||^2, s_k^T g_k$ and $y_k^T\ g_k$, etc. $a_k = \beta_k$ is a commonality. Here, β_k is a parameter $(0 < \beta_k < 1)$ and g_{k+1} represents $g(x_{k+1})$. There are a number of formulas for β_k, which are listed below.

In this context, where $|.|$ is the Euclidean norm, $g_{k+1} = g(x_{k+1})$ and $y_k = \bigtriangledown f_{k+1} - \bigtriangledown f_k$ are vectors. We should be sure that function value is transported down as expected and there are not many iterations. These criteria, including Wolfe and Goldstein, Armijo conditions that are widely used to compute the step length α^k actually. The line search (LS) process is usually addressed with an inexact line search (ILS), like the Strong Wolfe Conditions (SWC) that help also define which *alphak* assumes the statement above when conducting the theoretical convergence analysis of CG method. [7],

$$f(x_k+\alpha_k d_k) \le f(x_k)+\delta\alpha_k g_k^T p_k,\ 0 \le \delta \le \frac{1}{2}|p_k^T g(x_k+\alpha_k d_k)| \le -\sigma p_k^T g_k\ , \delta \le \sigma \le 1. \tag{5}$$

$\beta_k^{FR} = \frac{g_{k+1}^T g_{k+1}}{g_k^T g_k}$ [3]	$\beta_k^{CD} = \frac{g_{k+1}^T g_{k+1}}{-p_k^T g_k}$ [4]	$\beta_k^{BA1} = \frac{y_k^T y_k}{-p_k^T g_k}$ [10]
$\beta_k^{HS} = \frac{g_{k+1}^T y_{k+1}}{d_k^T y_k}$ [2]	$\beta_k^{LS} = \frac{g_{k+1}^T g_{k+1}}{-p_k^T g_k}$ [2]	$\beta_k^{BA2} = \frac{y_{k+1}^T y_{k+1}}{g_k^T g_k}$ [10]
$\beta_k^{PR} = \frac{g_{k+1}^T y_{k+1}}{g_k^T g_k}$ [7]	$\beta_k^{DY} = \frac{g_{k+1}^T g_{k+1}}{p_k^T y_k}$ [8]	$\beta_k^{BA3} = \frac{y_{k+1}^T y_{k+1}}{p_k^T y_k}$ [10]

Table 1: Classical Conjugate Gradient Conjugacy Parameters.

Recently, some scholars have presented innovative strategies and revised procedures, as evidenced in references [9–17]. In the subsequent sections, we will examine the given formula in detail, prove its attribute of decreasing, and offer valuable insights into its convergence.

2 New Direction for CG

Recent research has focused on enhancing the standard conjugate gradient approach by consolidating parameters inside the conjugate gradient methodology. Various hybrid algorithms were developed to use the strengths of classical conjugate gradient algorithms. Numerous hybrid methods were explored with the aim of obtaining conjugate gradient methods that were computationally efficient and exhibited favourable convergence features. Hybrid CG outperforms standard conjugated gradient algorithms [18, 19]. Malik *et al.* [20] have just created a novel β_k which is derived from the formula β_k^{NPRP}. The coefficient β_k is defined in the following manner:

$$\beta_k^{NPRP} = \begin{cases} X, & if \quad Y \\ \\ 0 & otherwise, \end{cases} \tag{6}$$

where

$$X = \frac{||g_k||^2 - \frac{||g_{k+1}||}{||g_k||}|g_{k+1}^T g_k| - |g_{k+1}^T g_k|}{||p_{k+1}||^2}, \tag{7}$$

$$Y = ||g_{k+1}||^2 > \left(\frac{g_{k+1}}{g_k} + 1\right)|g_{k+1}^T g_k|. \tag{8}$$

Using an equation similar to the one described above, we propose our approach which incorporates new computed values of β_k along with another spectral parameter θ_k. In Eq.(6), we integrate an X -equation into the modification of Eq. (7).

$$\beta_k^{NPRP} = \begin{cases} X, & if \quad Y \\ \\ 0 & otherwise, \end{cases} \tag{9}$$

$$X = \beta_k^{BA}. \tag{10}$$

β_k^{BA2}, as mentioned in Table 1 for Al-Bayati and Al-Asaady and $Y = ||g_{k+1}||^2 > \omega_k, |g_{k+1}^T g_k|, \omega_k = \frac{||g_{k+1}||}{||g_k||} + 1$, stay with the switch criteria. The imbalance of the formula BA2 is because the amount in the numerator is y^T y, it is the same problem found as in the Polak-Ribiere formula for conjugacy, where the method is frequently recovered when the slope in the new step is less than the old one. Also, frequent retrieval causes the

conjugacy parameter to become zero, slowing down the regression. Therefore, the return had to be done carefully and with the scale set below for that purpose. Furthermore, it is possible that the spectral search direction facilitates the rapid descent towards the optimal point. The main difference between standard and spectral conjugate gradient methods is the computation of the search direction P_k. The search direction of the normal conjugate gradient method is determined by applying the formula Eq. 3, but the search direction of the spectral conjugate gradient method is determined by scaling g_k using the formula

$$p_{k+1} = \begin{cases} -g_{k+1} & if\ k{=}0, \\ \\ -\theta_k g_{k+1} + \beta_k p_k, & if\ k{>}0. \end{cases} \tag{11}$$

In addition, Zhang et al. [21] also proposed a spectral conjugate gradient method which is called the SCD method. The SCD method is applied based on conjugate gradient coefficient (β_k) and spectral gradient parameter (θ_k):

$$\beta = \beta_k^{FR}\ and\ \theta_k = \frac{p_k^T y_k}{||g_k||^2}. \tag{12}$$

The conjugacy parameter (β^{MAR}) is imported and positioned in the second term of Eq.(6). The trend's ultimate manifestation is defined by newly established parameters:

$$\beta_k^{NPRP} = \begin{cases} X, & if \quad Y \\ \\ 0 & otherwise, \end{cases} \tag{13}$$

$$X = \beta_k^{NPRP}\ and\ Y = ||g_{k+1}||^2 > \omega_k, |g_{k+1}^T g_k|, \omega_k = \frac{||g_{k+1}||}{||g_k||} + 1. \tag{14}$$

Denote the conjugate parameter β_k^{NPRP} and spectral scaling for the gradient θ_k^{NPRP} as follows:

$$\theta_k = \frac{p_k^T y_k}{||g_k||^2}. \tag{15}$$

2.1 MAR-CG algorithm

Process (0): initialization, as start $k = 0$, set: $x_0 \epsilon \mathbb{R}^n$, compute all $f(x_0)$, $g(x_0)$, let $p_0 = -g_0$ and $\alpha_0 = 1/||g_0||_2$.
Process (1): Check for convergence: If $\|g_k\| \leq \epsilon$, then stop; x_k is the optimal solution; Else continue with Process (2).
Process (2): Second, obtain α_k in the line search process bearing in mind the Wolfe conditions and set variable $x_{k+1} = x_k + \alpha_k p_k$. Now coming to the input, find out f_{k+1}, g_{k+1}, y_k and p_k.
Process (3): Obtain the direction defined by $p_= - \theta_k^{MAR} g_{k+1} + \beta_k^{MAR} p_k$, β_k^{MAR} is set as described in Eq. (13).
Process (4): If we are satisfied with restarts from Powell's, set $p_{k+1} = -g_{k+1}$ and if not, set $p_{k+1} = p$.
Process (5): If we are satisfied with restarts from Powell's, set $(p_{k+1} = -g_{k+1})$ and if not set $(p_{k+1} = p)$
Process (6): Initialize the estimate with $\alpha_k = \alpha_{k-1} \left(\frac{||p_k||_2}{||pk-1||_2} \right)$, set $k = k+1$ and go back to Process (1).

3 Analysis of Convergence

We need to show that the new CG-Algorithms are globally convergent, which is a necessary condition.

3.1 Assumptions (H):

(i) We know that the set: $s = \{x : x \in R_n, f(x) \leq f(x_1)\}$ is bounded. Here, x_1 is the starting point and $c > 0$ is a constant. The following statement is true for all $B > 0$.
(ii) The model f is continuously-differentiable in the neighborhood Ω of S, and the gradient g satisfies a Lipschitz condition. Let $L \geq 0$ be a constant such that

$$||g(x) - g(y)|| \leq L||x - y|| \ \forall\, x, y \epsilon \Omega. \tag{16}$$

Now, by Assumption (H)(i), we can clearly find a positive constant D such that

$$B = max||x - y||, \ \forall\, x, y \epsilon S. \tag{17}$$

Define the set B to be the diameter of the domain Ω. From (H)(ii) we can actually deduce that there exists a positive constant $\Upsilon \geq 0$ such that:

$$||g(x)|| \leq \Upsilon, \ \forall\, x \epsilon S. \tag{18}$$

However this correct descent or descent condition is statistically problematic to ensure in general (see [3] for computational based methods in particular).

3.2 Theorem (Descendant property):

For simplicity, let us assume that Assumptions (H) are satisfied and that we use a line search method with strong Wolfe conditions as discussed in Sec. We prove in Eqs. (5) that the search directions p_k can be obtained from them. In (14) and (15), $c = \frac{(p_k^T y_k)}{||g_k||^2}$ immediately satisfies the required steering search sufficient condition;
$p_{k+1}^T g_{k+1} \leq -c||g_{k+1}||^2$.

Proof. Start with multiplying the direction p_{k+1} in Eq. (14) by the gradient g= g_{k+1},

$$p_{k+1}^T g = -\theta_k^| |g||^2 + \beta_k^{MAR} p_k^T g. \tag{19}$$

We have the condition $||g_{k+1}||^2 > \omega_k |g_{k+1}^T g_k|$ to switch between $\beta_k^{MAR} = 0$ or β_k^{BA}. In this case, $\beta_{k+1}^{MAR} = 0$ makes the descent hold directly.
Otherwise, set the value of the parameters β_k^{MAR} and θ_k,

$$p_{k+1}^T g_{k+1} = -\frac{p_k^T y_k}{||g_k||^2}||g_{k+1}||^2 + \frac{y_k^T y_k}{||g_k||^2} p_k^T g_{k+1}.$$

Utilize the reality given from the strong Wolfe conditions $p_k^T \ g_{k+1} < p_k^T \ y_k$, we get the inequality

$$p_{k+1}^T g_{k+1} \leq -\frac{p_k^T y_k}{||g_k||^2}||g_{k+1}||^2 + \frac{y_k^T y_k}{||g_k||^2} p_k^T y_k.$$

Or, we can rearrange the last term

$$p_{k+1}^T g_{k+1} \leq -\frac{p_k^T y_k}{||g_k||^2}||g_{k+1}||^2 + \frac{y_k^T y_k}{||g_k||^2} y_k^T y_k.$$

We have $y_k^T y_k = ||g_{k+1}||^2 + ||g_k||^2 - 2g_{k+1}^T g_k$, it implies that

$$p_{k+1}^T g_{k+1} \leq -\frac{(p_k^T y_k)}{||g_k||^2}||g_{k+1}||^2 + \frac{p_k^T y_k)}{||g_k||^2}(||g_{k+1}||^2 + ||g_k||^2 - 2g_{k+1}^T g_k)$$

$$p_{k+1}^T g_{k+1} \leq \frac{p_k^T y_k}{{g_k}^2}(||g_k||^2 - 2g_{k+1}^T g_k)$$

and A^T B$\leq \frac{1}{2}(A^2 + B^2)$ helps as in the second term

$$p_{k+1}^T g_{k+1} \leq \frac{p_k^T y_k}{||g_k||^2}||g_k||^2 - 2\frac{p_k^T y_k}{2{g_k}^2}(||g_{k+1}||^2 + ||g_k||^2)$$

$$p_{k+1}^T g_{k+1} \leq -c||g_{k+1}||^2$$

with c $= \frac{p_k^T y_k}{{g_k}^2}$.

3.3 Property (Boundedness of β_k)

Let us consider the existence of a generic conjugate gradient method and assume that [21]

$$\zeta \leq ||g_k|| \leq \Upsilon, \forall k \geq 0, \tag{20}$$

here ζ is positive. A CG-method is said to possess this characteristic if there are two constants $\lambda > 0$ and b > 1 that guaranty, for all k,

$$|\beta_k| \geq b \tag{21}$$

if

$$||p_k|| \leq \lambda \ , then \ |\beta_k| \leq \frac{1}{2b} \ \forall \lambda > 0. \tag{22}$$

3.4 Corollary (Boundedness of θ_k)

Since Assumptions (H) are satisfied, and by using line search with strong Wolfe conditions as described in Eq. (5) the search directions (p_k) are computed through Eqs. From both (14) and (15), we restrict θ_k.

Proof. Utilising the Cauchy-Schwarz inequality and the Lipschitz condition, we obtain

$$|\theta_k| = \left|\frac{p_k^T y_k}{g_k^T g_k}\right| = \frac{|p_k^T y_k|}{|g_k^T g_k|} \leq \frac{|d_k||y_k|}{||g_k||^2} < \frac{\lambda B}{\Upsilon^2} = \bar{b}.$$

3.5 Lemma (Boundedness of α_k)

Assuming that $\forall Y$ on the line segment from y to x, there exists a descent direction p_k and Lipshitz continuity is satisfied, let L be constant for all $\|g_k\|$ [7], thus line search direction satisfies Strong Wolfe condition.

$$\alpha_k \leq \frac{(1-\sigma)|p_k^T g_k|}{L{p_k}^2}. \tag{23}$$

Proof. employing the curvature inequality in Equation (5)

$$\sigma p_k^T g_k \leq p_k^T g_{k+1} \leq -\sigma p_k^T g_k \Rightarrow \sigma p_k^T g_k \leq p_k^T g_{k+1)}. \tag{24}$$

By subtracting $p_k^T g_k$ from both sides of (25) and applying the Lipschitz condition, the following results:

$$(1-\sigma) p_k^T g_k \leq p_k^T (g_{k+1} - g_k) \leq L\alpha_k ||p_k||^2 \tag{25}$$

Given that p_k represents the descending direction and $\sigma \leq 1$, the equation (24) is satisfied:

$$\alpha_k \geq \frac{(1-\sigma)|d_k^T g_k|}{L||d_k||^2}.$$

This lemma is referred to as the Zoutendijk condition [22] and then provide a global convergence proof for any nonlinear conjugate gradient method. From here, which first appeared in the strong Wolfe line search (Eq. (5). We will formulate this condition exactly next in the lemma.

3.6 Lemma

Suppose that Hypotheses (H) hold. Now, we will start analysing the iteration specified by Eqs. (2) and (3), where for each $k \geq 1$, we have descent condition ($p_k^T g_k = p_k^T g_k \leq 0$) and α_k satisfies (5). Subsequently,

$$\sum_{k\geq 0} \frac{(p_k^T g_k)^2}{(||p_k||^2)} < +\infty. \tag{26}$$

Proof. Using the inequality from before in Eq. (5), we obtain

$$f(x_{k+1}) - f(x_k) \leq \delta \alpha_k g_k^T p_k$$

The integration of this with the findings in the Lemma (Boundedness of α_k) produces

$$f_{k+1} - f_k \leq \left[\frac{\delta(1-\sigma)}{L}\right] \frac{(g_k^T p_k)^2}{||p_k||^2}. \tag{27}$$

By utilizing the boundedness of function f as stated in Assumptions (H), we get

$$\sum_{k>0} \frac{(g_k^T p_k)^2}{||p_k||^2} < \infty. \tag{28}$$

3.7 Theorem.

We assume that Assumption (H) holds and apply Eqs. (2),(3),(14), and (15) where α_k is using the strong Wolfe line search in Eq. (5),

$$\liminf_{k\to\infty} ||g_k|| = 0.$$

Proof. The contradiction method is employed to demonstrate that the conclusion is incorrect. Therefore, we assume that $||g_k|| \neq 0$, as previously stated. It is also established that there are constants ζ and Υ both greater than zero. $0 < \zeta \leq ||g_k|| \leq \Upsilon$, for all $k \geq 0$. Now, by calculating the square norm on both sides of our new direction

$$p_{k+1} = -\theta_k g_{k+1} + \beta_k^{MAR} p_k$$

$$\begin{aligned} p_{k+1} &= -\theta_k g_{k+1} + \beta_k^{MAR} p_k \\ &\leq \theta_{k+1}^M ||g_{k+1}|| + \beta_{k+1}^M ||d_k|| \\ &\leq ||g_{k+1}|| + \beta_{k+1}^M ||d_k|| \qquad (By\, the\, Cauchy - Schwarz\, property) \\ &< b\overline{\Upsilon} + b\lambda = C,\ where\, C = b\overline{\Upsilon} + b\lambda. \end{aligned}$$

Since $||p_{k+1}||^2 < (C)^2$, dividing by the quality $||g_{k+1}||^4$, we get

$$\frac{||p_{k+1}||^2}{||g_(k+1)||^4} < \frac{C^2}{||g_{k+1}||^4}.$$

$$\sum_{k=1}^{\infty} \frac{||p_{k+1}||^2}{||g_{k+1}||^4} > C^2 \Upsilon^{-2} = \infty.$$

This is in contradiction with Lemma, then $\liminf_{k\to\infty} ||g_k|| = 0$

4 Numerical Experiment Results

To determine the reliability of the proposed approaches, they are utilized for testing purposes. We compared our newly derived ways with standard approaches BA2 [23] and Malik CGM [20] and use comparable evaluation problems illustrated in Figures 1, 2, and 3. A comparison is made between several widely recognized test functions from CUTE [6], ranging in size from 100 to 1000, with an increasing number 300. The program was developed on Fortran 77 with employing double-precision arithmetic. The algorithm's relative performance is determined by the cumulative number of function evaluations, which usually involve the most expensive component in each iteration, as well as the total number of iterations. The prerequisites for convergence were

$$||g_{k+1}|| \ \leq 1 \times 10^{-5}. \tag{29}$$

A figure is shown to display the proportion P of issues that are completed in less than the desired time for each technique. The graph also shows the proportion of test questions that are solved quickly using a certain approach on the left side, and the percentage of test questions that each method solves correctly on the right side. The curve that demonstrates the greatest effectiveness in terms of problem-solving efficiency is represented as the uppermost curve. Figures 1, 2, and 3 compare MAR-New, BA2, and Malik CG-methods for a total of n various dimensions [100, 400, 700, 1000] for every assessment based on the measure of prefer ability in numerical optimization and the number of iterations and function evaluations; the fourth figure is CPU.

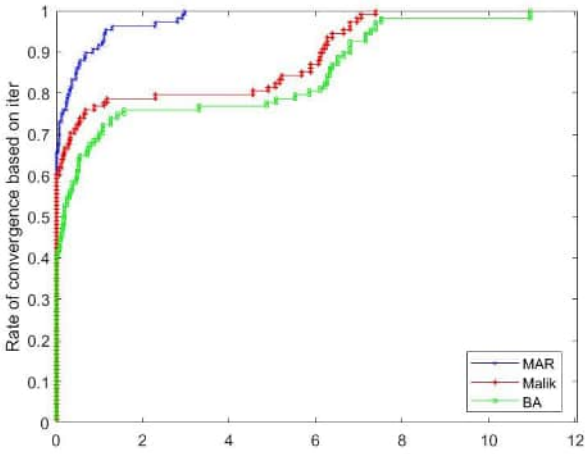

Figure 1: The performance of the compared methods in terms of iter.

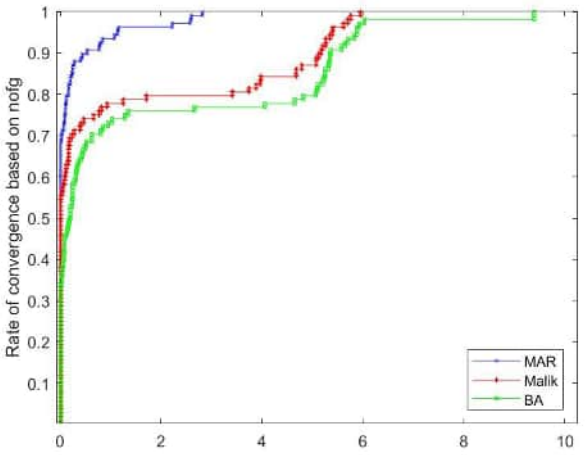

Figure 2: The performance of the compared methods in terms of nofg.

5 Conclusion

Ultimately, we propose robust conjugate gradient techniques (CG) that combine hybrid and spectral components, guided by the parameters β_k^{MAR} and θ_k^{MAR} to determine the search direction. These methods exhibit a notable advantage in ensuring satisfactory descent. Especially in the area of nonlinear dynamics, the gradient-based optimization frequently faces obstacles such as non-convexity, chaotic behavior, or stiff structures. Through a meticulous examination of descent qualities and global convergence for both uniformly convex and general nonlinear functions, we establish that our methodology is

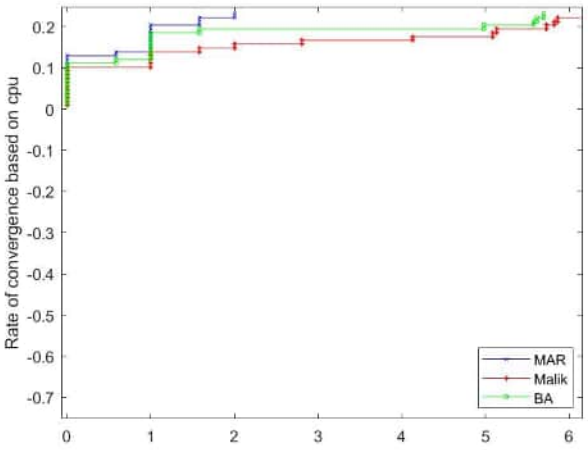

Figure 3: The time performance comparison of the approaches.

appropriately suited for dynamical systems governed by nonlinear equations, a fundamental issue in nonlinear dynamics. Additionally, the algorithms are proven to be globally convergent for both uniformly convex and general non-linear functions. The performance of the proposed CG algorithms against the traditional BA and Malik method is elucidated through some numerical experimentation results based on the essential parameters β_k^{MAR} and θ_k^{MAR}.

Acknowledgment

We thank the Ministry of Higher Education and Scientific Research Iraq, on its support of this project and assistance in completion, College of Science University of Kirkuk and the College of Environmental Sciences at successful University of Mosul for their kind cooperation in providing a suitable environment to complete this work.

References

[1] C. Souli and A. Leulmi. Study of a Penalty Method for Nonlinear Optimization Based on a New Approximate Function. *Nonlinear Dynamics and Systems Theory* **23** (5) (2023) 561–570.

[2] A. M. Jasim, A. A. Ali, I. H. Halil, F.Z. Ahmed and M. A. Shallal. Numerical Solution for Benjamin-Bona-Mahony-Burgers Equation Using Septic B-Spline Galerkin Method. *Nonlinear Dynamics and Systems Theory* **24** (3) (2025) 267–274.

[3] R. Fletcher and C. M. Reeves. Function minimization by conjugate gradients. *Comput J.* **7** (2) (1964) 149–154.

[4] R. Fletcher. *Practical Methods of Optimization.* John Wiley & Sons, 2000.

[5] M. L. Ouaoua, S. Khelladi and D. Benterki. New parameter of conjugate gradient method for unconstrained nonlinear optimization. *Statistics, Optimization and Information Computing* **13** (6) (2025) 2382–2390.

[6] N. Andrei. An Unconstrained Optimization Test Functions Collection. *Advanced Modeling and Optimization* (2008) 147–161.

[7] E. Polak and G. Ribiere. Note sur la convergence de méthodes de directions conjuguées. *ESAIM: Mathematical Modelling and Numerical Analysis-Modélisation Mathématique et Analyse Numérique* **3** (1) (1969) 35–43.

[8] Y. H. Dai and Y. Yuan. A nonlinear conjugate gradient method with a strong global convergence property. *SIAM Journal on Optimization* **10** (1) (1999) 177–182.

[9] Z. Dai, X. Chen and F. Wen. A modified Perry's conjugate gradient method-based derivative-free method for solving large-scale nonlinear monotone equations. *Applied Mathematics and Computation* **270** (2015) 378–386.

[10] M. Jameel, A. Al-Bayati and Z. Algamal. Scaled multi-parameter (SMP) nonlinear QN-algorithms. *In AIP Conference Proceedings* **2845** (1) (2023).

[11] P. Faramarzi and K. Amini. A modified spectral conjugate gradient method with global convergence. *Journal of Optimization Theory and Applications* **182** (2019) 667–690.

[12] Z. Sun, H. Li, J. Wang and Y. Tian. Two modified spectral conjugate gradient methods and their global convergence for unconstrained optimization.*International Journal of Computer Mathematics* **95** (10) (2018) 2082–2099.

[13] E. T. Hamed, R. Z. Al-Kawaz and A. Y. Al-Bayati. A new investigation for the liu-story scaled conjugate gradient method for nonlinear optimization. *Journal of Mathematics* (2020) 1–12.

[14] H. I. Ahmed, R. Z. Al-Kawaz and A. Y. Al-Bayati. Spectral three-term constrained conjugate gradient algorithm for function minimizations. *Journal of Applied Mathematics* (2019) 1–6.

[15] H. T. Saeed Chilmeran, E. T. Hamed, H. I. Ahmed and A. Y. Al-Bayati. A Method of Two New Augmented Lagrange Multiplier Versions for Solving Constrained Problems. *International Journal of Mathematics and Mathematical Sciences* (2022) 1–6.

[16] S. O. T. Mohammad, H. T. S. Chilmeran and R. Z. Al-Kawaz. A New Scalar of Conjugate Gradient Methods for Solving Unconstrained Minimization. *European Journal of Pure and Applied Mathematics* **16** (1) (2023) 233–242.

[17] H. Wu, L. Wang, and H. Zhang. An Improved Spectral Conjugate Gradient Algorithm Based on A Modified Wolfe Line Search. *arXiv preprint arXiv* **2302** (2023) 09816.

[18] Y. H. Dai. A family of hybrid conjugate gradient methods for unconstrained optimization. *Math Comput.* **72** (243) (2023) 1317–1328.

[19] D.Touati-Ahmed and C. Storey. Efficient hybrid conjugate gradient techniques.*J Optim Theory Appl.* **64** (2023) 379–397.

[20] M. Malik, M. Mamat, S. S. Abas and I. M. Sulaiman. A New Coefficient of the Conjugate Gradient Method with the Sufficient Descent Condition and Global Convergence Properties. *Engineering Letters* **28** (3) (2020) 1–11.

[21] L. Zhang and W. Zhou. Two descent hybrid conjugate gradient methods for optimization.*J Comput. Appl. Math.* **216** (1) (2008) 251—264.

[22] G. Zoutendijk. Nonlinear programming, computational methods. *Integer and nonlinear programming* (1970) 37–86.

[23] M. S. Jameel, A. A. Al-Arbo and R. Z. Al-Kawaz. Robust and Hybrid Conjugate Gradient Method for Modern Unconstrained Optimization Methods. *Mathematical Modelling of Engineering Problems* **12** (6) (2025) 2170–2176.

Nonlinear Dynamics and Systems Theory, **26** (2) (2026) 173–183

Advanced Kalman Filter Implementation for Estimating Yaw Coefficient in Amphibious Plane Motion Experiments

T. Herlambang [1], Y. F. Kusuma [2], S. Syamsuar [3], H. Hendrato [3], R. S. Marjianto [4*], Z. Othman [5] and M. Muhammad [3]

[1] *Information System Department, Faculty of Economy Business and Digital Technology, Universitas Nahdlatul Ulama Surabaya, Jalan Jemursari (Kompleks RSI Jemursari) 57, Surabaya 60237, Indonesia.*
[2] *Research Center for Hydrodynamic Technology, National Research and Innovation Agency, KS Said Djauharsjah Jenie, Sukolilo, Surabaya, East Java 60112, Indonesia.*
[3] *Research Center for Transportation Technology, National Research and Innovation Agency, KST B.J Habibie, Setu, South Tangerang, Banten 15314, Indonesia.*
[4] *Department of Engineering, Faculty of Vocational Studies, Universitas Airlangga, Indonesia.*
[5] *Department of Diploma Studies, Universiti Teknikal Malaysia Melaka, Malaysia.*

Received: December 17, 2025; Revised: March 24, 2026

Abstract: Indonesia is a maritime country with a larger ocean area than land. This issue must be addressed with proper supporting transportation that serves as both a method of mobilization and defence. Amphibious planes are versatile modes of transportation that are suitable for usage in Indonesian coastal areas. Amphibious aircraft are equipped with a navigation system and technology to move both in the air and on water. The amphibious aircraft's mobility is also engineered to allow it to take off and land on its intended trajectory. Several approaches have been developed to calculate the amphibious aircraft's trajectory. These approaches are continuously refined to achieve the desired level of accuracy. The commonly used estimation calculation methods are the Ensemble Kalman Filter and the Kalman Filter. The Ensemble Kalman Filter method is a development of the Kalman Filter which can be used to estimate linear and non-linear system models. The Kalman Filter is the forerunner of the Ensemble Kalman Filter method which can only be used to estimate linear dynamic system models. The Ensemble Kalman Filter method successfully obtained the best prediction error value with an RMSE value of 0.0876 with a total of 400 ensembles. Meanwhile, the Kalman Filter method successfully obtained the best prediction error value with an RMSE value of 0.000237.

Keywords: *amphibious plane; trajectory estimation; ensemble Kalman filter; Kalman filter.*

Mathematics Subject Classification (2020): 93E11, 93C41, 60G35.

* Corresponding author: mailto:rachmansinatriya@vokasi.unair.ac.id

1 Introduction

Indonesia is the biggest country in Southeast Asia region. In addition, Indonesia is also the world's largest archipelagic country, with a vast maritime area [1, 2]. This circumstance positioned the Indonesian sea as the gateway to the Indo-Pacific region, a strategic fishing area, a hub for trade and commerce, and the largest country in Southeast Asia [2]. Given the scattered nature of the islands, many of which are isolated by sea, a reliable and multifunctional transportation mode is required. Furthermore, it can be used to help the country maintain its sovereignty.

Amphibious planes are one type of supporting mode of transportation that may operate on both water and land. Amphibious planes are mostly employed as support vehicles for search and rescue operations, delivering products to isolated locations and underdeveloped areas, assisting with firefighting efforts, and so on [3]. Several experiments and research are being conducted to optimize the design and performance of amphibious aircraft. The main goal is to reduce the resistance force to allow for a faster takeoff with less engine power, resulting in lower fuel consumption [4].

Due to the variety of functions, careful consideration must be given to the design planning and acceleration calculations during takeoff and landing. Moreover, vertical acceleration is a more significant factor, which not only causes mental problems for the crew, but can cause structural damage to the fuselage when touching water. More attention should be given to the load characteristics of seaplanes when landing on water [5]. Therefore, for amphibious aircraft to move in accordance with their trajectory, sophisticated navigation technology and guidance systems are required.

The calibration in this study was conducted using the Kalman Filter Ensemble (EnKF) and Kalman Filter techniques. The Kalman Filter Ensemble approach (EnKF) is a modified estimation approach of the Kalman Filter algorithm that may be used to estimate linear and nonlinear system models by producing a number of ensembles for their error co-variants during the prediction stage [6]. The Kalman Filter is a widely used estimating tool in control and navigation systems [8]. In the previous research, the Ensemble Kalman Filter (EnKF) approach was used to estimate the position of autonomous vehicles [9]. Meanwhile, the Kalman Filter (KF) approach is used to determine the orientation and translation of UAV motions [10].

2 Data and Mathematical Modeling

The forces acting on unmanned seaplanes can be divided into four categories: aircraft mass, hydrodynamic force, aerodynamic force, and engine thrust, as seen in Figure 1. The following equation represents a nonlinear unmanned seaplane's longitudinal dynamic motion.

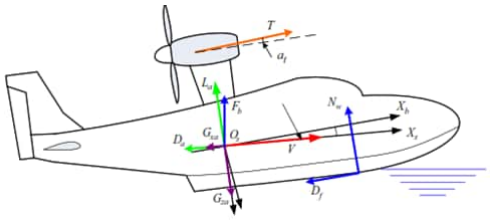

(a)

(b)

(c)

Figure 1: (a) and (b) The aerodynamic model of amphibious aircraft during the wind tunnel test [12].

It employs the Earth coordinate system $X_e; Y_e; Z_e$, then plane body coordinate system $X_b; Y_b; Z_b$ and the steady-translation coordinate system $X_s; Y_s; Z_s$.

$$\begin{aligned}
m\dot{V} &= T\cos(\alpha+\alpha_t) - D_a - N_w\sin\alpha - D_f\cos\alpha + G_{xa},\\
mV\dot{\alpha} &= mVq - T\sin(\alpha+\alpha_t) - L_a - N_w\cos\alpha + D_f\sin\alpha + G_{za},\\
I_y\dot{q} &= M_a + M_w + M_T,\\
\dot{\theta} &= q,\\
\dot{x}_g &= u\cos\theta + w\sin\theta,\\
\dot{z}_g &= -u\sin\theta + w\cos\theta.
\end{aligned}$$

The dataset used in this study is based on the research findings (primary data). The data in this study was analyzed using the Python programming language with a dataset similar to that in Table 2 below.

Symbol	Description	Symbol	Description
A	Angle of attack	m	Seaplane mass
Ø	Angle of Pitch	D_a	Aerodynamic drag force
V	Speed	G_{xa}	gravity along Xs
α_t	Angle between engine force to Xb	G_{za}	gravity along Zs
M_a	Total pitching moments from the air	X_g	position of aircraft along the Xe
M_w	Total pitching moments from the air	Z_g	aircraft positions along Ze
M_T	Total Pitching Moments from the Engine	u	aircraft speed components along Xb
T	Engine thrust	w	aircraft speed components along Zb
N_w	Normal directional water pressure at the bottom of the aircraft	q	Angular rate pitch (increase/ decrease of pitch angle
D_f	Water friction along the bottom of the aircraft	I_y	Seaplane moment of inertia against Yb
L_a	Aerodynamic lift force	$\dot{\theta}$	Increase/decrease of the angle of pitch
$\dot{V}$	Speed gain/decrease	$\dot{\alpha}$	Increase/decrease of the angle of attack

Table 1: Description of the amphibious aircraft model parameters.

2.1 Mathematical model of Ensemble Kalman Filter (EnKF)

$$x_{k+1} = f(k, x_k) + w_k, \tag{1}$$

$$z_k = Hx_k + v_k, \tag{2}$$

$$x_0 \sim N(\bar{x}_0, P_{x_0}),\ w_k \sim N(0, Q_k),\ v_k \sim N(0, R_k), \tag{3}$$

$$X_{0,i} = [x_{0,1}\ \ x_{0,2}\ \ x_{0,3}\ \ \cdots\ \ x_{0,N_e}], \tag{4}$$

$$\hat{x}_k^* = \frac{1}{N_e}\sum_{i=1}^{N_e} x_{k,i}, \tag{5}$$

$$P_k = \frac{1}{N_e - 1}\sum_{i=1}^{N_e}(\hat{x}_{k,i} - \hat{x}_k)(\hat{x}_{k,i} - \hat{x}_k)^T. \tag{6}$$

RUN	ALFA	BETA	CL	CY
13	-10,4	0	-0,567133333	-0,005233333
13	-9,393333333	0	-0,5438	-0,003833333
13	-8,35	0	-0,498733333	-0,005666667
13	-7,303333333	0	-0,440433333	-0,006466667
13	-6,24	0	-0,3466	-0,006866667
13	-5,18	0	-0,2584	-0,0046
13	-4,1	0	-0,150066667	-0,004233333
13	-3,03	0	-0,034	-0,003533333
13	-1,93	0	0,0798	-0,0025
13	-0,86	0	0,197133333	-0,0018
13	0,22	0	0,315566667	-0,001566667
13	1,29	0	0,438533333	-0,002833333
13	2,39	0	0,560533333	-0,0028
13	3,466666667	0	0,6812	-0,0023
13	4,56	0	0,802433333	-0,0015
13	5,65	0	0,924866667	-0,0012
13	6,73	0	1,0427	-0,001633333
13	7,81	0	1,160233333	-0,0017
13	8,89	0	1,279533333	-0,001366667
13	9,96	0	1,3949	-0,001366667
13	11,35	0	1,537083333	-0,000583333
13	12,395	0	1,636716667	-0,000116667
13	13,465	0	1,732683333	0,000416667
...	...	...	...	...
20	16,345	0	2,284183	-0,025583333

Table 2: Dataset.

2.2 Mathematical model of Kalman Filter (KF)

Kalman Filter (KF) is a method for solving state estimation problems. This method is commonly known as the Linear Quadratic Estimator (LQE) since it minimizes the quadratic function of estimate error in a linear dynamic system with white measurement and disturbance noise [8]. The Kalman Filter technique has the following mathematical function.

A discrete linear stochastic dynamic system is generally given in the form

$$x_{k+1} = A_k x_k + B_k u_k + G_k w_k, \tag{7}$$

$$z_k = H_k x_k + v_k, \tag{8}$$

$$x_0 \sim N(\bar{x}_0, P_{x_0}),\ w_k \sim N(0, Q_k),\ v_k \sim N(0, R_k), \tag{9}$$

where: x_0 : initialization of the system,
x_{k+1} : state variable at time $k+1$ and dimension $n \times 1$,
x_k : state variable at time k with initial estimated value $\bar{x}_0$ and early covariants P_{x_0}, $x_k \in \mathbb{R}^n$,
u_k : deterministic input vector at time k, $u_k \in \mathbb{R}^m$,

w_k : noise on the system with mean $\bar{w}_k = 0$ and covariants Q_k,
z_k : measurement variables, $z_k \in \mathbb{R}^p$,
v_k : noise on the measurement with mean $\bar{v}_k = 0$ covariants R_k,
A_k, B_k, G_k, H_k: the matrices with the values of their elements being the coefficients of their respective variables.

In the Kalman Filter, estimation is carried out in two stages: the prediction stage (time update) predicts state variables based on a dynamic system, and the correction stage (measurement update) corrects the measurement data to improve estimation results.

The prediction stage is influenced by the dynamics of the system by predicting state variables using the state variable estimation equation and the accuracy level is calculated using the error covariance equation. In the correction stage, the results of the estimation of the state variables obtained at the prediction stage are corrected using a measurement model. One part of this stage is to determine the Kalman Gain matrix that is used to minimize error covariance. The prediction and correction stages are carried out recursively by minimizing the covariance of estimation errors $(x_k - x\hat{k})$, x_k is a variable of actual circumstances and $x\hat{k}$ is an estimate of the variables of the situation.

3 Simulation Results

From the results of simulation using the Ensemble Kalman Filter method (EnKF) and Kalman Filter (KF), the visualization results in the form of prediction plot are shown in Figure 2 below.

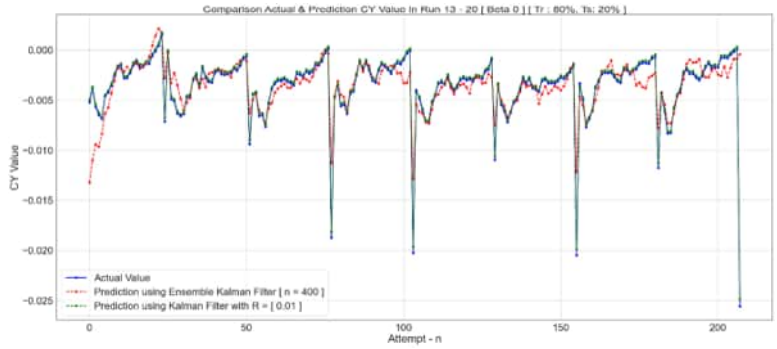

Figure 2: CY Value Prediction Plot using the EnKF method of 400 ensembles with observation models of 0.8 and KF.

The first simulation was carried out using the Kalman Filter Ensemble (EnKF) method with a total of 400 ensembles and Kalman Filter. At this stage, the observation model of the Ensemble Kalman Filter (EnKF) is set with a value of 0.8 with a total of 400 ensembles. The prediction results of the Ensemble Kalman Filter (EnKF) method produced an RMSE value of 0.0876. Then, for the Kalman Filter method with an R value of 0.01, it produced an RMSE value of 0.00023. The plot visualization of the Ensemble Kalman Filter (EnKF) method, indicated by the red line, looks close to the actual value with dynamic conditions. As for the plot visualization of the Kalman Filter

method indicated by the green line, it looks close to the actual value with a small margin of error.

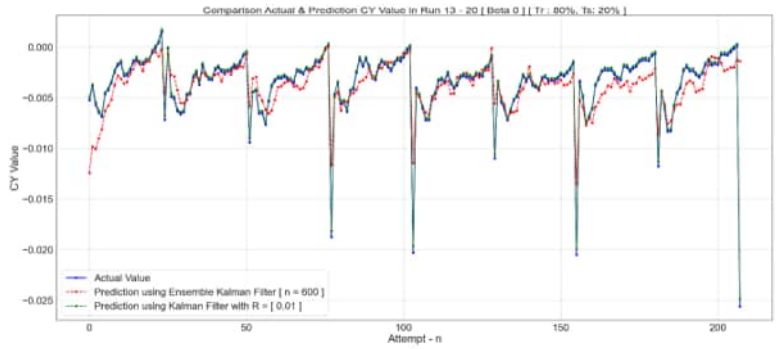

Figure 3: CY Value Prediction Plot using the EnKF method of 600 ensembles with observation models of 0.8 and KF.

The second simulation was carried out using the Kalman Filter Ensemble (EnKF) method with a total of 600 ensembles and Kalman Filter. At this stage, the observation model of the Kalman Filter Ensemble (EnKF) is set with a value of 0.8 with a total of 600 ensembles. The prediction results of the Ensemble Kalman Filter (EnKF) method produced an RMSE value of 0.0865. Then, for the Kalman Filter method with an R value of 0.01, it produced an RMSE value of 0.00023. The plot visualization of the Ensemble Kalman Filter (EnKF) method, indicated by the red line, looks close to the actual value with dynamic conditions. As for the plot visualization of the Kalman Filter method shown by the green line, it looks close to the actual value with a small margin of error. In this second simulation, the RMSE value of the Ensemble Kalman Filter (EnKF) method decreased by 0.0011.

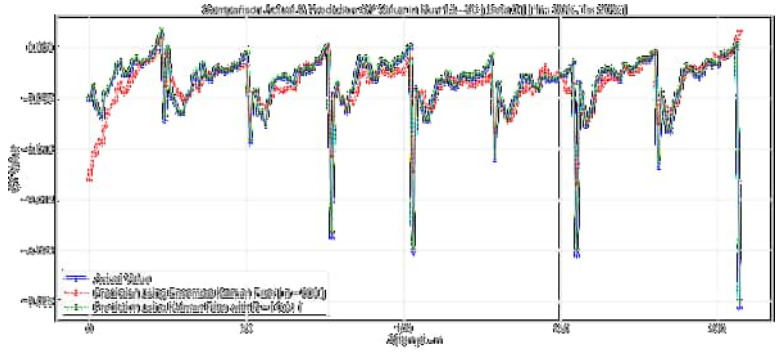

Figure 4: CY Value Prediction Plot using the EnKF method of 800 ensembles with observation models of 0.8 and KF.

The third simulation was carried out using the Kalman Filter Ensemble (EnKF) method with a total of 800 ensembles and Kalman Filter. At this stage, the observation model of the Ensemble Kalman Filter (EnKF) is set with a value of 0.8 with a total of 800 ensembles. The prediction results of the Ensemble Kalman Filter (EnKF) method produced an RMSE value of 0.0909. Then, for the Kalman Filter method with an R

value of 0.01, it produced an RMSE value of 0.00023. The plot visualization of the Ensemble Kalman Filter (EnKF) method, indicated by the red line, looks close to the actual value with dynamic conditions. As for the plot visualization of the Kalman Filter method shown by the green line, it looks close to the actual value with a small margin of error. In this third simulation, the RMSE value of the Ensemble Kalman Filter (EnKF) method increased by 0.0044.

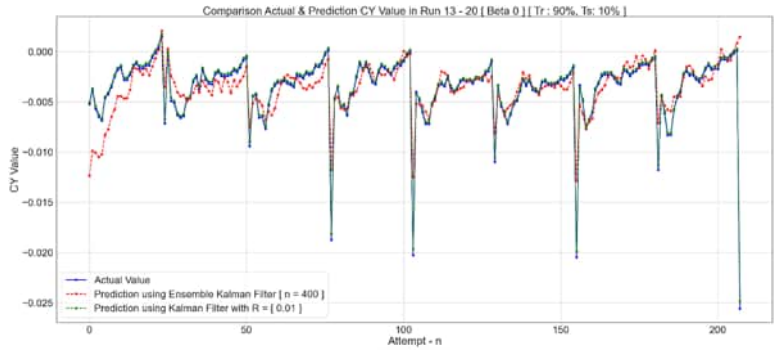

Figure 5: CY Value Prediction Plot using the EnKF method of 400 ensembles with observation models of 0.9 and KF.

The fourth simulation was carried out using the Kalman Filter Ensemble (EnKF) method with a total of 400 ensembles and Kalman Filter. At this stage, the observation model of the Kalman Filter Ensemble (EnKF) is set with a value of 0.9 with a total of 400 ensembles. The prediction results of the Ensemble Kalman Filter (EnKF) method produced an RMSE value of 0.0927. Then, for the Kalman Filter method with an R value of 0.01, it produced an RMSE value of 0.00023. The plot visualization of the Ensemble Kalman Filter (EnKF) method, indicated by the red line, looks close to the actual value with dynamic conditions. As for the plot visualization of the Kalman Filter method shown by the green line, it looks close to the actual value with a small margin of error. In this fourth simulation, the Kalman Filter method did not experience an increase or decrease in the error value (RMSE).

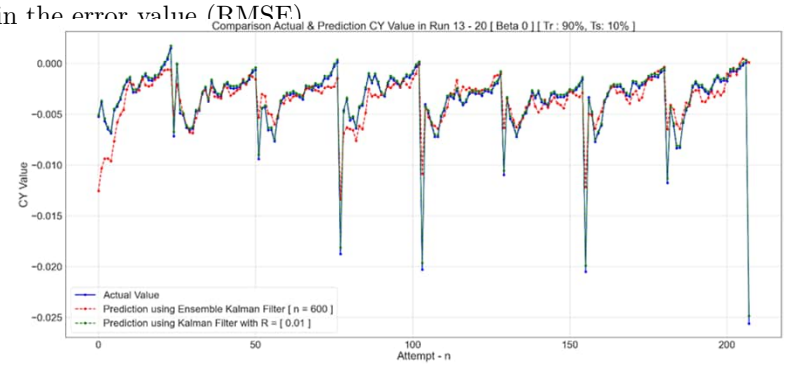

Figure 6: CY Value Prediction Plot using the EnKF method of 600 ensembles with observation models of 0.9 and KF.

The fifth simulation was carried out using the Kalman Filter Ensemble (EnKF)

method with a total of 600 ensembles and Kalman Filter. At this stage, the observation model of the Kalman Filter Ensemble (EnKF) is set with a value of 0.9 with a total of 600 ensembles. The prediction results of the Ensemble Kalman Filter (EnKF) method produced an RMSE value of 0.0889. Then, for the Kalman Filter method with an R value of 0.01, it produced an RMSE value of 0.00023. The plot visualization of the Ensemble Kalman Filter (EnKF) method, indicated by the red line, looks close to the actual value with dynamic conditions. As for the plot visualization of the Kalman Filter method shown by the green line, it looks close to the actual value with a small margin of error. In this fourth simulation, the Kalman Filter method did not experience an increase or decrease in the error value, and the Kalman Filter Ensemble method experienced a decrease in the error value (RMSE) of 0.0038.

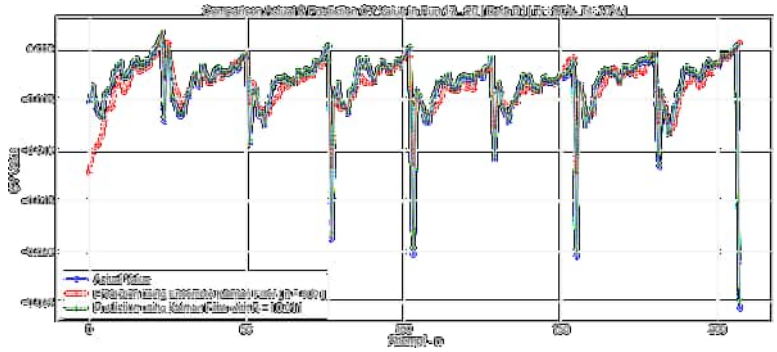

Figure 7: CY Value Prediction Plot using the EnKF method of 800 ensembles with observation models of 0.9 and KF.

The sixth simulation was carried out using the Kalman Filter Ensemble (EnKF) method with a total of 800 ensembles and Kalman Filter. At this stage, the observation model of the Kalman Filter Ensemble (EnKF) is set with a value of 0.9 with a total of 600 ensembles. The prediction results of the Ensemble Kalman Filter (EnKF) method produced an RMSE value of 0.0884. Then, for the Kalman Filter method with an R value of 0.01, it produced an RMSE value of 0.00023. The plot visualization of the Ensemble Kalman Filter (EnKF) method, indicated by the red line, looks close to the actual value with dynamic conditions. As for the plot visualization of the Kalman Filter method shown by the green line, it looks close to the actual value with a small margin of error. In this fourth simulation, the Kalman Filter method did not experience an increase or decrease in error value, and the Kalman Filter Ensemble method experienced a decrease in error value (RMSE) of 0.0005.

The simulation results of the Ensemble Kalman Filter (EnKF) method and the Kalman Filter method can be seen in Table 3 below.

Nilai Observation Model	Jumlah Nilai RMSE	Nilai RMSE Ensemble Kalman Filter	Nilai RMSE Kalman Filter
0,8	400	0,0876	0,00023
	600	0,0865	
	800	0,0909	
0,9	400	0,0927	
	600	0,0889	
	800	0,0884	

Table 3: Comparison of RMSE values.

Table 3 displays the entire series of simulations using the Ensemble Kalman Filter (EnKF) and Kalman Filter methods. The dynamic simulation by the Ensemble Kalman Filter (EnKF) method showed the best simulation results in the second simulation stage with an RMSE value of 0.0865. Meanwhile, the simulation by the Kalman Filter method showed constant results from the first simulation to the end.

4 Conclusion

Based on the simulation results, it can be concluded that the second simulation, which used the Ensemble Kalman Filter (EnKF) method, yielded the best prediction error (RMSE) of 0.0865. Furthermore, using the Kalman Filter method with R = 0.01 yielded the best prediction error (RMSE) of 0.00023 across all simulations. The results show that the Ensemble Kalman Filter (EnKF) and Kalman Filter methods produce good predictions with a 1% error rate and are consistent, thus they can be recommended for further research.

Acknowledgment

Our deep gratitude goes to Prof. Dr. Cuk Supriyadi Ali Nandar. as Head of the Energy and Manufacturing Research Organization, BRIN as the person in charge of the Indonesia Maju Research and Innovation Program with contract number 60/II/HK/2022 and 8/III.3/HK/2024, and also many thanks to LPPM Universitas Nahdlatul Ulama Surabaya (UNUSA) for supporting and facilitating the writing of this publication. Additionally, gratitude is extended to the Centre of Research and Innovation Management of Universiti Teknikal Malaysia Melaka (UTeM) for sponsoring the publication fees under the Tabung Penerbitan CRIM UTeM.

References

[1] I. M. Ali and D. Sianturi. Strategi pertahanan laut dalam menghadapi ancaman keamanan maritim di wilayah laut Indonesia. *Jurnal Education and Development* **10** (2) (2022) 372–379.

[2] M. R. Iswardhana, W. Adi and H. C. Chotimah. Strategi keamanan laut pemerintah Indonesia untuk menjaga keamanan maritim. *NUSANTARA: Jurnal Ilmu Pengetahuan Sosial* **8** (6) (2021) 1406–1428.

[3] A. Seth and R. P. Liem. Amphibious aircraft developments: computational studies of hydrofoil design for improvements in water-takeoffs. *Aerospace* **8** (1) (2020) 10.

[4] Y. F. Kusuma, Sulistiya, Hendrato, Muhammad, B. Halfina, I. Ansori, A. D. Kurniawan, G. Verma, D. H. Priatno, A. F. Paripurna and Widyawasta. The effect of floater shape on amphibious aircraft's drag coefficient using computational fluid dynamics method. *International Review of Aerospace Engineering* **17** (2) (2024) 50–59.

[5] Y. Lu, A. Del Buono, T. Xiao, A. Iafrati and S. Deng. Loads prediction at early stage of water landing on amphibious aircraft with a V-shaped hull.

[6] D. Agustin, E. Apriliani and H. Nurhadi. Implementasi ensemble Kalman filter pada estimasi gerak proyektil di bawah pengaruh faktor temperatur dan kecepatan angin.

[7] M. Sammang, F. Mahmuddin and H. Rivai. Sistem monitoring energi surya jarak jauh (wireless photovoltaic monitoring system). *Jurnal Penelitian Enjiniring* **26** (2) (2022) 67–75.

[8] M. Khuluq, A. Pratahtya and R. T. Imansyah. Pengembangan autonomous UAV untuk sistem delivery dengan optimator adaptive sliding mode control dan Kalman filter. *Buletin Pagelaran Mahasiswa Nasional Bidang Teknologi Informasi dan Komunikasi* **1** (1) (2023) 16–22.

[9] A. Wahyantika. *Estimasi posisi autonomous car menggunakan metode ensemble Kalman filter (EnKF) dengan kendali gerak sliding-mode.* PhD Thesis, Institut Teknologi Sepuluh Nopember, 2021.

[10] F. Kurniawan, E. Nasution, M. Ridlo, O. Dinaryanto and L. Lasmadi. Penentuan orientasi dan translasi gerakan UAV menggunakan data fusion berbasis Kalman filter. *Aviation Electronics, Information Technology, Telecommunications, Electricals, Controls* **3** (2) (2021) 99–116.

[11] Z. Liang, S. Fan, J. Feng, P. Yuan, J. Xu, X. Wang and D. Wang. An enhanced adaptive ensemble Kalman filter for autonomous underwater vehicle integrated navigation. *Drones* **8** (12) (2024) 711.

[12] S. Nurrahma, T. A. Berbudi, M. R. Firdaus, G. Izzaulhaq and I. Hudati. Implementasi kontrol PID pada kopel motor DC dengan menggunakan filter Kalman. *Jurnal Listrik, Instrumentasi, dan Elektronika Terapan* **4** (1).

[13] T. Herlambang, S. Syamsuar, F. Yudianto, A. Basuki, G. Wijiatmoko, A. Roschyntawati and R. S. Marjianto. Trajectory estimation of amphibious aircraft using H-infinity and ensemble Kalman filter methods. *Nonlinear Dynamics and Systems Theory* **24** (3) (2024) 259–266.

[14] T. Herlambang, D. Rahmalia, H. Nurhadi, A. Suryowinoto and A. Muhith. Estimation of remote operated vehicle motion in XY plane using unscented Kalman filter. In: *AIP Conference Proceedings* **2679** (1) (2023).

Nonlinear Dynamics and Systems Theory, **26** (2) (2026) 184–194

A New Hybrid Conjugate Gradient Method Based on RMIL, LS and CD Methods

Samia Khelladi * and Youcef Elhamam Hemici

Laboratory of Fundamental and Numerical Mathematics, Department of Mathematics, Faculty of Sciences, Setif 1 University Ferhat Abbas, 19000, Algeria.

Received: March 17, 2025; Revised: March 30, 2026

Abstract: We propose a new hybrid conjugate gradient method for unconstrained optimization problems. The method combines the RMIL, LS and CD formulas through a convex combination to build a more effective search direction. This approach aims to improve both convergence and numerical performance. The hybrid parameter β_k is updated to satisfy the conjugacy condition and global convergence is proven under the strong Wolfe line search. Numerical results on test problems show that the new method is better than other existing approaches in terms of iterations and CPU time.

Keywords: *unconstrained optimization; hybrid conjugate gradient method; descent direction; line search; global convergence.*

Mathematics Subject Classification (2020): 65K05, 90C26, 90C30, 93-10.

1 Introduction

Unconstrained optimization problems appear in many areas such as machine learning, data fitting, finance and control systems. These problems are generally written as

$$\begin{cases} \min\ f(x) \\ x \in \mathbb{R}^n, \end{cases} \tag{1}$$

where $f : \mathbb{R}^n \to \mathbb{R}$ is a continuously differentiable function.

When the dimension n is large, solving this problem efficiently becomes important. One of the most effective and memory-saving methods used is the nonlinear conjugate gradient (CG) method. These methods are known for their low storage requirements and

* Corresponding author: mailto:samia.boukaroura@univ-setif.dz

are widely used in practice due to their simplicity and strong performance. Moreover, the nonlinear CG method plays a crucial role in nonlinear dynamics [9, 11], where many problems such as trajectory optimization, equilibrium analysis and model calibration can be reformulated as large-scale unconstrained optimization problems. In such contexts, CG methods provide a computationally efficient framework to handle the high dimensions and complex structure typical of dynamical systems, without the need to compute or store second-order derivatives.

Starting from an initial point x_0, the conjugate gradient method updates the solution using the formula

$$x_{k+1} = x_k + \alpha_k d_k, \tag{2}$$

where $\alpha_k > 0$ is the step size, often found using a line search, and d_k is the search direction computed by

$$d_k = \begin{cases} -g_0, & \text{if } k = 0, \\ -g_k + \beta_k d_{k-1}, & \text{if } k \geq 1. \end{cases} \tag{3}$$

Here, $g_k = \nabla f(x_k)$ is the gradient of the objective function at the k-th step, and β_k is a scalar used to generate the new search direction.

Several formulas for β_k exist in the literature. Notable examples include those by Hestenes and Stiefel (HS), Fletcher and Reeves (FR), Polak–Ribière–Polyak (PRP) and Conjugate Descent (CD) [1]. In addition, see Liu and Storey (LS) [10], Dai and Yuan (DY) [2], and Rivaie et al. (RMIL) [13]. According to Hager and Zhang [7], methods like FR, CD, and DY have solid convergence properties, while others, such as HS, PRP and LS, often give better numerical results.

Some classical formulas for β_k are given by

$$\beta_k^{HS} = \frac{g_{k+1}^T y_k}{d_k^T y_k}, \quad \beta_k^{FR} = \frac{\|g_{k+1}\|^2}{\|g_k\|^2}, \quad \beta_k^{PRP} = \frac{g_{k+1}^T y_k}{\|g_k\|^2}, \quad \beta_k^{CD} = -\frac{\|g_{k+1}\|^2}{g_k^T d_k},$$

$$\beta_k^{LS} = -\frac{g_{k+1}^T y_k}{g_k^T d_k}, \quad \beta_k^{DY} = \frac{\|g_{k+1}\|^2}{d_k^T y_k}, \quad \beta_k^{RMIL} = \frac{g_{k+1}^T y_k}{\|d_k\|^2},$$

where $y_k = g_{k+1} - g_k$ and $\|\cdot\|$ denotes the Euclidean norm.

To improve the performance and stability of CG methods, researchers have developed hybrid formulas by combining two or more β_k expressions. Some are convex combinations, while others are non-convex. Many such combinations have been proposed in the literature [3, 4, 8, 12–14].

In this paper, we propose a new hybrid method called RMILCDLS, which blends the RMIL, CD and LS formulas using a convex combination. The aim is to take advantage of the strong global convergence of RMIL and CD, while also using the numerical performance of the LS method.

The rest of this paper is organized as follows. Section 2 presents the new β_k formula and algorithm. Section 3 contains the convergence analysis under the strong Wolfe conditions. Section 4 gives numerical results and Section 5 concludes the paper.

2 New Formula of β_k and Description of the Corresponding Algorithm

In this section, we propose a new hybrid conjugate gradient method for solving (1). The method is based on a convex combination of the RMIL, CD and LS conjugate gradient

formulas. The proposed parameter β_k^{New} is defined by

$$\beta_k^{\text{New}} = \lambda_k \beta_k^{\text{RMIL}} + \theta_k \beta_k^{\text{CD}} + (1 - \lambda_k - \theta_k)\beta_k^{\text{LS}}, \quad \lambda_k, \theta_k \in [0,1],\ \lambda_k + \theta_k \leq 1. \tag{4}$$

Substituting the expressions for the individual CG parameters, we get

$$\beta_k^{\text{New}} = \lambda_k \frac{g_{k+1}^T y_k}{\|d_k\|^2} + \theta_k \frac{\|g_{k+1}\|^2}{-g_k^T d_k} + (1 - \lambda_k - \theta_k)\frac{g_{k+1}^T y_k}{-g_k^T d_k}, \tag{5}$$

where $y_k = g_{k+1} - g_k$.

The search direction is generated using the recurrence

$$d_0 = -g_0, \quad d_{k+1} = -g_{k+1} + \beta_k^{\text{New}} d_k. \tag{6}$$

To ensure global convergence and sufficient descent condition, we employ the strong Wolfe line search conditions

$$f(x_k + \alpha_k d_k) \leq f(x_k) + \delta \alpha_k g_k^T d_k, \tag{7}$$

$$\sigma g_k^T d_k \leq g_{k+1}^T d_k \leq -\sigma g_k^T d_k, \tag{8}$$

where $0 < \delta \leq \sigma < \frac{4}{5}$.

The parameters λ_k and θ_k are chosen to satisfy the conjugacy condition

$$y_k^T d_{k+1} = 0. \tag{9}$$

Substituting (6) into (9) and using (4), we get

$$\begin{aligned} y_k^T d_{k+1} &= -y_k^T g_{k+1} + \beta_k^{\text{New}} y_k^T d_k = 0, \\ \Rightarrow y_k^T g_{k+1} &= \beta_k^{\text{New}} y_k^T d_k. \end{aligned} \tag{10}$$

Replacing β_k^{New} by its expression from (4), we obtain

$$\begin{aligned} y_k^T g_{k+1} &= \left[\lambda_k \beta_k^{\text{RMIL}} + \theta_k \beta_k^{\text{CD}} + (1 - \lambda_k - \theta_k)\beta_k^{\text{LS}}\right] y_k^T d_k \\ &= \lambda_k (\beta_k^{\text{RMIL}} - \beta_k^{\text{LS}}) y_k^T d_k + \theta_k (\beta_k^{\text{CD}} - \beta_k^{\text{LS}}) y_k^T d_k + \beta_k^{\text{LS}} y_k^T d_k. \end{aligned} \tag{11}$$

From (11), we get

$$\lambda_k = \frac{y_k^T g_{k+1} - \theta_k (\beta_k^{\text{CD}} - \beta_k^{\text{LS}}) y_k^T d_k - \beta_k^{\text{LS}} y_k^T d_k}{(\beta_k^{\text{RMIL}} - \beta_k^{\text{LS}}) y_k^T d_k}. \tag{12}$$

To ensure feasibility of the parameters, we enforce the following bounds:

$$\lambda_k = \begin{cases} 0, & \text{if } \lambda_k < 0, \\ 1, & \text{if } \lambda_k > 1, \\ 1 - \theta_k, & \text{if } \lambda_k + \theta_k > 1. \end{cases}$$

Depending on the values of λ_k and θ_k, the parameter β_k^{New} reduces to the known methods

$$\beta_k^{\text{New}} = \begin{cases} \beta_k^{\text{RMIL}}, & \lambda_k = 1,\ \theta_k = 0, \\ \beta_k^{\text{CD}}, & \lambda_k = 0,\ \theta_k = 1, \\ \beta_k^{\text{LS}}, & \lambda_k = 0,\ \theta_k = 0, \\ \lambda_k \beta_k^{\text{RMIL}} + (1 - \lambda_k)\beta_k^{\text{LS}}, & \theta_k = 0,\ \lambda_k \in (0,1), \\ \lambda_k \beta_k^{\text{RMIL}} + (1 - \lambda_k)\beta_k^{\text{CD}}, & \theta_k = 1 - \lambda_k,\ \lambda_k \in (0,1), \\ \theta_k \beta_k^{\text{CD}} + (1 - \theta_k)\beta_k^{\text{LS}}, & \lambda_k = 0,\ \theta_k \in (0,1), \\ \lambda_k \beta_k^{\text{RMIL}} + \theta_k \beta_k^{\text{CD}} + (1 - \lambda_k - \theta_k)\beta_k^{\text{LS}}, & \lambda_k, \theta_k \in (0,1),\ \lambda_k + \theta_k < 1. \end{cases} \tag{13}$$

Now we give the corresponding algorithm for our β_k^{New}.

Algorithm 2.1 (RMILCDLS)
Begin algorithm
Step 0: *Given a starting point $x_0 \in \mathbb{R}^n$ and a parameter $\varepsilon > 0$, compute $g_0 = \nabla f(x_0)$, then set $d_0 = -g_0$.*
Step 1: *If $\|g_k\| \leq \varepsilon$, **Stop**; otherwise go to **Step 2**.*
Step 2: *Compute the step-size α_k using (7) and (8).*
Step 3: *Update $x_{k+1} = x_k + \alpha_k d_k$.*
Step 4: *Compute $g_{k+1} = \nabla f(x_{k+1})$, $y_k = g_{k+1} - g_k$.*
Step 5: *If $g_{k+1}^T g_k = 0$, then set $\lambda_k = 0$;*
otherwise compute λ_k as in (12) with $0 \leq \theta_k \leq 1$.
Step 6: *Compute β_k^{New} using formula (5).*
Step 7: *Set $d_{k+1} = -g_{k+1} + \beta_k^{New} d_k$.*
Step 8: *If $\left|g_{k+1}^T g_k\right| \geq 0.2\|g_{k+1}\|^2$ (restart criterion of Powell [4]),*
then set $d_{k+1} = -g_{k+1}$.
Step 9: *Let $k = k + 1$ and go back to **Step 1**.*
End algorithm

3 Convergence Analysis

Throughout this section, we make the following assumptions.

Assumption (i): The level set $S = \{x \in \mathbb{R}^n : f(x) \leq f(x_0)\}$ is bounded, i.e., there exists a constant $B > 0$ such that

$$\|x\| \leq B, \text{ for all } x \in S. \tag{14}$$

Assumption (ii): In a neighborhood N of S, the function f is continuously differentiable and its gradient $\nabla f(x)$ is Lipschitz continuous, i.e., there exists a constant $0 < L < \infty$ such that

$$\|\nabla f(x) - \nabla f(y)\| \leq L \|x - y\|, \text{ for all } x, y \in N. \tag{15}$$

Under Assumptions **(i)** and **(ii)** on f, there exists a constant $\mu \geq 0$ such that

$$\|\nabla f(x)\| \leq \mu, \text{ for all } x, y \in N. \tag{16}$$

To establish the sufficient descent condition, we introduce the following theorem.

Theorem 3.1 *Let $\{d_k\}_{k\in\mathbb{N}}$ be given by (6), α_k satisfy (7) and (8), then*

$$g_{k+1}^T d_{k+1} \leq -c \|g_{k+1}\|^2, \ k = 0, 1, .., \tag{17}$$

where $c > 0$ and $\sigma < \frac{4}{5}$.

Proof. Induction is used to show (17). Since $d_0 = -g_0$, we get $g_0^T d_0 = -\|g_0\|^2 < 0$. Consider that (17) holds for $k > 0$.

We have

$$\left|g_{k+1}^T g_k\right| \geq 0.2 \|g_{k+1}\|^2. \tag{18}$$

If (18) holds, then $g_{k+1}^T d_{k+1}^{New} = -\|g_{k+1}\|^2 < 0$.

The search direction that meets the sufficient descent condition is achieved.
If (18) does not hold, then

$$\left|g_{k+1}^T g_k\right| < 0.2 \left\|g_{k+1}\right\|^2. \tag{19}$$

Using (8), we can get that

$$y_k^T d_k = (g_{k+1} - g_k)^T d_k \geq -(1-\sigma) g_k^T d_k. \tag{20}$$

And

$$\left|\frac{g_{k+1}^T d_k}{y_k^T d_k}\right| \leq \frac{\sigma}{(1-\sigma)}.$$

Multiplying both sides of (6) by g_{k+1}^T, we get

$$\begin{aligned} g_{k+1}^T d_{k+1}^{New} &= -\left\|g_{k+1}\right\|^2 + \lambda_k \beta_k^{RMIL} g_{k+1}^T d_k + \theta_k \beta_k^{CD} g_{k+1}^T d_k \\ &\quad + (1-\lambda_k-\theta_k)\beta_k^{LS} g_{k+1}^T d_k. \end{aligned}$$

We have seven cases.

Case 01: If $\lambda_k = 1$, $\theta_k = 0$, we have $g_{k+1}^T d_{k+1}^{New} = g_{k+1}^T d_{k+1}^{RMIL}$. For the RMIL direction $d_{k+1}^{RMIL} = -g_{k+1} + \beta_k^{RMIL} d_k$, it is proved in [13] that

$$g_{k+1}^T d_{k+1}^{RMIL} \leq -a_1 \|g_{k+1}\|^2 \text{ for all } k,$$

where $a_1 > 0$.

Case 02: If $\lambda_k = 0$, $\theta_k = 1$, we have $g_{k+1}^T d_{k+1}^{New} = g_{k+1}^T d_{k+1}^{CD}$. For the conjugate descent direction $d_{k+1}^{CD} = -g_{k+1} + \beta_k^{CD} d_k$, it is proved in [4] that

$$g_{k+1}^T d_{k+1}^{CD} \leq -a_2 \|g_{k+1}\|^2 \text{ for all } k,$$

where $a_2 > 0$.

Case 03: If $\lambda_k = 0$, $\theta_k = 0$, we have $g_{k+1}^T d_{k+1}^{New} = g_{k+1}^T d_{k+1}^{LS}$. For the Liu-Storey direction $d_{k+1}^{LS} = -g_{k+1} + \beta_k^{LS} d_k$, it is proved in [4] that

$$g_{k+1}^T d_{k+1}^{LS} \leq -a_3 \|g_{k+1}\|^2 \text{ for all } k,$$

where $a_3 > 0$.

Case 04: If $\lambda_k \in]0,1[$, $\theta_k = 0$, we have $g_{k+1}^T d_{k+1}^{New} = g_{k+1}^T d_{k+1}^{RMILLS}$.
We have

$$d_{k+1}^{New} = \lambda_k d_{k+1}^{RMIL} + \theta_k d_{k+1}^{CD} + (1-\lambda_k-\theta_k) d_{k+1}^{LS}.$$

Hence,

$$g_{k+1}^T d_{k+1}^{New} = \lambda_k g_{k+1}^T d_{k+1}^{RMIL} + \theta_k g_{k+1}^T d_{k+1}^{CD} + (1-\lambda_k-\theta_k) g_{k+1}^T d_{k+1}^{LS}. \tag{21}$$

With (21), we get

$$g_{k+1}^T d_{k+1}^{RMILLS} = \lambda_k g_{k+1}^T d_{k+1}^{RMIL} + (1-\lambda_k) g_{k+1}^T d_{k+1}^{LS}.$$

$\exists w_1, w_2 \in \mathbb{R} : 0 < w_1 < \lambda_k < w_2 < 1$, then

$$g_{k+1}^T d_{k+1}^{RMILLS} \leq -(w_1 a_1 + w_2 a_3) \left\|g_{k+1}\right\|^2 = -a_4 \left\|g_{k+1}\right\|^2,$$

where $a_4 > 0$.

Case 05: If $\theta_k = 1 - \lambda_k$ and λ_k, $\theta_k \in]0,1[$, we have $g_{k+1}^T d_{k+1}^{New} = g_{k+1}^T d_{k+1}^{RMILCD}$.
With (21), we get

$$g_{k+1}^T d_{k+1}^{RMILCD} = \lambda_k g_{k+1}^T d_{k+1}^{RMIL} + (1-\lambda_k) g_{k+1}^T d_{k+1}^{CD}.$$

Clearly, the sufficient descent condition is satisfied, which means that

$$g_{k+1}^T d_{k+1}^{RMILCD} \leq -a_5 \left\| g_{k+1} \right\|^2,$$

where $a_5 > 0$.

Case 06: If $\lambda_k = 0$, $\theta_k \in]0,1[$, we have $g_{k+1}^T d_{k+1}^{New} = g_{k+1}^T d_{k+1}^{CDLS}$.
With (21), we get

$$g_{k+1}^T d_{k+1}^{CDLS} = \theta_k g_{k+1}^T d_{k+1}^{CD} + (1-\theta_k) g_{k+1}^T d_{k+1}^{LS}.$$

Case 06 is the same as **Case 04** and **Case 05**. So, the sufficient descent condition is satisfied, which means that

$$g_{k+1}^T d_{k+1}^{CDLS} \leq -a_6 \left\| g_{k+1} \right\|^2,$$

where $a_6 > 0$.

Case 07: If λ_k, $\theta_k \in]0,1[$ and $0 < \lambda_k + \theta_k < 1$, we have

$$g_{k+1}^T d_{k+1}^{New} = \lambda_k g_{k+1}^T d_{k+1}^{RMIL} + \theta_k g_{k+1}^T d_{k+1}^{CD} + (1-\lambda_k-\theta_k) g_{k+1}^T d_{k+1}^{LS}.$$

$\exists k_1, k_2, k_3, k_4 \in \mathbb{R} : 0 < k_1 < \lambda_k < k_2 < 1$, $0 < k_3 < \theta_k < k_4 < 1$, then

$$\begin{aligned} g_{k+1}^T d_{k+1}^{New} &\leq -(k_1 a_1 + k_2 a_2 + (1-k_3-k_4) a_3) \left\| g_{k+1} \right\|^2 \\ &= -a_7 \left\| g_{k+1} \right\|^2, \end{aligned}$$

where $a_7 > 0$.

The proof is complete.

Lemma 3.1 *Suppose that Assumptions (i) and (ii) hold. Consider common iterate (2), where d_k is a descent direction that verifies (17) and α_k is determined by the strong Wolfe line search (7) and (8). Then the Zoutendijk condition*

$$\sum_{k \geq 0} \frac{(g_k^T d_k)^2}{\|d_k\|^2} < \infty \tag{22}$$

holds.

Proof. The proof follows directly from [15].

Lemma 3.2 *Suppose that Assumptions (i) and (ii) hold and $\alpha_k > 0$ is determined by the strong Wolfe line search (7) and (8). Then there exists $\alpha^* > 0$ such that*

$$\alpha_k \geq \alpha_* > 0 \text{ for all } k.$$

Proof. The proof follows directly from [4].

Theorem 3.2 *Consider the RMILCDLS conjugate gradient method and suppose that Assumptions (i), (ii) and (8) hold. Then either $g_k = 0$ for some k or*

$$\lim_{k\to\infty} \inf \|g_k\| = 0. \tag{23}$$

Proof. Suppose that $g_k \neq 0$ for all k. Then we are going to prove (23).
Suppose by contradiction that (23) does not hold. Then there exists $t > 0$ such that

$$\|g_k\| \geq t \text{ for all } k. \tag{24}$$

Let D denote the diameter of the level set S, and define the step $s_k = x_{k+1} - x_k = \alpha_k d_k$. From equation (4), we have

$$\left|\beta_k^{\text{New}}\right| \leq \left|\beta_k^{\text{RMIL}}\right| + \left|\beta_k^{\text{CD}}\right| + \left|\beta_k^{\text{LS}}\right|. \tag{25}$$

We begin by analyzing each of the components on the right-hand side. By definition,

$$\left|\beta_k^{\text{RMIL}}\right| = \frac{\left|g_{k+1}^T y_k\right|}{\|d_k\|^2}.$$

From equations (24) and (17), we have

$$\|d_k\|^2 \geq \frac{-(1-\sigma)g_k^T d_k}{L\alpha_k} \geq \frac{(1-\sigma)c\|g_k\|^2}{L\alpha_k} \geq \frac{(1-\sigma)ct^2}{L\alpha_k}.$$

Thus, we obtain the bound

$$\frac{1}{\|d_k\|^2} \leq \frac{L\alpha_k}{(1-\sigma)ct^2}. \tag{26}$$

Next, for $\left|g_{k+1}^T y_k\right|$, we have

$$\begin{aligned} \left|g_{k+1}^T y_k\right| &\leq \|g_{k+1}\| \, \|y_k\| \\ &\leq \mu \|g_{k+1} - g_k\| \\ &\leq \mu L \|x_{k+1} - x_k\| \\ &\leq \mu L \|s_k\| \\ \left|g_{k+1}^T y_k\right| &\leq \mu L D. \end{aligned} \tag{27}$$

Combining equations (26) and (27), we get

$$\left|\beta_k^{\text{RMIL}}\right| \leq \frac{\mu L^2 D \alpha_k}{(1-\sigma)ct^2}. \tag{28}$$

For $\left|\beta_k^{\text{CD}}\right|$, we have

$$\left|\beta_k^{\text{CD}}\right| \leq \frac{\|g_{k+1}\|^2}{-g_k^T d_k} \leq \frac{\mu^2}{c\|g_k\|^2} \leq \frac{\mu^2}{ct^2}. \tag{29}$$

Finally, for $\left|\beta_k^{\text{LS}}\right|$, we have

$$\left|\beta_k^{\text{LS}}\right| = \left|\frac{g_{k+1}^T y_k}{-g_k^T d_k}\right| \leq \frac{\|g_{k+1}\| \, \|y_k\|}{-g_k^T d_k} \leq \frac{\mu L D}{ct^2}. \tag{30}$$

From (28), (29) and (30), we can write

$$\left|\beta_k^{New}\right| \leq \frac{\mu L^2 D\alpha_k}{(1-\sigma)ct^2} + \frac{\mu^2 + \mu LD}{ct^2}. \tag{31}$$

Now, we can write

$$\|d_{k+1}\| \leq \|g_{k+1}\| + \left|\beta_k^{New}\right| \|d_k\|. \tag{32}$$

We have $s_k = \alpha_k d_k$. So, we can write $d_k = \dfrac{s_k}{\alpha_k}$. Then, from (31) and (32), we get

$$\begin{aligned} \|d_{k+1}\| &\leq \mu + \left(\frac{\mu L^2 D\alpha_k}{(1-\sigma)ct^2} + \frac{\mu^2 + \mu LD}{ct^2}\right)\frac{\|s_k\|}{\alpha_k} \\ &\leq \mu + \left(\frac{\mu L^2 D\alpha_*}{(1-\sigma)ct^2} + \frac{\mu^2 + \mu LD}{ct^2}\right)\frac{D}{\alpha_*} = P. \end{aligned} \tag{33}$$

This implies that

$$\sum_{k\geq 1} \frac{1}{\|d_{k+1}\|^2} = \infty. \tag{34}$$

On the other hand, from (18), (24) and from the Zoutendijk condition (22), it follows that

$$c^2 t^4 \sum_{k\geq 0} \frac{1}{\|d_k\|^2} \leq \sum_{k\geq 0} \frac{c^2\|g_k\|^4}{\|d_k\|^2} \leq \sum_{k\geq 0} \frac{(g_k^T d_k)^2}{\|d_k\|^2} < \infty,$$

which contradicts (34). Therefore, (24) does not hold. Then $\lim\limits_{k\to\infty} \inf \|g_k\| = 0$.

This completes the proof.

4 Numerical Experiments

In this section, we present several numerical tests to evaluate the performance of RMIL-CDLS algorithm. We select various test functions given in Table 4, taken from the CUTE library [1, 6] for different dimensions, from $n = 10$ to $n = 800000$. At the same time, we present a numerical comparison with other conjugate gradient algorithms, namely RMIL, LS, CD and HSDYCD [8]. The stopping criterion is $\|g_k\| \leq \varepsilon$, where $\varepsilon = 10^{-6}$, or the iteration number > 4000. The step-size α_k is computed by the strong Wolfe line search with $\sigma = 0.01$ $\delta = 0.1$. In order to evaluate the data of iterations number, CPU time and for gradient evaluation and objective function evaluation, we use the performance profile of Dolan and Moré [5] presented in Figure 1.

4.1 Commentaries

The performance profile results, as depicted in Figures 1 (a), (b), (c) and (d), show that our proposed conjugate gradient method RMILCDLS, using β_k^{New}, consistently outperforms the other methods based on β_k^{RMIL}, β_k^{CD}, β_k^{LS} and β_k^{HSDYCD}.

Functions	Dimensions	Functions	Dimensions
Genrose	10000	Pen1	200, 1000
Osb2	10	Rosex	500, 1000
Eg2	100	Diagonal3	500, 2000
Freuroth	460	Singx	1000, 2000
Pen2	160	Diagonal1	800, 2000
Dixon3dq	150	Trid	500, 8000
Fletcbv3	100	Ie	500, 1500
Power1	150	Raydan1	500, 5000
Biggsb1	300	Lin	100, 1300
Dixmaani	360	Nonscomp	5000, 80000
Bv	2000, 20000	Dqrtic	5000, 150000
Liarwhd	6000, 30000	Dqdrtic	9000, 90000
Woods	150000, 200000	Dixmaana	6000, 90000
Quartc	80000, 50000	Dixmaanb	24000, 48000
Dixmaanc	2700, 27000	Dixmaand	12000, 90000
Dixmaane	2400, 48000	Dixmaanf	15000, 60000
Dixmaang	12000, 90000	Edensch	7000, 40000, 50000
Diagonal2	8000, 50000	Cosine	6000, 100000, 800000
Dixmaank	12000, 12000	Fletchcr	1000, 50000, 200000
Dixmaanl	2400, 24000	Exdenschnb	6000, 24000, 300000
Himmelbg	70000, 240000	Exdenschnf	90000, 280000, 600000
Dixmaanh	6000, 150000	Raydan2	2000, 20000, 500000
Dixmaanj	3000, 15000	Sine	100000, 250000, 500000

Table 1: List of test functions and their dimensions.

5 Conclusion

In this paper, we have proposed a new hybrid conjugate gradient method for solving unconstrained optimization problems, where the parameter β_k^{New} is a convex combination of β_k^{RMIL}, β_k^{CD} and β_k^{LS}.

We have provided the proof of the sufficient descent condition for the search direction and the global convergence of our proposed method for nonlinear functions using the strong Wolfe line search.

The numerical tests carried out confirm the effectiveness of our proposed RMILCDLS algorithm in terms of iterations number, computation time, gradient evaluation and objective function evaluation compared with other standard conjugate gradient methods, namely the RMIL, LS, CD and HSDYCD algorithms.

In particular, the convex combination strategy introduced in the construction of β_k^{New} offers a new balance between convergence reliability and computational efficiency. This makes the RMILCDLS algorithm a valuable tool for solving large-scale problems arising in various fields such as nonlinear dynamics, optimal control, machine learning, image processing and compressive sensing.

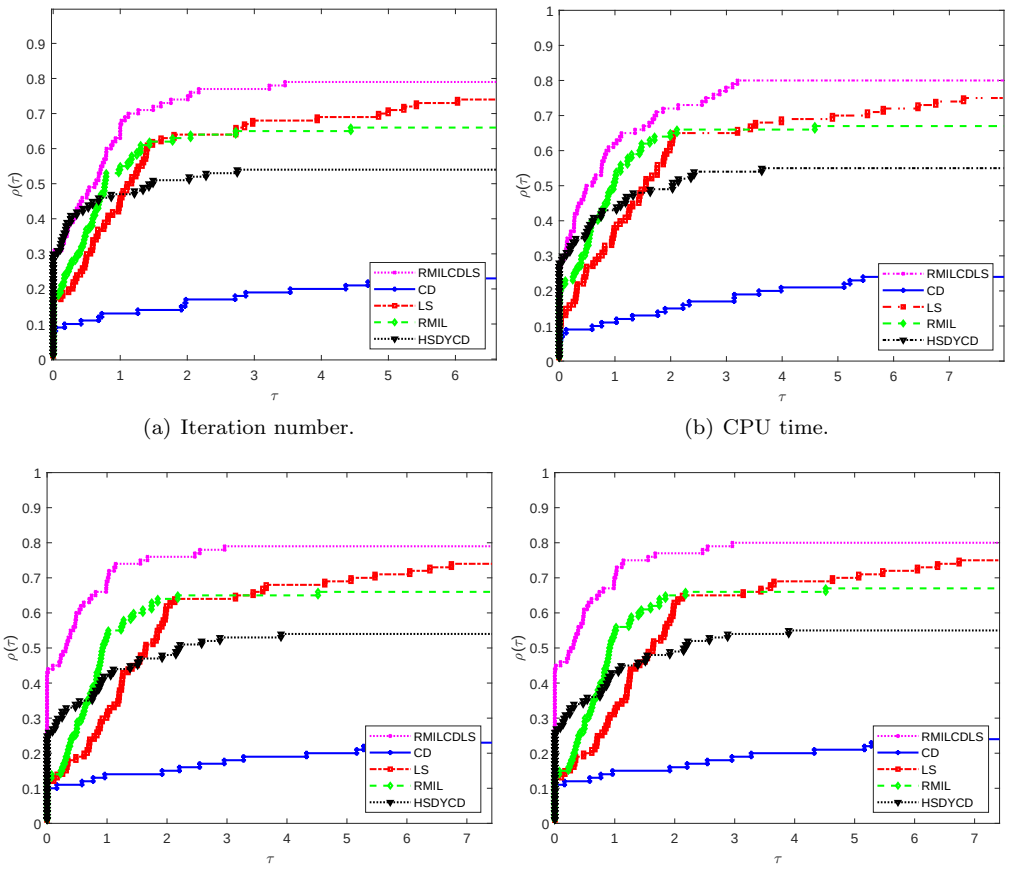

(a) Iteration number.

(b) CPU time.

(c) Objective function evaluation.

(d) Gradient evaluation.

Figure 1: Performance profile of RMILCDLS, RMIL, CD, LS and HSDYCD algorithms.

References

[1] N. Andrei. Nonlinear conjugate gradient methods for unconstrained optimization. *Springer Optimization and its Applications* **158** (2020).

[2] Y. H. Dai and Y. Yuan. A nonlinear conjugate gradient method with a strong global convergence property. *SIAM J. Optim.* **10** (1) (1999) 177–182.

[3] S. Delladji, M. Belloufi and B. Sellami. New hybrid conjugate gradient method as a convex combination of FR and BA methods. *J. Inf. Optim. Sci.* **42** (3) (2021) 591–602.

[4] S. Djordjevic. New Hybrid Conjugate Gradient Method as a Convex Combination of LS and CD methods. *Filomat* **31** (6) (2017) 1813–1825.

[5] E. D. Dolan and J. J. Moré. Benchmarking optimization software with performance profiles. *Math. Program.* **91** (2002) 201–213.

[6] N. I. M. Gould, D. Orban and Ph. L. Toint. CUTEr and SifDec: A constrained and unconstrained testing environment, revisited. *ACM Trans. Math. Softw.* **29** (4) (2003) 373–394.

[7] W. W. Hager and H. Zhang. A survey of nonlinear conjugate gradient methods. *Pac. J. Optim.* **2** (2006) 35–58.

[8] A. Hallal, M. Belloufi and B. Sellami. An efficient new hybrid CG-method as convex combination of DY and CD and HS algorithms. *RAIRO Oper. Res.* **56** (2022) 4047–4056.

[9] M. D. Johansyah, A. Sambas, S. Vaidyanathan, R. Amira, F. Hannachi and N. Hamri. A new chaotic supply chain model, its bifurcation analysis, multi-stability and synchronization using backstepping control. *Nonlinear Dyn. Syst. Theory* **24** (3) (2024) 275–288.

[10] Y. Liu and C. Storey. Efficient generalized conjugate gradient algorithm. Part 1: Theory. *J. Optim. Theory Appl.* **69** (1) (1991) 129–137.

[11] M. Labid and N. Hamri. Chaos anti-synchronization between fractional-order Lesser Date Moth chaotic system and integer-order chaotic system by nonlinear control. *Nonlinear Dyn. Syst. Theory* **23** (2) (2023) 153–163.

[12] M. L. Ouaoua and S. Khelladi. Efficient Descent Direction of a Conjugate Gradient Algorithm for Nonlinear Optimization. *Nonlinear Dyn. Syst. Theory* **25** (1) (2025) 91–100.

[13] M. Rivaie and M. Mustafa. A new class of non linear conjugate gradient coefficients with exact and inexact line searches. *Appl. Math. Comput.* **268** (2015) 1152–1163.

[14] X. Yang, Z. Luo and X. Dai. A global convergence of LS-CD hybrid conjugate gradient method. *Adv. Numer. Anal.* **2013** (2013) 5 pages.

[15] G. Zoutendijk. Nonlinear programming, computational methods. In: Abadie, J. (ed.) Integer and Nonlinear Programming, 1970, 37–86.

Nonlinear Dynamics and Systems Theory, **26** (2) (2026) 195–202

A Quintic Nonlinear Differential System with a Non-Algebraic Limit Cycle Around a Non-Elementary Singular Point

A. Kina [1,2*] and A. Bendjeddou [2]

[1] *Department of Mathematics and Computer Science, Université de Ghardaia, 47 000 Algeria.*
[2] *Laboratory of Applied Mathematics, Department of Mathematics, Faculty of Sciences, University Ferhat Abbas Setif 1, Algeria.*

Received: June 11, 2025; Revised: April 13, 2026

Abstract: In this paper, we consider a class of quintic planar polynomial differential systems with a non-elementary singular point. We establish sufficient conditions for the existence of a hyperbolic non-algebraic limit cycle surrounding this singularity. Moreover, the limit cycle is explicitly expressed in polar coordinates. To demonstrate the applicability of our results, a concrete example is provided along with its corresponding phase portrait.

Keywords: *polynomial differential system; non-algebraic limit cycle; first integral; Riccati differential equation.*

Mathematics Subject Classification (2020): 34A05, 70K05, 34C05, 34C07, 34C25.

1 Introduction

One of the main problems in the qualitative theory of differential equations is the study of limit cycles, that is, isolated periodic solutions among all periodic solutions of planar differential systems of the form

$$\begin{cases} \dot{x} = \frac{dx}{dt} = P(x, y), \\ \dot{y} = \frac{dy}{dt} = Q(x, y), \end{cases} \tag{1}$$

where P and Q are real polynomials in the variables x and y. The degree n of the polynomial system of differential equations is the maximum of the degrees of the polynomials

* Corresponding author: mailto:abdelkrimkina@gmail.com

P and Q. Limit cycles of plane vector fields were first proposed by French mathematician Poincaré in his very famous classical papers entitled "Integral curves defined by differential equations" (1881, 1882, 1885, 1886). Later on van der Pol [16] in 1926, Lienard in 1928, and Andronov [2] in 1929, showed that the periodic solution of a self-sustained oscillation of a circuit in a vacuum tube was a limit cycle in the sense defined by Poincaré.

Hilbert proposed a list of 23 problems to guide the advancement of mathematical science, sparking intensive research throughout the 20th century. Among these, only the Riemann hypothesis and the second part of Hilbert's 16th problem remain unsolved to this day. The second part of the 16th Hilbert problem consists of two components: it seeks an upper bound on the number of possible limit cycles and their positions for planar polynomial differential systems of a given degree [5]. The theory of limit cycles, serving as an indispensable mathematical tool, has found broad and significant applications in modern physics, chemistry, biology, and other disciplines. In turn, the progress in these fields continues to drive research on limit cycles.

Let Ω be a non-empty open and dense subset of $\mathbb{R}^2$. We say that a non–locally constant C^1 function $\varphi : \Omega \to \mathbb{R}$ is a first integral of the polynomial differential (2) in Ω if φ is constant on the trajectories of the polynomial differential system (2) contained in Ω, i.e., if

$$\frac{d\varphi(x,y)}{dt} - \frac{\partial\varphi(x,y)}{\partial x}P(x,y) - \frac{\partial\varphi(x,y)}{\partial y}Q(x,y) \equiv 0 \text{ at the points of } \Omega.$$

Let us take into consideration a not closed set $F \subseteq \mathbb{R}^2$ and function V of class $C^1(F)$ defined by $V(x,y) : \mathbb{R}^2 \supseteq F \longrightarrow \mathbb{R}$. We say that the curve defined by means of the equation $V(x,y) = 0$ is an invariant curve of the system (2) under the condition that the following equation is satisfied:

$$P(x,y)\frac{\partial V}{\partial x}(x,y) + Q(x,y)\frac{\partial V}{\partial y}(x,y) = K(x,y)\,V(x,y)$$

with $K(x,y)$ being a polynomial in the variables x and y such as $\deg K(x,y) \leq q-1$. The polynomial $K(x,y)$ is known as the cofactor of the polynomial curve $V(x,y) = 0$.

The study of nonlinear differential systems is of central importance for understanding complex dynamical behaviors that cannot be captured by linear models. In particular, limit cycles play a key role in describing self-sustained oscillations in physical, biological, and engineering systems [4,8,9,12,15]. While linear systems provide foundational insight, they fail to account for the intricate behaviors introduced by nonlinearities. Therefore, investigating the existence and characteristics of limit cycles in nonlinear planar systems, especially those with higher-degree nonlinearities and non-elementary singularities, contributes significantly to the theoretical development and practical understanding of nonlinear dynamics.

In the qualitative theory of planar differential systems, an algebraic limit cycle of degree p is an oval of an irreducible invariant algebraic curve $V(x,y) = 0$ of degree p, which is a limit cycle of the system, otherwise it is called non-algebraic, see [11, 14]. In general, the orbits of a polynomial differential system (1) are contained in analytic curves that are not algebraic, see for example [1,6,10], an even more difficult problem is to give an explicit form of them, for example, the well-known limit cycle of the van der Pol differential system presented in 1926, was not proved until 1995, when Odani [13] showed that it was non-algebraic and the der Pol differential system can be written as a polynomial differential system (1) of degree 3, but its limit cycle is not known

explicitly. The first examples of explicit non-algebraic limit cycles appeared in the works of A.Gasull, Giacomini and Torregrosa [6] and J.Giné and M.Grau [7], Al-Dossary [1] for $n = 5$, and Benterki Lilibre [3] for $n = 3$.

In this work, we consider a class of quintic planar polynomial differential systems that feature a non-elementary singular point. We establish sufficient conditions for the existence of a hyperbolic, non-algebraic limit cycle surrounding this singularity. Moreover, we derive an explicit expression for the limit cycle, contributing both to the theoretical understanding and practical identification of such cycles. To illustrate the applicability of our results, a specific example is constructed, and its phase portrait is presented.

2 Main Result

As our main result, we shall prove the following theorem.

Theorem 2.1 *Consider the quintic polynomial differential systems*

$$\begin{cases} \dot{x} = 2hy\left(a^2y^2+x^2\right)+wax\left(-\left(x^2+y^2\right)^2+h\left(x^2+y^2\right)\right), \\ \dot{y} = -2hx\left(a^2y^2+x^2\right)+way\left(-\left(x^2+y^2\right)^2+h\left(x^2+y^2\right)\right), \end{cases} \tag{2}$$

then the following statements hold.

(1) If $a \in \mathbb{R}^*$, $w \in \mathbb{R}^*$ and $h > 0$, the system (2) has the first integral

$$I(x,y) = \frac{\exp\int_0^{\arctan\frac{y}{x}} \frac{2}{\sqrt{h}}\phi(s)ds}{\sqrt{x^2+y^2}-\sqrt{h}} + \int_0^{\arctan\frac{y}{x}} \left(\exp\int_0^s \frac{2}{\sqrt{h}}\phi(\eta)d\eta\right)\frac{1}{h}\phi(s)ds,$$

where $\phi(\theta) = \frac{wa}{2(a^2\sin^2\theta+\cos^2\theta)}$.

(2) If $wa < 0$ and $h > 0$, the system (2) possesses exactly one non-algebraic limit cycle around a non-elementary singular point, this limit cycle is explicitly given in polar coordinates (r,θ) by the expression

$$r(\theta, r_*) = \sqrt{h} + \frac{\left(\exp\int_0^\theta \frac{-2}{\sqrt{h}}\phi(s)ds\right)^{-1}}{\frac{1}{r_*-\sqrt{h}} - \int_0^\theta \left(\exp\int_0^s \frac{2}{\sqrt{h}}\phi(\eta)d\eta\right)\frac{1}{h}\phi(s)ds}$$

with

$$r_* = \frac{\left(\exp\int_0^{2\pi} \frac{2}{\sqrt{h}}\phi(s)ds\right)^{-1}-1}{\int_0^{2\pi}\left(\exp\int_0^s \frac{2}{\sqrt{h}}\phi(\eta)d\eta\right)\frac{1}{h}\phi(s)ds} + \sqrt{h}.$$

Proof. Firstly, we prove that the origin is the unique equilibrium non-elementary point of the system (2).

We note that

$$\begin{aligned} x\dot{y}-y\dot{x} &= x\left(-2hx\left(a^2y^2+x^2\right)+way\left(-\left(x^2+y^2\right)^2+h\left(x^2+y^2\right)\right)\right) \\ &\quad -y\left(2hy\left(a^2y^2+x^2\right)+wax\left(-\left(x^2+y^2\right)^2+h\left(x^2+y^2\right)\right)\right) \\ &= -2h\left(a^2y^2+x^2\right)\left(x^2+y^2\right), \end{aligned}$$

thus, the equilibrium points of system (2) are present in the curve's equation

$$-2h\left(a^2y^2+x^2\right)\left(x^2+y^2\right)=0 \tag{3}$$

because $h\neq 0$ and $a\neq 0$. Then the origin of coordinates is the only solution to the equation (3), we conclude that the origin, also known as an equilibrium point, is a degenerate non-elementary singular point of the system (2), for the reason that the linear part of this system is identically zero.

The Jacobian matrix of the differential system (2) at the origin $O(0,0)$ is

$$D_j(0,0)=\begin{pmatrix}0 & 0\\ 0 & 0\end{pmatrix}.$$

So the origin $(0,0)$ is a non-elementary point.

(1) To prove statements (1) and (2), we write the polynomial differential system (2) in polar coordinates $(r;\theta)$, then these system becomes

$$\begin{cases}\dot{r}=war\left(-r^4+hr^2\right),\\ \dot{\theta}=-2hr\left(a^2r^2\sin^2\theta+r^2\cos^2\theta\right).\end{cases} \tag{4}$$

Taking θ as an independent variable, we can rewrite the system (4) as the Riccati differential equation as follows:

$$\frac{dr}{d\theta}=\frac{1}{h}\phi(\theta)r^2-\phi(\theta), \tag{5}$$

where $\phi(\theta)=\frac{wa}{2(a^2\sin^2\theta+\cos^2\theta)}$.

Note that since $h\in\mathbb{R}_+^*$, we have $\theta'=-2hr\left(a^2r^2\sin^2\theta+r^2\cos^2\theta\right)<0$ for all $\theta\in\mathbb{R}$. So, the orbits $r(\theta)$ of the differential equation (5) reverse their orientation with respect to the orbits $(r(t);\theta(t))$ or $((x(t);y(t))$ of the differential systems (4) and (2), respectively.

Fortunately, the equation (5) is integrable since it possesses the particular solution $r=\sqrt{h}$, the general solution of equation (5) is given by

$$r=\left(\sqrt{h}+\frac{1}{\rho}\right), \tag{6}$$

where ρ is a function of the variable θ. Indeed, substituting the solution $r=\left(\sqrt{h}+\frac{1}{\rho}\right)$ into the Riccatti equation (5), we obtain the linear equation

$$\frac{d\rho}{d\theta}=-\frac{2}{\sqrt{h}}\,\phi(\theta)\rho-\frac{1}{h}\phi(\theta). \tag{7}$$

The general solution of linear equation (7) is

$$\rho(\theta,c)=\left(\exp\int_0^\theta\frac{2}{\sqrt{h}}\phi(s)ds\right)^{-1}\left(c+\int_0^\theta\left(\exp\int_0^s\frac{2}{\sqrt{h}}\phi(\eta)d\eta\right)\left(\frac{-1}{h}\phi(s)\right)ds\right),$$

where $c\in\mathbb{R}$. Going back through the changes of variables (6), we obtain the general solution of (5)

$$r(\theta,c)=\sqrt{h}+\frac{\exp\int_0^\theta\frac{2}{\sqrt{h}}\phi(s)ds}{c-\int_0^\theta\left(\exp\int_0^s\frac{2}{\sqrt{h}}\phi(\eta)d\eta\right)\frac{1}{h}\phi(s)ds}, \tag{8}$$

where $\phi(\theta) = \frac{wa}{2(a^2\sin^2\theta+\cos^2\theta)}$. By passing to Cartesian coordinates, we deduce the first integral

$$I(x,y) = \frac{\exp\int_0^{\arctan\frac{y}{x}} \frac{2}{\sqrt{h}}\phi(s)ds}{\sqrt{x^2+y^2}-\sqrt{h}} + \int_0^{\arctan\frac{y}{x}} \left(\exp\int_0^s \frac{2}{\sqrt{h}}\phi(\eta)d\eta\right)\frac{1}{h}\phi(s)ds.$$

The trajectories of the system (2) are the level curves $I(x,y) = c$, $c \in \mathbb{R}$, and since these curves are obviously non-algebraic except for the curve (Γ) which corresponds to $c \to +\infty$, any other limit cycle, if it exists, should also be non-algebraic. Hence, statement (1) is proved.

(2) If we put $\theta = 0$ in the solution (8), we have

$$r(0,c) = \sqrt{h} + \frac{1}{c}.$$

Let $r_0 = \sqrt{h} + \frac{1}{c}$, so $r(0,r_0) = r_0 > 0$, corresponds to the value $c = \frac{1}{r_0-\sqrt{h}}$, which allows to rewrite the general solution of (8) as

$$r(\theta,r_0) = \sqrt{h} + \frac{\exp\int_0^\theta \frac{2}{\sqrt{h}}\phi(s)ds}{\frac{1}{r_0-\sqrt{h}} - \int_0^\theta \left(\exp\int_0^s \frac{2}{\sqrt{h}}\phi(\eta)d\eta\right)\frac{1}{h}\phi(s)ds},$$

where $r_0 = r_0(0)$ and $\phi(\theta) = \frac{wa}{2(a^2\sin^2\theta+\cos^2\theta)}$.

The periodic solutions of system (2) must satisfy the following condition:

$$r(2\pi,r_0) = r(0,r_0). \tag{9}$$

The condition (9) is equivalent to

$$r_0 = r_* = \frac{\exp\int_0^{2\pi} \frac{-2}{\sqrt{h}}\phi(s)ds - 1}{\int_0^{2\pi} \left(\exp\int_0^s \frac{2}{\sqrt{h}}\phi(\eta)d\eta\right)\frac{1}{h}\phi(s)ds} + \sqrt{h}, \tag{10}$$

r_* is the intersection of the periodic orbit with the positive $x-$semi-axis.

Let us show that the right-hand side of (10) is strictly positive.

Indeed, since $aw < 0$ and $h > 0$, then $\phi(\theta) = \frac{wa}{2(a^2\sin^2\theta+\cos^2\theta)} < 0$ and $\frac{1}{\exp\int_0^\theta \frac{2}{\sqrt{h}}\phi(s)ds} - 1 < 0$ for all $\theta \in \mathbb{R}$, so

$$\begin{aligned} r_* &= \frac{\exp\int_0^{2\pi} \frac{-2}{\sqrt{h}}\phi(s)ds - 1}{\int_0^{2\pi} \left(\exp\int_0^s \frac{2}{\sqrt{h}}\phi(\eta)d\eta\right)\frac{1}{h}\phi(s)ds} + \sqrt{h} \\ &= \frac{\frac{1}{\exp\int_0^\theta \frac{2}{\sqrt{h}}\phi(s)ds} - 1}{\int_0^{2\pi} \left(\exp\int_0^s \frac{2}{\sqrt{h}}\phi(\eta)d\eta\right)\frac{1}{h}\phi(s)ds} + \sqrt{h} > 0. \end{aligned}$$

Substituting the value of r_* into (2), we get the candidate solution

$$r(\theta,r_*) = \sqrt{h} + \left(\exp\int_0^\theta \frac{2}{\sqrt{h}}\phi(s)ds\right)\left(\frac{1}{r_*-\sqrt{h}} - \int_0^\theta \left(\exp\int_0^s \frac{2}{\sqrt{h}}\phi(\eta)d\eta\right)\frac{1}{h}\phi(s)ds\right)^{-1}.$$

Next, we prove that $r(\theta, r_*) > 0$. Indeed, since $aw < 0$ and $h > 0$, we have $\phi(\theta) = \frac{wa}{2(a^2 \sin^2\theta + \cos^2\theta)} < 0$ for all $\theta \in \mathbb{R}$, so

$$\begin{aligned} r(\theta, r_*) &= \sqrt{h} + \frac{\exp \int_0^\theta \frac{2}{\sqrt{h}}\phi(s)ds}{\frac{1}{r_* - \sqrt{h}} + \int_0^\theta \left(\exp \int_0^s \frac{2}{\sqrt{h}}\phi(\eta)d\eta\right)\left(\frac{-1}{h}\phi(s)\right)ds} \\ &= \sqrt{h} + \frac{\exp \int_0^\theta \frac{2}{\sqrt{h}}\phi(s)ds}{\frac{\left(\exp \int_0^{2\pi} \frac{2}{\sqrt{h}}\phi(s)ds\right)^{-1} - 1}{\int_0^{2\pi}\left(\exp \int_0^s \frac{2}{\sqrt{h}}\phi(\eta)d\eta\right)\frac{1}{h}\phi(s)ds} + \int_0^\theta \left(\exp \int_0^s \frac{2}{\sqrt{h}}\phi(\eta)d\eta\right)\left(\frac{-1}{h}\phi(s)\right)ds} > 0 \end{aligned}$$

for all $\theta \in \mathbb{R}$. To prove that the periodic orbit is a hyperbolic limit cycle, we consider (2) and introduce the Poincare return map $r_0 \mapsto P(r_0) = r(2\pi, r_0)$, see [14].

We compute

$$\left.\frac{dr(2\pi, r_0)}{dr_0}\right|_{r=r_*} = \exp \int_0^{2\pi} \frac{2}{\sqrt{h}}\phi(s)ds < 1.$$

Since $\phi(\theta) < 0$ for all $\theta \in \mathbb{R}$, we have $\int_0^{2\pi} \frac{2}{\sqrt{h}}\phi(s)ds < 0$,

therefore

$$\left.\frac{dr(2\pi, r_0)}{dr_0}\right|_{r=r_*} < 1.$$

For this reason, the limit cycle for the ordinary differential equation (5) is stable. Finally, system (2) has exactly one non-algebraic limit cycle which is the only existing limit cycle. Consequently, this is an unstable and hyperbolic limit cycle for the differential system (2). This completes the proof of statement (2) of Theorem 2.1.

Example 2.1 When $a = -2, h = 4, w = 1$, system (2) reads

$$\begin{cases} \dot{x} = 8y\left(4y^2 + x^2\right) + 2x\left(x^4 + y^4\right) - 8x\left(x^2 + y^2\right) + 4x^3y^2, \\ \dot{y} = -8x\left(4y^2 + x^2\right) + 2y\left(x^4 + y^4\right) - 8y\left(x^2 + y^2\right) + 4x^2y^3, \end{cases} \tag{11}$$

the system (11) satisfies the conditions of the statement (2) of Theorem 2.1, hence the system (11) possesses one non-algebraic limit cycle which is an unstable and hyperbolic limit cycle for the differential system (11) as shown in Figure 1 and it is explicitly given in polar coordinates (r, θ) by the expression

$$r(\theta, r_*) = 2 + \left(\exp \int_0^\theta \phi(s)ds\right)\left(\frac{1}{r_* - 2} - \frac{1}{4}\int_0^\theta \left(\exp \int_0^s \phi(\eta)d\eta\right)\phi(s)ds\right)^{-1}$$

with $\phi(\theta) = \frac{-1}{4\sin^2\theta + \cos^2\theta}$, and

$$r_* = \frac{\left(\exp \int_0^{2\pi} \phi(s)ds\right)^{-1} - 1}{\int_0^{2\pi}\left(\exp \int_0^s \frac{2}{\sqrt{h}}\phi(\eta)d\eta\right)\frac{1}{h}\phi(s)ds} + 2 \simeq 2.25.$$

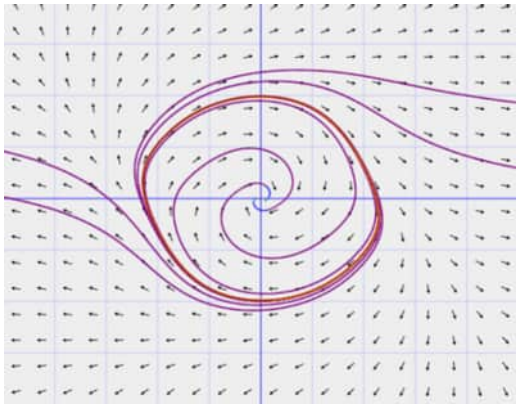

Figure 1: Limit cycle of the system (11) in the Poincare disc.

3 Conclusion

In this paper, we studied a class of quintic planar polynomial differential systems featuring a non-elementary singular point. We established sufficient conditions for the existence of a hyperbolic, non-algebraic limit cycle surrounding this singularity. Furthermore, we provided an explicit expression for the limit cycle in polar coordinates. To demonstrate the applicability of our theoretical findings, a concrete example was constructed, and its corresponding phase portrait was presented. These results contribute to the qualitative theory of nonlinear differential systems and offer valuable insights into the dynamics near non-elementary singularities.

References

[1] I. T. Al-Dosary Khalil. Non-algebraic limit cycles for parametrized planar polynomial systems. *Int. J. Math.* **18** (2)(2007) 179–189.

[2] A. A. Andronov. Les cycles limites de Poincaré et la théorie des oscillations auto-entretenues. *C.R. Acad. Sci. Paris* **89** (1929) 559–561.

[3] R. Benterki and J. Llibre. Polynomial differential systems with explicit non-algebraic limit cycles. *Elect. J. of Diff. Equ.* **2012** (78) (2012) 1–6.

[4] R. Boukoucha. First Integral of a class of two-dimensional Kolmogorov systems. *Nonlinear Dynamics and Systems Theory* **22** (1) (2022) 13–20.

[5] F. Dumortier, J. Llibre and J. Artés. *Qualitative Theory of Planar Differential Systems.* Universitext, Springer-Verlag, Berlin, 2006.

[6] A. Gasull, H. Giacomini and J. Torregrosa. Explicit non-algebraic limit cycles for polynomial systems. *J. Comput. Appl. Math.* **200** (1) (2007) 448–457.

[7] J. Gine and J. Llibre. Integrability and algebraic limit cycles for polynomial differential systems with homogeneous nonlinearities. *J. Differential Equations* **197** (1) (2004) 147–161.

[8] J. Guckenheimer and P. Holmes. *Nonlinear Oscillations, Dynamical Systems and Bifurcations of Vector Fields.* Springer Science and Business Media, 2013.

[9] A. Kina and A. Bendjeddou. On the Dynamics of a class of planar differential systems. *Nonlinear Dynamics and Systems Theory* **22** (4) (2022) 400–406.

[10] A. Kina, A. Berbache and A. Bendjeddou. Integrability and limit cycles for a class of multi-parameter differential systems with unstable node point. *Rend. Circ. Mat. Palermo 2.* **72** (3) 1937–1946 (2023).

[11] J. Llibre, J. Antonio and E. Teruel. *Introduction to the Qualitative Theory of Differential Systems.* Springer Basel, 2014.

[12] A. Menaceur and A. Makhlouf. Limit Cycles for a Class of Generalized Liénard Polynomial Differential Systems via the First-Order Averaging Method. *Nonlinear Dynamics and Systems Theory* **25** (5) (2025) 563–572.

[13] K. Odani. The limit cycle of the van der Pol equation is not algebraic. *J. of Diff. Equ.* **115** (1) (1995) 146–152.

[14] L. Perko. *Differential Equations and Dynamical Systems.* Springer-Verlag, New York, 2000.

[15] S.H. Strogatz. *Nonlinear Dynamics and Chaos: With Applications to Physics, Biology, Chemistry and Engineering.* Chapman and Hall/CRC, 2024.

[16] B. Van der Pol. On relaxation-oscillations. *Phil. Mag.* **2** (1) (1926) 978–992.

Nonlinear Dynamics and Systems Theory, **26** (2) (2026) 203–213

Systematic Review of Students' Attitudes and Motivation Using Dynamical System Models

A. Maryati [1*], N. Anggriani [2], A. K. Supriatna [2] and E. Carnia [2]

[1] *Doctoral at the Department of Mathematics, Faculty of Mathematics and Natural Sciences, Universitas Padjadjaran, Bandung, Indonesia.*

[2] *Department of Mathematics, Faculty of Mathematics and Natural Sciences, Universitas Padjadjaran, Bandung, Indonesia.*

Received: June 13, 2025; Revised: April 11, 2026

Abstract: The study investigates students' negative attitudes toward learning mathematics, often linked to low motivation, anxiety, and disinterest. These issues are widespread and influenced by factors such as misinformation and avoidance of challenging math courses. To understand the spread of such attitudes, the research uses mathematical modeling through a Systematic Literature Review (SLR) covering studies from 2013–2023, using databases including Scopus, Science Direct, Google Scholar, and Dimensions. Analysis follows the PRISMA method and uses bibliometric tools such as VOSviewer. The findings reveal that since 2020, very few studies have focused on mathematical models analyzing students' attitudes toward mathematics learning, and none have addressed both attitudes and motivation simultaneously–highlighting a significant research gap.

Keywords: *mathematical model; dynamic analysis; optimal control; anxiety; hostility towards mathematics; motivation; interest.*

Mathematics Subject Classification (2020): 70K75, 92D30, 93A30, 93C15, 97C70.

* Corresponding author: mailto:nursanti.anggriani@unpad.ac.id

1 Introduction

Mathematics holds significant potential in cultivating highly competent human resources suited for the demands of the globalization era. This potential can be realized when mathematics education effectively equips students with a strong grasp of mathematical concepts and the ability to apply and integrate them in other scientific disciplines. The advancement of science and technology, along with the economic progress of various nations, is inseparable from the foundational role of mathematics, which is essential for understanding a wide array of fields including science, technology, business, social sciences, engineering, and the arts [1]. Despite its importance, mathematics education faces considerable challenges. Factors such as students' attitude, teaching methods, and teacher competence greatly influence educational quality. One key issue is student anxiety during mathematics lessons, which acts as a psychological barrier to achievement [2]. This anxiety can lead to avoidance and disengagement from math learning. In more severe cases, students may develop outright hostility towards mathematics [3]. Such negative attitudes are often associated with the so-called Strawberry Generation-young people known for their potential, but also for their psychological fragility and difficulty in coping with academic and life pressure [4].

Nonlinear dynamics provides a robust framework to capture the feedback loops, thresholds, and stability conditions inherent in such educational phenomena, allowing researchers and educators to understand not only how negative attitudes propagate, but also how timely interventions can shift the system toward a more motivated and engaged student population. Hence, integrating nonlinear dynamical systems into this educational context enables a deeper, quantitatively grounded insight into the evolution and control of students' attitudes and motivation in mathematics learning.

The persistence of students' negative attitudes toward learning mathematics is a longstanding concern that significantly impacts their motivation and interest in the subject [5]. These attitudes are shaped by various factors, including personal motivation, teacher influence, and social interactions such as peer support [6]. When students lack motivation or experience negative emotions—such as anxiety, fear, hatred, or discouragement—these psychological conditions can spread and hinder the mathematics learning environment. Addressing this issue requires teachers to foster a classroom atmosphere that nurtures positive emotions and encourages student motivation [7]. Situational factors greatly influence emotional experiences, which in turn affect students' attitudes and confidence levels during math learning. By implementing effective teaching strategies, educators can stimulate the transmission of positive emotions and motivation not only between teachers and students but also among peers. This interaction builds students' emotional resilience in facing challenges in learning mathematics. Research also indicates that emotional contagion—especially in close-knit social environments—is more likely to spread positive feelings than negative ones [8].

The approach of mathematical modeling using deterministic methods is a scientific effort to connect and discover real-world situations [9]. A mathematical model is a model that consists of mathematical concepts such as coefficients, constants, variables, functions, equations, and so on. The mathematical model of epidemics in the spread of students' negative attitudes toward mathematics learning is one part of applied mathematics which discusses various aspects of epidemics of psychological diseases, and mathematical modeling is the knowledge to translate a problem into mathematical language [10]. Mathematical modeling is a tool that can be used to analyze the spread of students'

learning attitudes and motivation towards learning mathematics. This research aims to identify future research gaps regarding mathematical modeling in analyzing the dynamics of students' attitudes and learning motivation in mathematics learning.

This study employs the Systematic Literature Review (SLR) method to analyze research on mathematical modeling related to the spread of students' attitudes and motivation in mathematics learning, using data from Scopus, ScienceDirect, Google Scholar, and Dimensions databases from 2013–2023, and analyzed through the PRISMA method and bibliometric visualization. Deterministic mathematical models have long been used to study the spread of physical and psychological phenomena such as diseases in humans and plants, racism and corruption and cultural dissemination [11, 12]. These variations in modeling arise from differing assumptions, making each model unique [13]. Given the limited studies focusing specifically on the dynamics of students' attitudes and motivation in mathematics, this literature review seeks to identify research gaps and encourage future developments in modeling approaches and methodologies in this field.

2 Methodology

2.1 Data search strategy

The PRISMA method is an analytical technique used to identify elements of papers in a database. This method explores papers related to the research topic to uncover gaps as novel aspects of this study. In the PRISMA method, the first step is to collect related papers for this research using keywords ("Stability analysis" OR "Mathematical model" OR "Mathematical modeling" OR "Dynamical Analysis" OR "Dynamical System") AND "Optimal Control" AND (("motivation" OR "animosity" OR "anxiety") AND "towards mathematics") across four databases: Scopus, ScienceDirect, Google Scholar, and Dimensions. Based on these keywords, papers are obtained from each database, as detailed in Table 1.

Database	**Scopus**	**ScienceDirect**	**Dimensions**	**Google Scholar**
Number of Papers	2	1	2	18

Table 1: Number of papers collected from each database.

2.2 Selection of relevant papers

Database	**Scopus**	**Science Direct**	**Dimensions**	**Google Scholar**
Number of Papers	2	1	2	16

Table 2: Contribution of papers from each database after duplicate selection.

As shown in Table 1, a total of 23 papers were initially identified as related to the study of mathematical modeling concerning the spread of students' motivation and interest in learning mathematics. The next step involved filtering these papers to remove duplicates and retain those relevant to the research topic. Using Scopus as the primary reference, duplicates across ScienceDirect, Google Scholar, and Dimensions were identified and

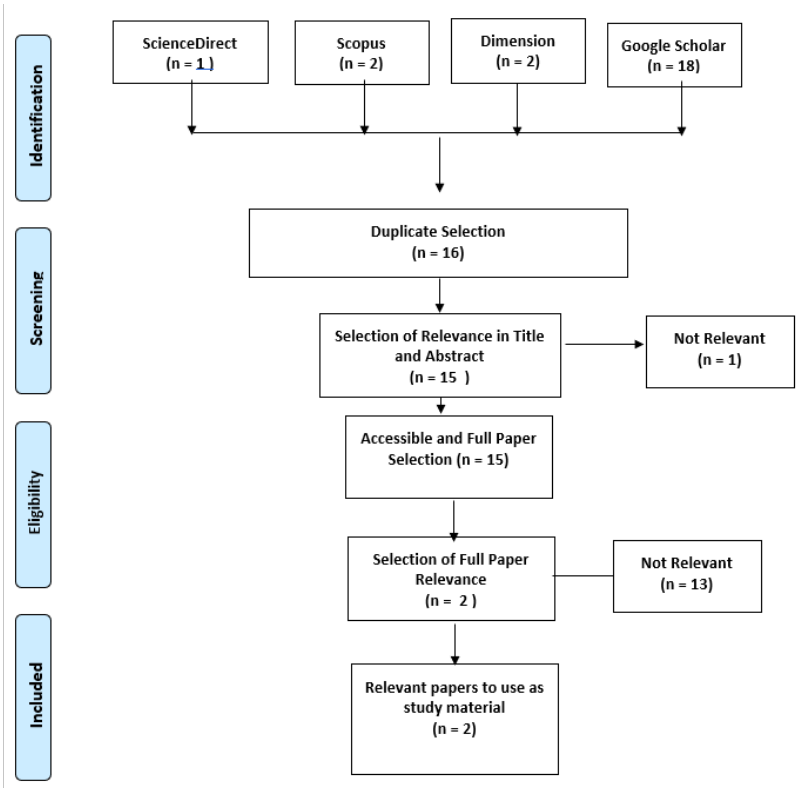

Figure 1: PRISMA analysis flowchart.

excluded, resulting in 15 papers, as presented in Table 2. The selection process continued by evaluating the relevance of the papers titles and abstracts, narrowing the list to 15 papers that matched the specified keywords. A more detailed relevance check was then conducted by skimming these papers to determine alignment with the research scope, which focuses on continuous dynamic systems and the application of optimal control [14]. This rigorous filtering ultimately led to two unique papers deemed most relevant to the study. The PRISMA-based selection process is summarized in the flowchart, see Figure 1.

2.3 Data analysis

The data analysis was carried out in four stages: first, by examining mathematical representations related to the distribution of students' attitudes and motivation toward learning mathematics to identify potential areas for model development; second, by reviewing the findings from previous studies; third, by pinpointing aspects that require further exploration in the context of mathematical models addressing students' attitudes and motivation; and finally, by conducting a bibliometric analysis to assess the novelty of the research, providing insight into existing literature and highlighting gaps within the field.

3 Results

3.1 Previous model overview

The outcome of paper selection based on the use of specific keywords ("Stability analysis" OR "Mathematical model" OR "Mathematical modeling" OR "Dynamical Analysis" OR "Dynamical System") AND "Optimal Control" AND (("motivation" OR "animosity" OR "anxiety") AND "towards mathematics") shows that after duplicative selection, there are 15 relevant papers. A summary of the papers in question can be seen in Table 3. From the initial 15 papers, only 2 were deemed relevant after the screening, eligibility, and inclusion process, and these were used as key references. Their models, detailed in Table 4, represent the earliest efforts to apply mathematical modeling to analyze the transmission of students' attitudes toward mathematics learning.

As illustrated in Table 4, the researchers employed several subpopulations and parameters to build their mathematical models. In the model proposed in [2], the vulnerable subpopulation, denoted by $P(t)$, consists of students who either have the potential to perform well academically or are at risk of developing anxiety related to mathematics. On the other hand, Teklu and Terefe [7] identify their vulnerable group, represented by $S(t)$, as college students who initially do not possess a strong aversion to mathematics—some of whom may even show interest in the subject—but may develop animosity upon interaction with already affected peers. Regarding the exposed subpopulation, Nathan and Jackob [2] do not include this category in their model. However, Teklu and Terefe [7] introduce an exposed group, denoted by $E(t)$, comprising students who are currently enrolled in mathematics courses and have frequent contact with those expressing negative sentiments about the subject. These exposed individuals may or may not become negatively influenced. Furthermore, in Nathan and Jackob's model, the group of students who have developed anxiety toward mathematics is categorized as the infectious subpopulation, represented by $A_x(t)$.

Meanwhile, in the Teklu and Terefe model [7], students are infected with animosity towards mathematics. A group of students who strongly dislike or display hostility towards mathematics and tend to perform poorly in university are denoted by $A(t)$. Subpopulation that recovered due to treatment, in the Nathan and Jackob model [2], students who recovered due to efforts or treatments to become students with the potential to perform well, are denoted by $A_a(t)$. Meanwhile, in the model of Teklu and Terefe [7], the students who recovered, that is, those who received treatment aimed at eliminating hostility towards mathematics, namely a group of students who received different psychological guidance and treatments from their mentors and professors, are referred to as treated students and denoted by $T(t)$.

In comparing the models by Teklu and Terefe [7] and Nathan and Jackob [2], key differences in parameter usage are evident. The η parameter, which governs the return of treated individuals to the vulnerable group, appears only in the Teklu and Terefe model. Both models utilize the parameter β to describe transmission, but in Teklu and Terefe's model, it represents the transition from vulnerable to exposed, while in Nathan and Jackob's model, it signifies the transition from vulnerable to infected. The parameter γ also differs in meaning: it defines the transition from exposed to infected in Teklu and Terefe's model, and that from infected to recovered in Nathan and Jackob's one. Similarly, δ denotes the transition from infected to recovered in the Teklu and Terefe model, whereas in Nathan and Jackob's model, it indicates the transition from vulnerable to recovered.

No	Writer	Research Topics	Summary	Method/model	Description
1.	Kendall (2013) [1]	Estimated Future Trends in the Development Of Mathematics and of its relations with the Non-Mathematical world	Classify the branches of Mathematics into (1) which is rarely or never used in statistics; (2) which is used occasionally but not in depth; (3) things that are important to the subject and adding a fourth category,(4) categories that must be discovered or developed by statisticians	-	The development of mathematics and its relationship with the non-mathematical world Not relevant
2	Nathan & Jackob. (2020) [2]	Mathematical Modeling and Analysis of Mathematics Anxiety Behavior on Mathematics Performance in Kenya	Constructing a deterministic model that describes the dynamics of students who have abilities to perform well on mathematics tests and engage in careers that require its application and the negative influence of individuals with mathematics anxiety on student potential	Model: Susceptible- Infectious-Removed (SIR) Method: Dynamic Analysis	Students who have abilities for achievement and the influence of negative attitudes, namely anxiety towards learning mathematics, on student potential.
3.	Teklu & Terefe (2022) [3]	Mathematical modeling analysis on the dynamics of university students animosity towards mathematics with optimal control theory	Formulate a new SEATS compartmental mathematical model with optimal control theory to analyze the dynamics of student animosity towards mathematics	Model: Susceptible- Exposed-Animosity Infectious- Treated-susceptible (SEATS) Method: Dynamic Analysis	university students animosity towards mathematics
4.	Kotola & shewafera (2022) [4]	A Mathematical Modeling Analysis of Racism and Corruption Codynamics with Numerical Simulation as Infectious Diseases	Formulate the dynamics of racism and corruption that coexist in society, using a deterministic compartmental model to analyze and suggest appropriate control strategies to stakeholders	Deterministic compartment model	Racism and corruption coexist in society,full paper is not suitable.
5.	Terefe (2022) [5]	Mathematical Model Analysis on the Diffusion of Violence	Formulate and test a mathematical model of direct violence with five different classes of human populations (vulnerable, exposed to violence, violent, negotiated, and reconciled)	Model: Susceptible, exposed, Violently infectious, Negotiated, reconciled SEPHR	Violence against humans full paper is not suitable
6.	Teklu & Mamo (2022) [6]	A nonlinear system dynamics and simulation analysis of fractional order modelling on employees negative attitude towards their workplace with intervention strategies	Formulate and analyze the Caputo fractional order mathematical model with intervention strategies for employees' negative attitudes towards the workplace.	Model: susceptible, protected, exposed, employees who have ordinary negative attitude, employees who have permanent negative attitude, employees recoverd from negative attitude (SPEAQR)	Employee negative attitudes towards the workplace. Full paper is not suitable.
7.	Teklu & Terefe (2022) [7]	Mathematical Modeling Investigation of Violence and Racism Coexistence as a Contagious Disease Dynamics in a Community	Developing and testing a new mathematical model of the coexistence of violence and racism with eight different classes of human populations (vulnerable, violence-infected, negotiated, racist, violence-racism co-infected, recovering from violence, recovering against racism, and recovering from co-infection)	Model:SVUR1,2,3.	Violence and racism full paper is not suitable.
8.	Teklu (2023) [8]	Analysis of fractional order model on higher institution students' anxiety towards mathematics with optimal control theory	Formulate and analyze the Caputo fractional order mathematical model with optimal control strategies for college students' anxiety towards mathematics.	SPEAQR Method: caputo fractional order	College students' anxiety about mathematics.
9.	Teklu et al. (2023) [9]	Analysis of tinea capitis epidemic fractional order model with optimal control theory	Formulating the transmission dynamics of tinea captis infection using Caputo's fractional derivative approach.	Model : susceptible, exposed, infected, recoverd (SEIR)	Transmission of tinea captis infection full paper is not suitable.
10.	Asih et al. (2023) [10]	Weights Optimization Using Firefly Algorithm for Dengue Fever Optimal Control Model by Vaccination, Treatment, and Abateseae	Optimal control model for minimizing the spread and cost of dengue fever transmission in Indonesia using the Firefly Algorithm	Model: vaccination, treatment, and larvicide (abateseae) strategies	Examining the dynamics of Dengue Fever in the vaccination phase. full paper is not suitable.
11.	Quedraogo & Guiro (2023) [11]	Analysis of Dengue Disease Transmission Model with General Incidence Functions	analyze a nonlinear dengue fever transmission model involving general incidence functions that describe interactions between humans and mosquito vectors	Model: SIRSI	Dengue fever transmission model full paper is not suitable.
12.	Baba et al. (2023) [12]	A fractional order model that studies terrorism and corruption codynamics as epidemic disease	Formulate a fractional order mathematical model to study the dynamics of the coexistence of terrorism and corruption in society.	Model: SCDRT	Terrorists and corruption full paper is not suitable.
13.	Olaniyi et al. (2023) [13]	Lyapunov Stability and Economic Analysis of Monkeypox Dynamics with Vertical Transmission and Vaccination	Formulate a new nonlinear mathematical model to understand the dynamics of monkeypox disease	-	Monkeypox disease Full paper cannot be opened
14.	Teklu (2023) [14]	Investigating the Effects of Intervention Strategies on Pneumonia and HIV/AIDS Coinfection Model	Formulate a compartment epidemic model on the dynamics of the spread of HIV/AIDS and pneumonia coinfection to investigate the impact of protective and treatment intervention mechanisms on the spread of coinfection in the community	Model: SCHPT	HIV/AIDs and pneumonia full paper is not suitable.
15.	Mamo & Mengstie (2023) [15]	Racism Dissemination Model and Simulation Analysis Considering Crowd Classification with Intervention Strategies	Analyze compartmental mathematical models to understand how racists spread their opinions and influence society with intervention strategies	Model: S-H-R-C-I	Racist full paper is not suitable.

Table 3: Summary of relevant papers.

	$\frac{dP}{dt} = \eta - \beta P(t)A_x(t) - \delta P(t) - \mu P(t)$
4*Model 1 (Nathan and Jackob, 2020) [2]	$\frac{dA_x}{dt} = \beta P(t)A_x(t) - \gamma A_x(t) - \mu A_x(t)$
	$\frac{dA_a}{dt} = \gamma A_x(t) + \delta P(t) - \mu A_a(t)$
	$\frac{dS(t)}{dt} = \eta + \alpha T(t) - \beta S(t)A(t) - \mu S(t)$
4*Model 2 (Teklu and Terefe, 2022) [3]	$\frac{dE(t)}{dt} = \beta S(t)A(t) - (\mu + \gamma)E(t)$
	$\frac{dA(t)}{dt} = \gamma E(t) - \mu + \delta A(t)$
	$\frac{dT(t)}{dt} = \delta A(t) - \mu + \alpha T(t)$

Table 4: Model of the distribution of attitudes towards previous mathematics learning.

3.2 Results that have been achieved in previous studies

In [2], the mathematical models represent the first attempts to apply mathematical modeling to examine the transmission of students' attitudes toward mathematics learning. In the first model, the student population is categorized into three groups: vulnerable students, students experiencing anxiety related to learning mathematics, and high-achieving students. In contrast, the second model divides the population into four compartments: vulnerable students, those exposed to hostility toward mathematics, students infected with such hostility, and students undergoing tutorial interventions to recover from negative attitudes. Both models employ dynamic systems approaches, including analysis of equilibrium points, calculation of the basic reproduction number, and assessment of system stability. Additionally, the second model incorporates optimal control strategies using Pontryagin's maximum principle to evaluate the effectiveness of intervention efforts.

Based on the models developed in [2], several limitations have been identified. Notably, both models focus solely on negative attitudes such as anxiety and hatred toward mathematics, without incorporating motivational variables or the positive influence of teachers as motivators in implementing interventions. Furthermore, the preventive strategies used are implicitly limited to subgroups of students receiving treatment, lacking comprehensive mitigation involving the broader student population. Additionally, the interventions applied are general in nature and do not incorporate STEM-based quantum teaching-learning strategies, which have the potential to significantly boost students' motivation and engagement. A comparative overview of the elements within both models and their alignment with the research context on the dissemination of students' attitudes and motivation toward mathematics learning is provided in Table 5.

3.3 Research gaps that may be developed

After reviewing studies related to the modeling of the spread of students' attitudes and motivation toward learning mathematics, it becomes apparent that compartmental models are still rarely applied in this context. This is supported by the identification of only two relevant papers, indicating a significant research gap despite the increasing application of compartmental modeling in various fields. Existing studies primarily focus on modeling the dissemination of negative attitudes such as anxiety and hostility toward mathematics, without addressing the positive aspects of motivation and student interest. Furthermore, prior research has yet to incorporate control strategies involving specific learning approaches aimed at enhancing students' motivation in mathematics education. The development of Model 1 and Model 2 involves constructing a modified model that

No.	Author	Research Topics	Summary	Method/model
1.	Nathan & Jackob. (2020) [2]	Students who have the ability to achieve and the negative influence of individuals with mathematics anxiety on student potential	Constructing a deterministic model that depicts the dynamics of students who have the ability to excel in mathematics exams and are involved in careers that demand its application, and the negative influence of individuals with mathematics anxiety on student potential.	Model: Susceptible-Infectious- Removed (SIR) Method: Dynamic Analysis
2.	Shewafera & Birhanu (2022) [3]	Student animosity towards mathematics	Formulating a new SEATS compartmental mathematical model with optimal control theory to analyze the dynamics of student animosity towards mathematics.	Model: Susceptible-Exposed- Animosity Infectious- Treated-susceptible (SEATS) Method: Dynamic Analysis

Table 5: Summary of papers.

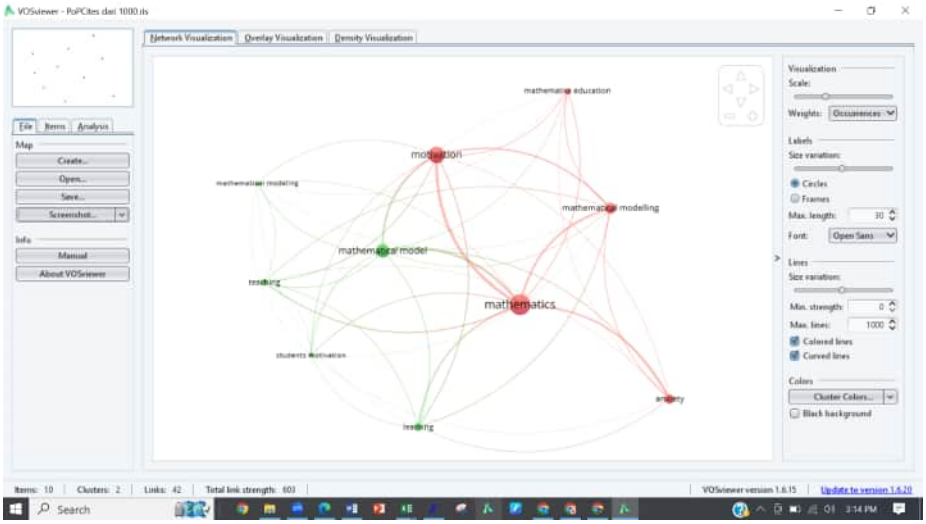

Figure 2: Research mapping the distribution of students' attitudes.

incorporates the spread of both negative and positive student attitudes toward learning mathematics, while also taking into account the application of a motivating learning strategy. This modification aims to decrease the number of students with negative attitudes and reduce the presence of unmotivating teachers, while simultaneously increasing the population of students with positive attitudes and teachers who actively motivate mathematics learning. Additionally, the model includes control strategies designed to enhance student motivation and engagement in mathematics while minimizing the associated implementation costs.

3.4 Blibiometric analysis

Based on the keywords outlined in Section 2.2, a total of 16 papers were identified after duplicate removal, and additional 15 papers were selected based on the relevance of their references. The bibliometric network visualization of these selected papers, generated using VOSviewer software, is shown in Figure 2.

Figure 2 shows that the nodes representing students' attitudes and motivation to-

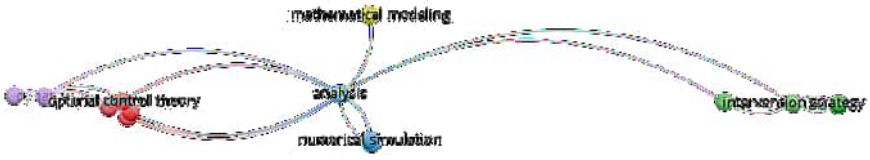

Figure 3: Visualization of the interrelationships among all reference papers.

ward learning mathematics in the context of mathematical modeling are relatively small, indicating that only a limited number of researchers have explored this area. Additionally, the figure reveals a lack of connections between models addressing the spread of negative and positive attitudes, students' learning motivation, and mathematics learning strategies. This gap highlights a valuable opportunity for future researchers to develop comprehensive mathematical models that integrate these aspects to better predict and understand the dynamics of students' attitudes and motivation toward mathematics learning.

Based on Figure 1, the mapping results in Figures 2 and 3, and the summary of papers in Table 5, it is evident that no existing research has integrated a mathematical model of the spread of students' attitudes and learning motivation toward mathematics with optimal control to predict these dynamics. This represents a novel and promising opportunity for future research in this area. Additionally, all reference papers were mapped using VOSviewer to visualize their interconnections, as illustrated in Figure 3.

4 Discussion

The current study highlights a significant gap in the application of mathematical modeling to the dynamics of students' attitudes and motivation toward mathematics learning. Despite the extensive use of compartmental models in fields such as epidemiology, social sciences, and psychology, their application to educational contexts particularly modeling students' emotional and motivational dynamics—remains limited. Only two relevant studies were identified, both focusing predominantly on the spread of negative attitudes such as anxiety and animosity. These models employed classical deterministic approaches, including stability analysis and basic reproduction number calculations, and in one case, optimal control theory to explore intervention strategies. However, neither model incorporated variables that capture positive psychological constructs such as motivation or interest in mathematics.

This limited focus presents a critical shortcoming, as motivation plays a crucial role in shaping students' learning experiences and academic performance. The exclusion of motivational factors and teacher influences from previous models results in a narrow representation of the learning environment. Furthermore, while both existing models introduced control strategies, they were mostly limited to generic psychological treatments or tutorials, without considering pedagogical innovations such as STEM-based or quantum learning approaches. These omissions suggest that current mathematical models may underestimate the potential for positive intervention and support systems

in reversing negative attitudes and promoting long-term engagement with mathematics.

The bibliometric analysis further supports this conclusion, revealing a fragmented research landscape with few interconnections between studies modeling emotional and motivational dynamics in mathematics education. There is an urgent need for comprehensive models that not only capture the spread of negative emotions but also account for the diffusion of positive attitudes and motivational interventions. Future models should integrate dynamic interactions between students, peer groups, and educators, and evaluate the effectiveness of specific teaching strategies through optimal control frameworks. Such advancements would provide a more holistic and actionable understanding of the emotional and motivational factors influencing students' success in mathematics.

5 Conclusions

This study reveals a significant research gap in the application of nonlinear dynamical models to analyze the dynamics of students' attitudes and motivation toward mathematics learning. Through a systematic literature review and bibliometric analysis, we identified that existing models have primarily focused on negative psychological responses such as anxiety and animosity, while largely neglecting the role of motivation and positive learning influences. The novelty of this work lies in highlighting the absence of integrated models that simultaneously account for both negative and positive student attitudes, including the impact of motivational strategies within a control-theoretic framework. By synthesizing findings from recent mathematical modeling efforts and mapping their limitations, this paper offers a new research direction: the development of more comprehensive, optimally controlled compartmental models that incorporate emotional contagion, teacher influence, and motivational interventions. These models are crucial for predicting, understanding, and managing the evolving psychological dynamics in mathematics education from a nonlinear systems perspective.

Acknowledgement

The authors would like to thank the Ministry of Education, Culture, Research, and Technology through the PDD 2024 with contract number 3968/UN6.3.1/PT.00/2024.

References

[1] M. Kendall. Estimated Future Trends in the Development of Mathematics and of its Relations with the Non-Mathematical World. *Mathematics in the Real World* (2013) 34–52.

[2] O. M. Nathan and K. O. Jackob. Mathematical Modeling and Analysis of Mathematics Anxiety Behavior on Mathematics Performance in Kenya. *J. Adv. Math. Comput. Sci.* **35** (4) (2020) 46–62. doi: 10.9734/jamcs/2020/v35i430269.

[3] S. W. Teklu and B. B. Terefe. Mathematical modeling analysis on the dynamics of university students animosity towards mathematics with optimal control theory. *Sci. Rep.* **12** (1) (2022) 1–19. doi: 10.1038/s41598-022-15376-3.

[4] B. S. Kotola and S. W. Teklu. A Mathematical Modeling Analysis of Racism and Corruption Codynamics with Numerical Simulation as Infectious Diseases. *Comput. Math. Methods Med.* **2022** (4) (2022). doi: 10.1155/2022/9977727.

[5] B. B. Terefe. Mathematical Model Analysis on the Diffusion of Violence. *Int. J. Math. Math. Sci.* (2022). doi: 10.1155/2022/4776222.

[6] S. W. Teklu, D. K. Mamo and D. Ketema Mamo. A nonlinear system dynamics and simulation analysis of fractional order modelling on employees negative attitude towards their workplace with intervention strategies. *Research Square* (2022). doi: 10.21203/rs.3.rs-2368423/v1.

[7] S. W. Teklu and B. B. Terefe. Mathematical Modeling Investigation of Violence and Racism Coexistence as a Contagious Disease Dynamics in a Community. *Comput. Math. Methods Med.* (2022). doi: 10.1155/2022/7192795.

[8] S. W. Teklu. Analysis of fractional order model on higher institution students' anxiety towards mathematics with optimal control theory. *Sci. Rep.* **13** (1) (2023) 1–20. doi: 10.1038/s41598-023-33961-y.

[9] S. W. Teklu, A. A. Meshesha and S. Ullah. Analysis of tinea capitis epidemic fractional order model with optimal control theory. *Informatics Med. Unlocked* **42** (2009) 101379. doi: 10.1016/j.imu.2023.101379.

[10] A. Y. P. Asih, B. Gunawan, N. Hidayati, T. Herlambang, D. Rahmalia and K. Oktafianto. Weights Optimization Using Firefly Algorithm for Dengue Fever Optimal Control Model by Vaccination, Treatment, and Abateseae. *Nonlinear Dynamics and Systems Theory* (23) (3) (2023) 237–248.

[11] H. Quedraogo and A. Guiro. Analysis of Dengue Disease Transmission Model with General Incidence Funcstions. *Nonlinear Dynamics and Systems Theory* **23** (1) (2023) 79–94.

[12] I. A. Baba, F. A. Rihan and E. Hincal. A fractional order model that studies terrorism and corruption codynamics as epidemic disease. *Chaos* **169** (2023). doi: 10.1016/j.chaos.2023.113292.

[13] S. Olaniyi and F. M. Chuma. Lyapunov Stability and Economic Analysis of Monkeypox Dynamics with Vertical Transmission and Vaccination. *Int. J. Appl. Comput. Math.* **9** (85) (2023) 1–28.

[14] S. W. Teklu. Investigating the Effects of Intervention Strategies on Pneumonia and HIV/AIDS Coinfection Model. *Biomed Res. Int.* (2023). doi: 10.1155/2023/5778209.

[15] D. K. Mamo and T. K. Mengstie. Racism Dissemination Model and Simulation Analysis Considering Crowd Classification with Intervention Strategies. *Biomed Res. Int.* (2023). doi: 10.1155/2023/5778209.

Nonlinear Dynamics and Systems Theory, **26** (2) (2026) 214–228

Fractional-Order 5D Hyperchaotic System: Stability and Modified Projective Synchronization

A. Senouci [1*], B. Laadjel [1] and S. Senouci [2]

[1] *Department of Mathematics, University of Biskra, Biskra, Algeria.*
[2] *School of Computer Science and Engineering, University of Electronic Science and Technology of China, Chengdu, 611731, Sichuan, People's Republic of China.*

Received: August 31, 2025; Revised: April 13, 2026

Abstract: This paper introduces a novel five-dimensional fractional-order hyperchaotic system derived as a modification of the Lorenz model. The proposed system exhibits richer dynamics than its integer-order counterpart, including multiple coexisting attractors and complex bifurcation structures. The stability conditions of equilibrium points are derived using an extended fractional Routh–Hurwitz criterion, and Lyapunov exponent analysis confirms the existence of hyperchaotic behavior across a broad parameter range. To further explore its practical relevance, a Modified Projective Synchronization (MPS) strategy is applied to both identical and non-identical systems. Numerical simulations validate the theoretical analysis and highlight the potential of the proposed system for secure communication applications.

Keywords: *stability, 5D fractional-order system, Routh–Hurwitz criteria, modified projective synchronization.*

Mathematics Subject Classification (2020): 34A08, 34D06, 37D45, 70K05, 93C41, 93D05.

1 Introduction

Fractional calculus, whose origins go back more than three centuries, has gained much attention in recent studies because it can model complicated physical, chemical, and engineering systems with greater precision [7]. Fractional-order methods differ from conventional integer-order approaches in that they embrace memory and hereditary properties, enabling them to describe real-world phenomena more accurately. There have

* Corresponding author: mailto:assia.senouci@univ-biskra.dz

been profound theoretical advances in this domain, particularly in relation to the formalization of stability criteria for fractional-order differential equations [3], thereby reinforcing the foundational theoretical underpinnings of the discipline. In nonlinear dynamics, chaos synchronization of chaotic systems, where two or more chaotic systems synchronize their behavior through coupling or external drive, has emerged as a research topic of paramount interest. The groundbreaking study by Pecora and Carroll in 1990, established that two identical chaotic systems could achieve synchronization, thus catalyzing a vast array of applications, with secure communication emerging as one of the most pivotal. Following this breakthrough, numerous synchronization approaches have been proposed, including complete synchronization (CS) [6], phase synchronization (PS), lag synchronization (LS) [9], generalized synchronization (GS) [14], and projective synchronization [10]. Building on these foundational approaches, recent work has further expanded this repertoire: Hannachi and Amira [5] demonstrated full-state hybrid projective (FSHP) synchronization for 3D chaotic systems with three nonlinearities, while Ghettout et al. [4] investigated the adaptive synchronization of 4D hyperchaotic systems with infinite equilibria. Each of these paradigms offers a distinct perspective on chaos theory, contributing unique theoretical insights and practical advantages within its respective domain.

The present study is intended to add to the theoretical foundation of chaos research by conducting an in-depth investigation of stability and synchronization of fractional-order hyperchaotic systems. Specifically, it introduces a novel five-dimensional fractional-order hyperchaotic system and, in detail, investigates its stability with different parameter settings. Moreover, an improved MPS scheme is applied to the system and prove to be efficient in synchronizing fractional-order hyperchaotic system dynamics. These findings not only enhance current discussions in chaos theory but also provide a foundation for additional research on high-dimensional fractional-order synchronization methods. Table 1 presents a comparative analysis to emphasize the uniqueness and benefits of the suggested system. Important characteristics of a number of representative fractional-order chaotic and hyperchaotic systems from the literature are compiled in this table, including their dimensionality, equilibrium structure, dynamical behavior, and synchronization strategies. It offers a framework that illustrates how the current work surpasses previous contributions, especially with regard to dimensional extension complexity and synchronization robustness.

The originality of this work in the context of nonlinear dynamics and systems theory is manifested through several key aspects. Unlike fractional-order hyperchaotic models, the system proposed in this paper extends the generalized Lorenz framework to five dimensions by introducing a quadratic self-coupling term $x_4(x_4+1)$ in the first equation, which fundamentally alters the phase space topology and enables richer nonlinear interactions not present in the conventional Lorenz-type extensions. This unique structure produces both second– and third–order hyperchaos within the same parameter configuration. Unlike systems exhibiting only one type of hyperchaotic behavior, our system demonstrates controllable transitions between order-2 and order-3 hyperchaos through dual parameter control (fractional order q and system parameter d). This property is rare in the literature and provides enhanced flexibility for applications requiring tunable complexity. Furthermore, the modified projective synchronization (MPS) scheme developed here achieves guaranteed convergence for both identical and non-identical high-dimensional systems, thereby generalizing existing projective and adaptive synchronization approaches. These innovations place the present study at the intersection of nonlinear dynamics and control

theory, offering new tools for secure communication, encryption, and the coordination of complex dynamical networks.

To highlight advances in fractional-order chaotic and hyperchaotic systems between 2020 and 2025, Table 1 summarizes representative models, their system properties, and synchronization methods.

system	dim.	fo	equilibrium	chaos	synchronization	ref.
wang et al.	n/a	yes	not defined	hyperchaotic	improved projective	[12]
chen et al.	4d	yes	single point	hyperchaotic	adaptive tracking	[1]
shao et al.	4d	yes	single point	hyperchaotic	sliding mode	[8]
eshaghi et al.	4d	yes	single point	hyperchaotic	chaos control in laser system	[2]
yaghoubi et al.	4d	yes	stable origin	hyperchaotic	robust adaptive synchronization (satellite system)	[13]
proposed	5d	yes	unstable point	hyperchaotic	mps	this work

Table 1: Comparison of recent fractional-order hyperchaotic systems (2020–2025).

1.1 Key contributions

The main contributions of this study are outlined as follows:

- The proposed novel five-dimensional fractional-order hyperchaotic system is derived from a Lorenz-type structure, exhibiting rich and complex dynamics.
- The system exhibits rich dynamical phenomena, including both chaotic and hyperchaotic attractors of orders 2 and 3, adjustable using fractional order and system parameters q.
- A rigorous theoretical analysis is conducted using the fractional Routh–Hurwitz criterion and eigenvalue-based stability conditions to determine local equilibrium behavior.
- A modified projective synchronization (MPS) scheme is successfully developed and applied to both identical and non-identical systems, achieving convergence through analytically derived control laws.
- The analytical framework is validated by high-resolution numerical simulations using the Adams–Bashforth–Moulton method, confirming robust synchronization and dynamic transitions.

These contributions advance the theoretical and applied study of fractional-order hyperchaotic systems and provide practical tools for control and synchronization in complex dynamical networks.

2 Fundamental Definitions and Preliminary Concepts

2.1 Fractional calculus

Fractional calculus generalizes classical differential calculus to arbitrary non-integer orders, represented by the fundamental operator, enabling a more precise characterization

of complex dynamics ${}_aD_q^t$, where a and t are the bounds of the operation and $q \in \mathbf{R}$. The continuous differential integration operator is expressed as

$${}_aD_q^t = \begin{cases} \frac{d^q}{dt^q}, & q > 0, \\ 1, & q = 0, \\ \int_a^t (d\tau)^q, & q < 0. \end{cases}$$

Within the present analysis, the Caputo fractional derivative is adopted and mathematically defined as

$${}_aD_q^t f(t) = \frac{1}{\Gamma(n-q)} \int_a^t \frac{f^n(\tau)}{(t-\tau)^{q-n+1}} d\tau \quad \text{for } n-1 < q < n.$$

Numerical schemes resolve fractional equations while ensuring stability. The predictor-corrector method excels in chaos simulations, leveraging the Adams-Bashforth-Moulton framework.

2.2 Analytical examination of stability in fractional-order dynamics

Examine a nonlinear fractional-order autonomous system expressed as

$$\begin{cases} D^{q_1} x_1(t) = g_1(x_1, x_2, \ldots, x_n), \\ D^{q_2} x_2(t) = g_2(x_1, x_2, \ldots, x_n), \\ \vdots \\ D^{q_n} x_n(t) = g_n(x_1, x_2, \ldots, x_n), \end{cases} \tag{1}$$

where $0 < q_i \leq 1$ for $i = 1, 2, \ldots, n$. If $q_1 = q_2 = \ldots = q_n = q$, the system (1) is designated as a commensurate-order system; otherwise, it is categorized as an incommensurate-order system.

Definition 2.1 An equilibrium point $(x_1^{eq}, x_2^{eq}, \ldots, x_n^{eq})$ of the fractional dynamic system (1) is defined as

$$g_i(x_1^{eq}, x_2^{eq}, \ldots, x_n^{eq}) = 0, \quad \forall i = 1, 2, \ldots, n.$$

Theorem 2.1 *Within the framework of the commensurate nonlinear fractional-order system* (1) *with* $0 < q_1 = q_2 = \ldots = q_n = q \leq 1$*, the equilibrium states of* (1)*, denoted as* $x^{eq} = (x_1^{eq}, x_2^{eq}, \ldots, x_n^{eq})$*, are locally asymptotically stable if every eigenvalue* λ_i *of the Jacobian matrix* J *evaluated at the equilibrium points has the following condition:*

$$J = \begin{bmatrix} a_{11} & a_{12} & \cdots & a_{1n} \\ a_{21} & a_{22} & \cdots & a_{2n} \\ \vdots & \vdots & \cdots & \vdots \\ a_{n1} & a_{n2} & \cdots & a_{nn} \end{bmatrix},$$

where $a_{ij} = \left.\frac{\partial f_i}{\partial x_j}\right|_{x^{eq}}$ *for* $i, j = 1, 2, \ldots, n$*, and we say stability is ensured:*

$$|\arg(\lambda_i)| > \frac{q\pi}{2}.$$

These criteria define the basic stability conditions for partially ordered systems and create a sound theoretical basis for investigating the dynamical properties in both partially ordered, chaotic, and highly chaotic systems.

2.3 Routh-Hurwitz criteria for fractional-order systems

Examine the following commensurate fractional-order system:

$$D^q x = f(x),$$

where $q \in]0,1]$, $x \in \mathbf{R}^3$. Suppose x_{eq} represents an equilibrium point of this system. The associated characteristic equation can be expressed as

$$P(\lambda) = \lambda^3 + a_1\lambda^2 + a_2\lambda + a_3 = 0.$$

The discriminant of this equation is expressed as

$$D(P) = 18a_1a_2a_3 + (a_1a_2)^2 - 4a_3(a_1)^3 - 4(a_2)^3 - 27(a_3)^2.$$

According to the Routh-Hurwitz fractional criteria, the following conditions provide the necessary and sufficient requirements for the equilibrium point x_{eq} and to achieve local asymptotic stability in a fractional system:

1. If $D(P) > 0$, the system achieves local asymptotic stability provided that $a_1 > 0$, $a_3 > 0$, and $a_1a_2 - a_3 > 0$.
2. If $D(P) < 0$, $a_1 \geq 0$, $a_2 \geq 0$, $a_3 > 0$, stability is ensured when $q < 2/3$. In contrast, if $D(P) < 0$, $a_1 < 0$, $a_2 < 0$, $q > 2/3$, the equilibrium point is unstable.
3. If $D(P) < 0$, $a_1 > 0$, $a_2 > 0$, $a_1a_2 - a_3 = 0$, then local asymptotic stability is preserved for all $q \in]0,1[$.
4. A fundamental requirement for the equilibrium point x_{eq} is that it must be locally asymptotically stable if $a_3 > 0$.

3 Formal Characterization and Analytical Examination of the Models

3.1 Formulation of the five-dimensional hyperchaotic system

Q. Yang et al. [15] presented an advanced five-dimensional hyperchaotic extension of the generalized Lorenz system

$$\begin{cases} D^q x_1 &= a(x_2 - x_1), \\ D^q x_2 &= cx_1 + dx_2 - x_1x_3 + x_5, \\ D^q x_3 &= -bx_3 + x_1^2, \\ D^q x_4 &= ex_2 + fx_4, \\ D^q x_5 &= -kx_5 - rx_1, \end{cases}$$

where $a > 0$, $b > 0$, and $d > -c$, with a, b, c, d, and f denoting system parameters, while e represents the coupling coefficient and r, k are control parameters.

Expanding upon this framework, a fractional-order counterpart of the system is formulated as follows:

$$\begin{cases} D^q x_1 &= a(x_2 - x_1) + x_4(x_4 + 1), \\ D^q x_2 &= bx_1 + dx_2 - x_1x_3, \\ D^q x_3 &= -cx_3 + x_1^2, \\ D^q x_4 &= x_2 - x_4, \\ D^q x_5 &= -kx_5 - rx_4, \end{cases} \tag{2}$$

where $q \in [0,1]$ denotes the fractional-order parameter. The constraints on the parameters remain consistent, where $a > 0$, $c > 0$, and a, b, c, d serve as system coefficients, while r and k are control parameters that influence system stability and chaotic dynamics.

4 Investigation of Dynamical Properties in a Fractional-Order Hyperchaotic Framework

This section examines the dynamic characteristics of fractional-order hyperchaotic systems.

4.1 Fractional-order stability

The equilibrium points of the system described in (2) are identified by solving the equation $g(x_1, x_2, x_3, x_4, x_5) = 0$. After a simple calculation, it is found that this system has one trivial equilibrium point $E_0 \equiv (0,0,0,0,0)$, which always exists.

The stability of the equilibrium point E_0 relies on the Jacobian matrix, evaluated at this point and expressed as follows:

$$J = \begin{pmatrix} -a & a & 0 & 1 & 0 \\ b & d & 0 & 0 & 0 \\ 0 & 0 & -c & 0 & 0 \\ 0 & 1 & 0 & -1 & 0 \\ 0 & 0 & 0 & -r & -k \end{pmatrix}.$$

Hence, its characteristic polynomial is

$$P(\lambda) = -(c+\lambda)(k+\lambda)\left(\lambda^3 + (a-d+1)\lambda^2 + (-ab-ad+a-d)\lambda - ab - ad - b \quad\right). \tag{3}$$

This polynomial yields the roots $\lambda_1 = -c$, $\lambda_2 = -k$, and

$$P_2(\lambda) = \lambda^3 + a_1\lambda^2 + a_2\lambda + a_3, \tag{4}$$

where $a_1 = a - d + 1$, $a_2 = -ab - ad + a - d$, $a_3 = -ab - ad - b$.

Following the Routh–Hurwitz criterion, the conditions under which all the eigenvalues of (4) lie within the angular sector $|\arg(\lambda_i)| > q\frac{\pi}{2}$, ensuring the stability of the fractional-order system if $D(p) > 0$, are as follows: $a_1 > 0$, $a_3 > 0$ and $a_1 a_2 - a_3 > 0$. These conditions, along with the constraints $c > 0, k > 0$, lead to the following system of inequalities:

$$\begin{cases} a > d - 1, \\ ab + ad + b < 0, \\ a + b - d - a^2 b + ad^2 - a^2 d - 2ad + a^2 + d^2 + abd > 0. \end{cases} \tag{5}$$

Consequently, $E_0(0,0,0,0,0)$ exhibits local asymptotic stability for all $q \in]0,1[$.

When the parameters (a, c, b, d, r, k) are set to $(10, 28, \frac{8}{3}, -2, 5, 0.05)$, the condition $ab + ad + b = 9.33 > 0$ violates the second requirement of equation (5). Solving the characteristic equation yields four negative real eigenvalues and one positive real eigenvalue: $\lambda_1 = -28$, $\lambda_2 = 0.05$, $\lambda_3 = -12.51$, $\lambda_4 = -1.14$, and $\lambda_5 = 0.65$. This indicates that the equilibrium point $E_0(0,0,0,0,0)$ is a saddle of index one and hence unstable. Additionally, the condition $\min|\arg(\lambda_i)| > q\frac{\pi}{2}$ for $i = 1,2,3,4$ is satisfied. As a result,

it is possible to assess the potential for chaos within the system described by equation (2) when the order $q > 0$, in line with the five necessary conditions for the presence of a chaotic attractor in fractional-order systems. However, it remains impossible to ascertain the minimum order at which chaos manifests in the fractional-order system with the specified parameters.

4.2 Fixed system parameters and variable fractional order q

In this subsection, the system parameters are kept constant at $(a, c, b, d, r, k) = \left(10, 28, \frac{8}{3}, -2, 5, 0.05\right)$, while the fractional order q is varied within the range $[0.8, 1]$. The initial values of the state variables are set to $(3, 5, 9, 13, 0.1)$.

Fig.1(a) depicts the Lyapunov exponents of system (2) for different values of the fractional order q. The bifurcation diagram of system (2) as a function of q is shown in Fig.1(b). Table 2 presents the calculated Lyapunov exponents of system (2) and their corresponding dynamic behaviors for various values of the fractional order q.

Additionally, Fig.2 illustrates the projections of the order-2 hyper-chaotic attractor of system (2) when $q = 0.99$.

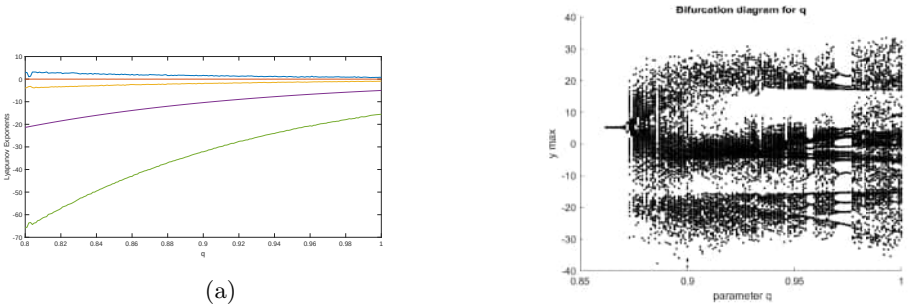

(a) (b)

Figure 1: (a) Lyapunov exponents of fractional system (2) with $(a, c, b, d, r, k) = (10, 28, \frac{8}{3}, -2, 5, 0.05)$ and $q \in [0.8, 1]$; (b) Bifurcation diagram of system (2) versus q

q	LE_1	LE_2	LE_3	LE_4	LE_5	Dynamics
0.810	2.8522	-0.0024	-3.6231	-20.0310	-61.8718	Chaotic
0.813	3.1708	0.0006	-3.6179	-19.6049	-60.8646	Hyperchaotic (order 2)
0.856	2.0145	0.0022	-2.5577	-14.3831	-44.4397	Hyperchaotic (order 2)
0.993	0.8303	0.0038	0.9752	-5.4538	-16.4516	Hyperchaotic (order 3)

Table 2: Lyapunov exponents of fractional systems with $(a, c, b, d, r, k) = (10, 28, \frac{8}{3}, -2, 5, 0.05)$.

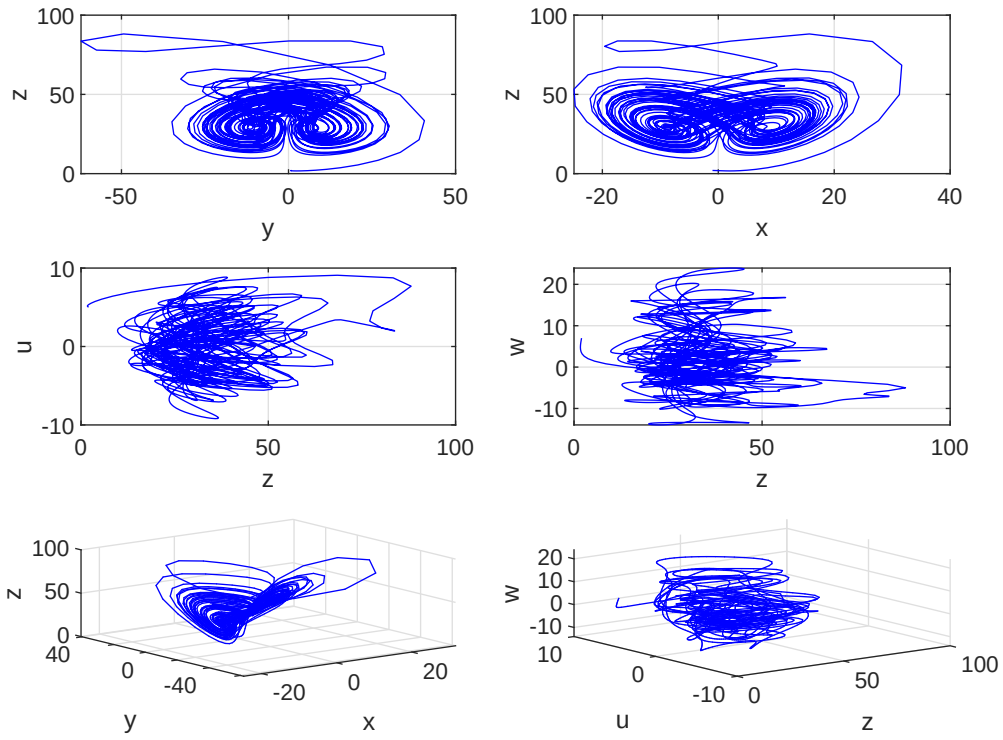

Figure 2: Hyperchaotic attractor of system (2) for $(a, c, b, d, r, k) = (10, 28, \frac{8}{3}, -2, 5, 0.05)$ and $q = 0.99$.

4.3 Fixed fractional order and variable system parameter d

In this subsection, the system parameters are $(a, c, b, r, k) = (10, 28, \frac{8}{3}, 5, 0.05)$, with $q = 0.99$, while exploring the impact of varying $d \in [-15, 0]$. The initial values for state variables are set to (3 5 9 13 0.1). The lyapunov exponents of equation (2) with respect to d are illustrated in Fig.3(a). The bifurcation diagram for the system described in equation (2) with $d \in [-15, 1]$ is depicted in Fig.3(b), using $(a, c, b, r, k) = (10, 28, \frac{8}{3}, 5, 0.05)$ and $q = 0.99$.

Table 3 presents the Lyapunov exponents of system (2) for various values of d. The corresponding dynamic behaviors for different d values are described. Additionally, Fig.4 displays the projections of the second-order hyperchaotic attractor for system (2) with $d = -6$ and $q = 0.99$.

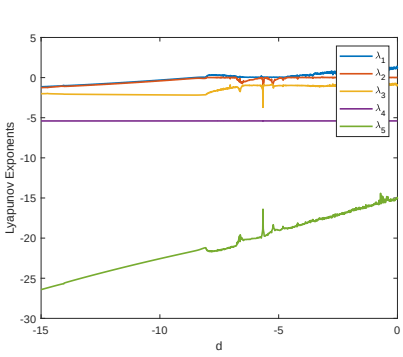

(a)

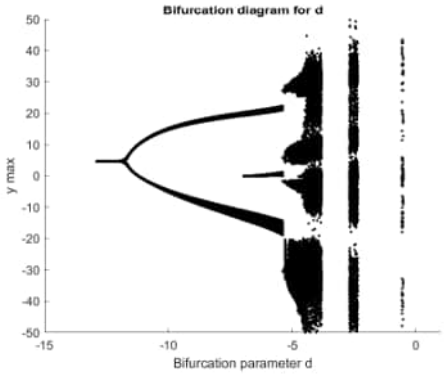

(b)

Figure 3: (a) Lyapunov exponents of fractional system (2) with $(a, c, b, r, k) = (10, 28, \frac{8}{3}, 5, 0.05)$ and $q = 0.99$, while $d \in [-15, 0]$; (b) Bifurcation diagram of system (2) versus d with $q = 0.99$.

d	LE_1	LE_2	LE_3	LE_4	LE_5	Dynamics
-6	0.2550	-0.0007	-0.9901	-1.1339	-18.2360	Chaotic
-4	0.6434	0.0002	-1.0325	-1.1256	-17.4954	Hyperchaotic (order 2)
-2	0.7419	0.0140	0.0525	-5.4538	-16.5421	Hyperchaotic (order 3)

Table 3: lyapunov exponents for fractional systems with $(a, c, b, r, k) = (10, 28, \frac{8}{3}, 5, 0.05)$, $q = 0.99$, and varying d.

5 Modified Projective Synchronization Framework

5.1 Synchronization of identical hyperchaotic systems via modified projective approach

Two identical hyperchaotic frameworks evolve, with drive dynamics defined as follows:

$$\begin{cases} D^q x_1 &= a(x_2 - x_1) + x_4(x_4 + 1), \\ D^q x_2 &= bx_1 + dx_2 - x_1 x_3, \\ D^q x_3 &= -cx_3 + x_1^2, \\ D^q x_4 &= x_2 - x_4, \\ D^q x_5 &= -kx_5 - rx_4. \end{cases} \tag{6}$$

The corresponding response system is formulated as

$$\begin{cases} D^q y_1 &= a(y_2 - y_1) + y_4(y_4 + 1) + \mu_1, \\ D^q y_2 &= by_1 + dy_2 - y_1 y_3 + \mu_2, \\ D^q y_3 &= -cy_3 + y_1^2 + \mu_3, \\ D^q y_4 &= y_2 - y_4 + \mu_4, \\ D^q y_5 &= -ky_5 - ry_4 + \mu_5. \end{cases} \tag{7}$$

Five control nonlinear functions, denoted μ_i $(i = 1, 2, 3, 4, 5)$, were introduced in (7) to synchronize the two identical systems in the sense of MPS.

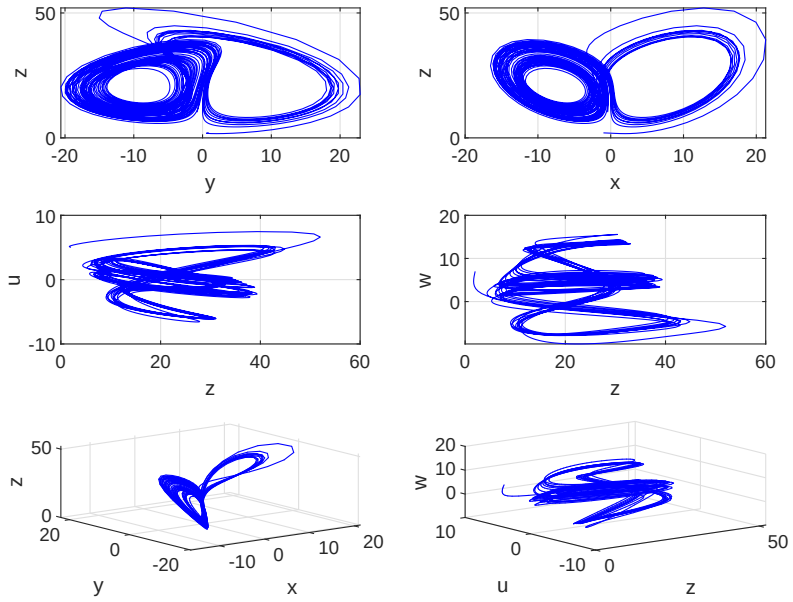

Figure 4: Hyperchaotic attractor of system (2) for $(a, c, b, r, k) = (10, 28, \frac{8}{3}, 5, 0.05)$, $d = -6$, and $q = 0.99$.

Defining the synchronization error as

$$e_i = y_i - \alpha_i x_i \quad \text{for} \quad i = 1, 2, 3, 4, 5,$$

the error dynamics can be derived by subtracting the response system from the drive system:

$$\begin{cases} D^q e_1 = a(e_2 - e_1) + e_4 + a(\alpha_2 - \alpha_1)x_2 + y_4^2 + (\alpha_4 - \alpha_1)x_4 + \mu_1, \\ D^q e_2 = de_2 + by_1 - y_1 y_3 - b\alpha_2 x_1 + \alpha_2 x_1 x_3 + \mu_2, \\ D^q e_3 = -ce_3 + y_1^2 + \alpha_3 x_1^2 + \mu_3, \\ D^q e_4 = -e_4 + y_2 - \alpha_4 x_2 - \alpha_4 x_5 + \mu_4, \\ D^q e_5 = -ry_4 - ke_5 + r\alpha_5 x_4 + \mu_5. \end{cases} \tag{8}$$

Construct appropriate control laws

$$\begin{aligned} \mu_1 &= -a(\alpha_2 - \alpha_1)x_2 - y_4^2 - (\alpha_4 - \alpha_1)x_4 - e_4, \\ \mu_2 &= -by_1 + y_1 y_3 + b\alpha_2 x_1 - \alpha_2 x_1 x_3, \\ \mu_3 &= -y_1^2 - \alpha_3 x_1^2, \\ \mu_4 &= -y_2 + \alpha_4 x_2 + \alpha_4 x_5, \\ \mu_5 &= ry_4 - r\alpha_5 x_4. \end{aligned} \tag{9}$$

Substituting these into the error dynamics yields a system of decoupled linear differ-

ential equations:

$$\begin{cases} D^q e_1 = a(e_2 - e_1), \\ D^q e_2 = de_2, \\ D^q e_3 = -ce_3, \\ D^q e_4 = -e_4, \\ D^q e_5 = -ke_5. \end{cases} \tag{10}$$

Taking the Laplace transformation on both sides of (10) gives

$$E_i(s) = \mathcal{L}(e_i(t)).$$

Given

$$\mathcal{L}\left(\frac{d^q e_i(t)}{dt^\alpha}\right) = s^q E_i(s) - s^{q-1} e_i(0) \quad i = 1, 2, 3, 4, 5,$$

results in the following system of equations:

$$\begin{aligned} &s^q E_1(s) - s^{q-1} e_1(0) = -aE_1(s) + aE_2(s), \\ &s^q E_2(s) - s^{q-1} e_2(0) = dE_2(s), \\ &s^q E_3(s) - s^{q-1} e_3(0) = -cE_3(s), \\ &s^q E_4(s) - s^{q-1} e_4(0) = -E_4(s), \\ &s^q E_5(s) - s^{q-1} e_5(0) = -kE_5(s). \end{aligned} \tag{11}$$

From 11, it follows that

$$\begin{cases} E_1(s) &= \frac{s^{q-1} e_1(0) + aE_2(s)}{s^q + a}, \\ E_2(s) &= \frac{s^{q-1} e_2(0)}{s^q - d}, \\ E_3(s) &= \frac{s^{q-1} e_3(0)}{s^q + c}, \\ E_4(s) &= \frac{s^{q-1} e_4(0)}{s^q + 1}, \\ E_5(s) &= \frac{s^{q-1} e_5(0)}{s^q + k}. \end{cases}$$

By applying the Laplace transformation and utilizing the final value theorem, it follows that

$$\begin{cases} \lim_{t\to\infty} e_2(t) &= \lim_{s\to 0^+} sE_2(s) = \lim_{s\to 0^+} \frac{s^q e_2(0)}{s^q - d} = 0, \\ \lim_{t\to\infty} e_1(t) &= \lim_{s\to 0^+} sE_1(s) = \lim_{s\to 0^+} \frac{s^q e_1(0) + saE_2(s)}{s^q + a} = 0, \\ \lim_{t\to\infty} e_3(t) &= \lim_{s\to 0^+} sE_3(s) = \lim_{s\to 0^+} \frac{s^q e_3(0)}{s^q + c} = 0, \\ \lim_{t\to\infty} e_4(t) &= \lim_{s\to 0^+} sE_4(s) = \lim_{s\to 0^+} \frac{s^q e_4(0)}{s^q + 1} = 0, \\ \lim_{t\to\infty} e_5(t) &= \lim_{s\to 0^+} sE_5(s) = \lim_{s\to 0^+} \frac{s^q e_5(0)}{s^q + k} = 0. \end{cases}$$

Therefore, both the response system (6) and the driving system (7) have attained MPS.

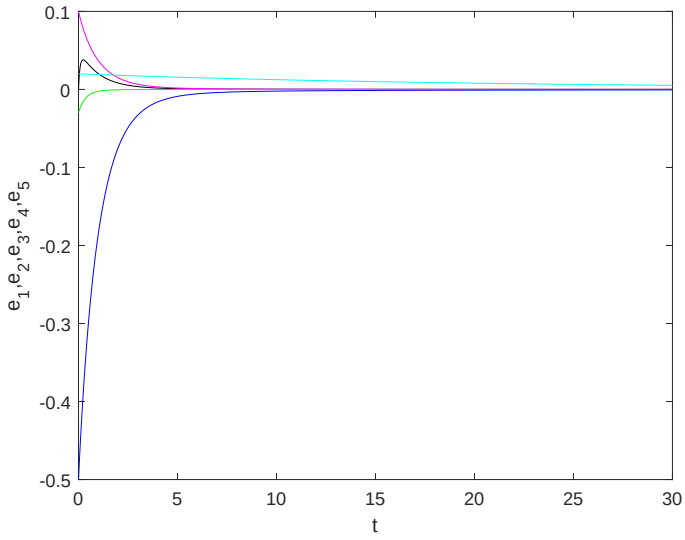

Figure 5: Synchronization errors between identical systems with $q = 0.95$.

5.2 Synchronization of non-identical hyperchaotic systems via modified projective approach

Suppose the system is the slave system [11], and its control is formulated as

$$\begin{cases} D^q y_1 = a_1(y_2 - y_1) + y_4 + \mu_1, \\ D^q y_2 = c_1 y_1 - y_1 y_3 + y_5 + \mu_2, \\ D^q y_3 = -b_1 y_3 + y_1 y_2 + \mu_3, \\ D^q y_4 = -h_1 y_4 - y_1 y_3 + \mu_4, \\ D^q y_5 = -k_1 y_1 - k_2 y_2 + \mu_5, \end{cases} \tag{12}$$

where μ_i, $i = 1, 2, 3, 4, 5$, are nonlinear control functions. The master system is given by

$$\begin{cases} D^q x_1 &= a(x_2 - x_1) + x_4(x_4 + 1), \\ D^q x_2 &= bx_1 + dx_2 - x_1 x_3, \\ D^q x_3 &= -cx_3 + x_1^2, \\ D^q x_4 &= x_2 - x_4, \\ D^q x_5 &= -kx_5 - rx_4. \end{cases} \tag{13}$$

Define the error variables as $e_i = y_i - l_i x_i$, where $i = 1, 2, 3, 4, 5$. Then the error

dynamical system is given by

$$\begin{cases} D^q e_1 = a_1(e_2 - e_1) + l_1(a - a_1)x_1 + (l_1 a_1 - l_1 a)x_2 + e_4 + (l_1 + l_4)x_4 + l_1 x_4^2 + \mu_1, \\ D^q e_2 = c_1 e_2 - (l_2 b + c_1 l_1)x_1 - y_1 y_3 + y_5 + l_2 x_1 x_3 + d l_2 x_2 + \mu_2, \\ D^q e_3 = -b_1 e_3 + y_1 y_2 - l_3 x_1^2 + l_3(c + b_1)x_3 + \mu_3, \\ D^q e_4 = -h_1 e_4 - y_1 y_3 - l_4(h_1 - 1)x_4 - l_4 x_2 + \mu_4, \\ D^q e_5 = -k e_5 - k_1 y_1 - k_2 y_2 + k l_5 x_5 + r l_5 x_4 - k y_5 + \mu_5. \end{cases} \tag{14}$$

Then the active control μ_i $(i = 1, 2, 3, 4, 5)$ is defined as

$$\begin{aligned} \mu_1 &= -l_1 (a - a_1) x_1 - (l_2 a_1 - l_1 a) x_2 - (l_1 + l_4)x_4 - l_1 x_4^2, \\ \mu_2 &= -(l_2 b + c_1 l_1)x_1 + y_1 y_3 - y_5 - l_2 x_1 x_3 - d l_2 x_2, \\ \mu_3 &= -y_1 y_2 + l_3 x_1^2 - l_3(c + b_1)x_3, \\ \mu_4 &= y_1 y_3 + l_4(h_1 - 1)x_4 + l_4 x_2, \\ \mu_5 &= k_1 y_1 + k_2 y_2 - k l_5 x_5 - r l_5 x_4 + k y_5. \end{aligned} \tag{15}$$

Substituting (15) into (14) leads to

$$\begin{cases} D^q e_1 &= a_1 (e_2 - e_1) + e_4, \\ D^q e_2 &= c_1 e_2, \\ D^q e_3 &= -b_1 e_3, \\ D^q e_4 &= -h_1 e_4, \\ D^q e_5 &= -k e_5. \end{cases} \tag{16}$$

Take the Laplace transformation on both sides of (16) in a way similar to that in Subsection 5.1. It is found that $\lim\limits_{t \longrightarrow +\infty} e_i(t) = 0$ for $i = 1, 2, 3, 4, 5$. Therefore, the MPS of the systems (12) and (13) is achieved under the control law (15).

Therefore, both the response system (13) and the driving system (12) have attained MPS.

5.3 Numerical simulations

This section presents the findings of the simulation that illustrate the efficacy of the suggested synchronization scheme. The ABM method is used to solve the systems. For these numerical simulations, the parameters for the slave and master systems are set as $\big(10, \frac{8}{3}, 28, -1, 5, 0.05\big)$.

The experiments are carried out with a fixed fractional-order value of $q = 0.95$. The starting conditions for the master and slave systems are given as $(2, 6, 4, -1.5, 7.5)$ and $(8, 5.5, 6, 4.5, 1)$, respectively. The results confirm successful synchronization, as illustrated in Fig. 5, where the errors e_i, for $i = 1, 2, ..., 5$, converge to zero.

Additional simulations further validate the scheme. The parameters of the master system are $(35, 7, 35, -5, 5, 0.05)$, while the parameters of the slave system are $\big(10, 28, \frac{8}{3}, -2, 0, 12\big)$. With $q = 0.98$, the initial conditions are $(3, 5, 4, 2, 6)$ and $(8, 10, 6, 8, 1)$. As shown in Fig.6, synchronization is achieved with the errors converging to zero.

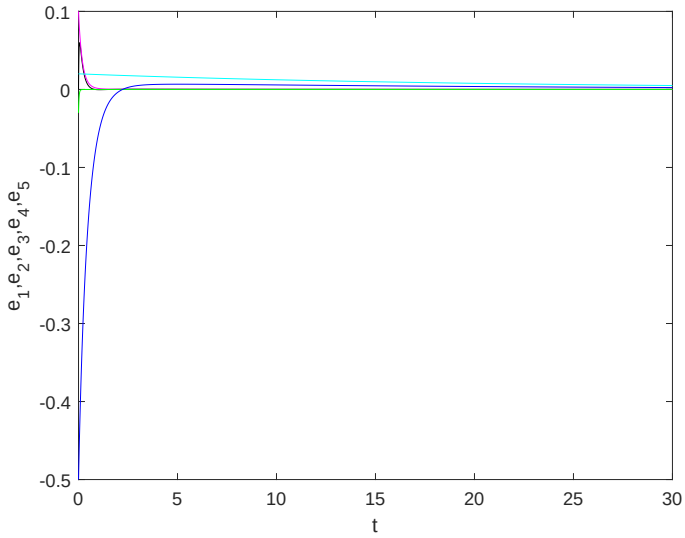

Figure 6: Synchronization errors between nonidentical systems with $q = 0.98$.

6 Discussion

The stability regions and synchronization results obtained demonstrate that the proposed five-dimensional hyperchaotic system with fractional order provides a flexible platform for investigating high-dimensional nonlinear dynamics. In particular, its ability to create second and third-order hyperchaos and synchronize identical and non-identical systems in the MPS distinguishes it from existing models. It increases its applicability in secure communication and control of complex networks.

7 Conclusion

This paper presents a five-dimensional fractional-order hyperchaotic system derived from a modified generalized Lorenz framework. Unlike previously reported fractional-order models, the proposed system introduces a nonlinear cross-coupling term together with tunable fractional orders, enabling both second- and third-order hyperchaotic attractors within a single parameter configuration.

Using the fractional Routh–Hurwitz criterion, we derived explicit stability conditions that map the parameter regions of chaotic and hyperchaotic behavior. Building on this analysis, we designed a modified projective synchronization (MPS) scheme and proved analytically that it synchronizes both identical and non-identical fractional-order systems. High-resolution numerical simulations support the theory and show robust convergence of synchronization errors.

Overall, the results extend the understanding of high-dimensional fractional-order nonlinear systems and offer practical tools for secure communications, encryption, and control of complex dynamical networks. The proposed system and synchronization approach also open promising directions for future research on high-dimensional fractional-order chaotic and hyperchaotic dynamics.

Acknowledgment

The authors express sincere gratitude to the reviewers for their valuable comments and suggestions, which have helped improve the quality of this work.

References

[1] Y. Chen, H. Zhang and X. Kong. A new fractional-order hyperchaotic system and its adaptive tracking control. *Discrete Dynamics in Nature and Society* **2021** (2021) 6625765.

[2] H. Eshaghi, S. Khanmohammadi and R. Alizadeh. Chaos control and synchronization of a new fractional laser chaotic system. *Qualitative Theory of Dynamical Systems* **23** (2) (2024).

[3] A. Farghaly and A. Shoreh. Some complex dynamical behaviors of the new 6D fractional-order hyperchaotic Lorenz-like system. *Journal of the Egyptian Mathematical Society* **26** (1) (2018) 138–155.

[4] Y. Ghettout, L. Meddour, T. Hamaizia and R. Ouahabi. Dynamic analysis of a new hyperchaotic system with infinite equilibria and its synchronization. *Nonlinear Dynamics and Systems Theory* **24** (2) (2024) 147–158.

[5] F. Hannachi and R. Amira. On the dynamics and FSHP synchronization of a new chaotic 3-D system with three nonlinearities. *Nonlinear Dynamics and Systems Theory* **23** (3) (2023) 283–294.

[6] G. M. Mahmoud and E. E. Mahmoud. Complete synchronization of chaotic complex nonlinear systems with uncertain parameters. *Nonlinear Dynamics* **62** (4) (2010) 875–882.

[7] K. Oldham and J. Spanier. *The fractional calculus: Theory and applications of differentiation and integration to arbitrary order*. Elsevier Science, Netherlands, 1974.

[8] K. Shao, Z. Xu and T. Wang. Robust finite-time sliding mode synchronization of fractional-order hyper-chaotic systems based on adaptive neural network and disturbance observer. *International Journal of Dynamics and Control* **9** (2021) 541–549.

[9] E. M. Shahverdiev, S. Sivaprakasam and K. A. Shore. Lag synchronization in time-delayed systems. *Physics Letters A* **292** (6) (2002) 320–324.

[10] X. Wang and Y. He. Projective synchronization of fractional order chaotic system based on linear separation. *Physics Letters A* **372** (4) (2008) 435–441.

[11] S. Wang and R. Wu. Dynamic analysis of a 5D fractional-order hyperchaotic system. *International Journal of Control, Automation and Systems* **15** (3) (2017) 1003–1010.

[12] S. Wang, L. Hong, J. Jiang and X. Li. Synchronization precision analysis of a fractional-order hyperchaos with application to image encryption. *Chaos* **30** (6) (2020) 063113.

[13] M. Yaghoubi, H. Faraji and G. Erjaee. Robust adaptive synchronization of a chaotic fractional-order satellite system. *IET Control Theory & Applications* **19** (5) (2025).

[14] J. Yang, J. Xiong, J. Cen and W. He. Finite-time generalized synchronization of non-identical fractional order chaotic systems and its application in speech secure communication. *PLOS ONE* **17** (2) (2022) e0263007.

[15] Q. Yang and M. Bai. A new 5D hyperchaotic system based on modified generalized Lorenz system. *Nonlinear Dynamics* **88** (1) (2016) 189–221.